COMBUSTION & FLAME

Quarterly Journal of The Combustion Institute

Contents

VOLUME 1 NO. 3 SEPTEMBER 1957

	Page
Behaviour of Inverted Propane–Hydrogen Sulphide Flames at the Blow-off Limits. *P. F. Kurz*	257
An Investigation of the Behaviour and Reaction Mechanisms of Nitric Acid–Hydrocarbon Flames. *M. H. Boyer and P. E. Friebertshauser*	264
Extraction of Ions from a Flame. *J. Deckers and A. van Tiggelen*	281
I. Predicting the Laminar Flame Speed in Gases with Temperature-explicit Reaction Rates. *D. B. Spalding*	287
II. One-dimensional Laminar Flame Theory for Temperature-explicit Reaction Rates. *D. B. Spalding*	296
Flame Decomposition of the Propyl Nitrates. *J. Powling and W. A. W. Smith*	308
Detonations in Gaseous Fuming Nitric Acid–Hydrocarbon Mixtures. *D. H. Wayman and R. L. Potter*	321
A Method for Determining Minimum Ignition Energies: Results for a Neopentane–Air Mixture. *I. W. Wolf and V. T. Burkett*	330
Temperature Stability of the Laminar Combustion Wave. *J. F. Wehner and J. B. Rosen*	339
Present Status of Information on Transport Properties Applicable to Combustion Research. *A. A. Westenberg*	346
Scale Effect in a Gas Turbine Combustion Chamber Fitted with a Swirl Atomizer, Part I. *M. V. Herbert and J. A. Bamford*	360
Recent Developments and Notes. *W. A. Kirkby*	379

Published quarterly. Annual subscription including postage—U.K. £5 5s. 0d.; U.S.A. $15.00. Combined subscription with Fuel*—U.K. £8 8s. 0d.; U.S.A. $25.00. Editorial Offices, Showroom, Binding and Trade Departments:* 4-5 Bell Yard, Temple Bar, London, W.C.2. *Telephone:* Chancery 6681. *Publishing and Advertising Offices:* 88 Kingsway, London, W.C.2. *Telephone:* Holborn 6900. *Distributors: U.S.A., Interscience Publishers Inc., 250 Fifth Avenue, New York 1, N.Y. All other countries except U.K., Canada, Australia, New Zealand and South Africa: I. R. Maxwell & Co. Ltd. 4-5 Fitzroy Square, London, W.1.*

BUTTERWORTHS SCIENTIFIC PUBLICATIONS

Behaviour of Inverted Propane–Hydrogen Sulphide Flames at the Blow-off Limits

P. F. KURZ

Blow-off studies with inverted propane–hydrogen sulphide flames show that at the lean limit propane appears to contribute its proportionate share to the stability of the mixed fuel, whereas the burning of hydrogen sulphide is inhibited in the presence of propane. At rich blow-off, hydrogen sulphide appears to inhibit the burning of propane in all mixtures, and when the fuel mixture contains more than 50 volume per cent hydrogen sulphide the component fuels are mutually inhibiting.

THIS PAPER describes the behaviour of propane–hydrogen sulphide flames at lean and rich blow-off on a 19·1 mm inverted Bunsen–Smithells burner. The Smithells[1] tube excludes ambient air from the environs of the burner port; its presence is necessary if inverted flames are to be studied quantitatively.

Earlier work[2] with hydrocarbons burning on a 19·1 mm burner showed that the blow-off limits of a given fuel were the same whether the burner was upright or inverted. Indeed, the flames of a given hydrocarbon appeared essentially the same in shape and colour whether they were upright or inverted, except for the split 'cone' which burned at the outlet of the Smithells tube. However, when hydrogen sulphide was burned alone with air on the inverted burner, rich flames of this fuel were quite different from those observed on an upright burner. The inverted rich flames of hydrogen sulphide were almost white and rather intense with just a faint tinge of purple, whereas upright rich flames observed earlier on another burner were lavender-white and not nearly as bright. It was considered possible, therefore, that inverted flames of hydrocarbon–hydrogen sulphide mixtures might show different mutual effects at blow-off from upright flames, but unfortunately circumstances did not permit the completion of the study of upright flames, so the desired comparison could not be made.

It was found that the presence of hydrogen sulphide in propane–air mixtures inhibited the burning processes of propane in all rich mixtures at blow-off. When more than about 50 vol. per cent hydrogen sulphide was present in rich-limit mixtures the component fuels were mutually inhibiting. However, in lean mixtures at blow-off it appeared that propane contributed its proportionate share to the stability of the mixture, and that the burning of hydrogen sulphide was inhibited in the presence of propane.

APPARATUS AND GASES

The inverted burner and auxiliaries for metering gas flows and controlling flash-back have been described earlier[2]. Briefly, the burner was brass, of 19·1 mm i.d., and water-cooled to maintain a uniform temperature at the port. Gas flows were metered with critical-flow orifices, and compressed

air in commercial cylinders was used to ensure close control over the pressure in the air lines at all times. The propane used was C.P. grade, specified as 99 mol per cent pure, and the hydrogen sulphide was 99·9 mol per cent pure.

EXPERIMENTAL PROCEDURE

The use of a Smithells tube or other method of shielding to exclude ambient air from the environs of the burner port permitted observation of both the lean blow-off and the rich blow-off limits, as inverted flames could not be studied quantitatively in the presence of random air currents in the laboratory.

At any given air rate within the range of laminar flow, the blow-off limits may be observed by adjusting the rate of fuel input to the burner. Thus, the lean blow-off limit was obtained by decreasing the fuel flow rate, and rich blow-off occurred when the rate of fuel input was increased until the flame dropped from the burner port. The procedure was as follows. A convenient rate of air flow was established and held constant throughout the experiment, the lean blow-off limit of propane was observed at the chosen air rate, and then hydrogen sulphide was introduced at a predetermined low rate of flow, and the flow rate of propane was decreased until the lean blow-off limit of the mixed-fuel flame was reached. Next, the flow rate of hydrogen sulphide was increased by a convenient amount and the flow rate of propane was decreased until the flame blew off again.

The addition of successive increments of hydrogen sulphide was continued, each time reducing the flow of propane required just sufficiently to maintain a stable flame, until the only combustible present was hydrogen sulphide, and then the lean blow-off limit of hydrogen sulphide was observed.

The procedure for observing rich blow-off limits of propane–hydrogen sulphide flames was similar to that described above; the rich limit of propane was observed at the chosen air rate, then hydrogen sulphide was introduced in a stepwise manner. Successive increments of hydrogen sulphide permitted observation of rich limits for a series of binary propane–hydrogen sulphide mixtures, and finally the rich blow-off limit of hydrogen sulphide was observed.

The blow-off limits of binary fuel mixtures were observed at two different rates of air flow using the procedure outlined above, and the complete range of fuel compositions from 100 per cent propane to 100 per cent hydrogen sulphide was thus studied.

EXPERIMENTAL RESULTS

Figure 1 shows lean and rich blow-off limit curves for propane–hydrogen sulphide flames at two air flow rates on the 19·1 mm shielded inverted burner. The coordinate scales are in units of the critical velocity gradient[3], $g = -8U/D$, and the composition of the fuel–air mixture is expressed as the percentage of stoichiometric air present in the mixture.

It is evident that the rich blow-off limits of all binary mixtures are at leaner compositions than are the limits shown for propane flames at the

two different air flow rates. Likewise, they are almost all leaner than are the rich blow-off limits of hydrogen sulphide flames.

The lean blow-off limits of all binary mixtures are at richer compositions than are the limits of hydrogen sulphide flames, although many of them are leaner than the limits of propane flames, the reversal of the curvature suggests that this is so only because the lean blow-off limits of propane and hydrogen sulphide flames are so very different.

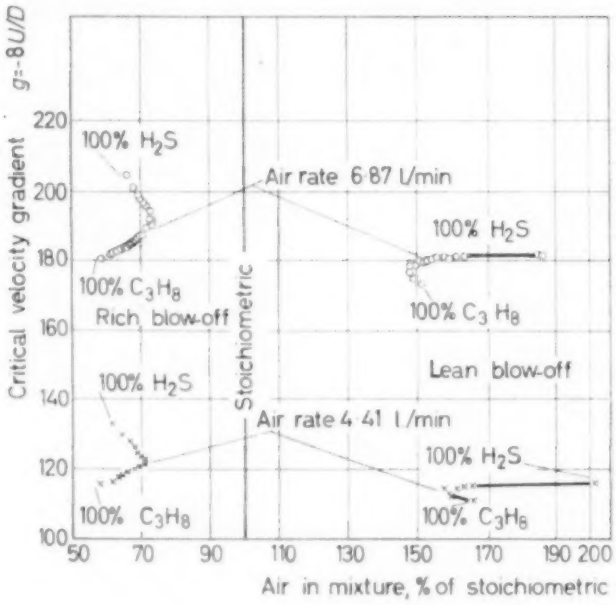

Figure 1. Lean and rich blow-off limits of propane–hydrogen sulphide flames on an inverted burner

Figure 2 shows the relation between fuel composition expressed as equivalent per cent[4] and the lean and rich blow-off limits of propane–hydrogen sulphide flames on the inverted burner. It is evident that the lean blow-off limit is narrowed much more than is the rich blow-off limit by an increase of about 50 per cent in the air rate (from about 4·4 to about 6·9 l./min).

ANALYSIS OF THE DATA

A convenient graphical method for examining the data from these stability experiments is to use coordinates which are in units of $V_{C_3H_8}/V^*_{C_3H_8}$ and $V_{H_2S}/V^*_{H_2S}$. $V_{C_3H_8}$ and V_{H_2S} are the volumetric flow rates of propane and hydrogen sulphide at the blow-off limit and $V^*_{C_3H_8}$ and $V^*_{H_2S}$ are the volumetric flow rates of these fuels, each burning separately with air at the same blow-off limit. Thus, the ratios $V_{C_3H_8}/V^*_{C_3H_8}$ and $V_{H_2S}/V^*_{H_2S}$ are measures of the effectiveness of the contributions of the component fuels to the flame properties of the mixture as related to the flame properties of the individual fuels when burning alone with air. If each component fuel contributes its proportionate share to the stability of the mixture, according to its ability, $V_{C_3H_8}/V^*_{C_3H_8} + V_{H_2S}/V^*_{H_2S}$ will be unity. Thus, the fuels will be compatible and non-interfering in the flame. Under these

conditions, the graphical relationship between $V_{C_3H_8}/V^*_{C_3H_8}$ and $V_{H_2S}/V^*_{H_2S}$ will be linear. The development of an equation for evaluating the additivity of the contributions of component fuels to the behaviour of a mixture at the blow-off limit has been described elsewhere[4], and is based

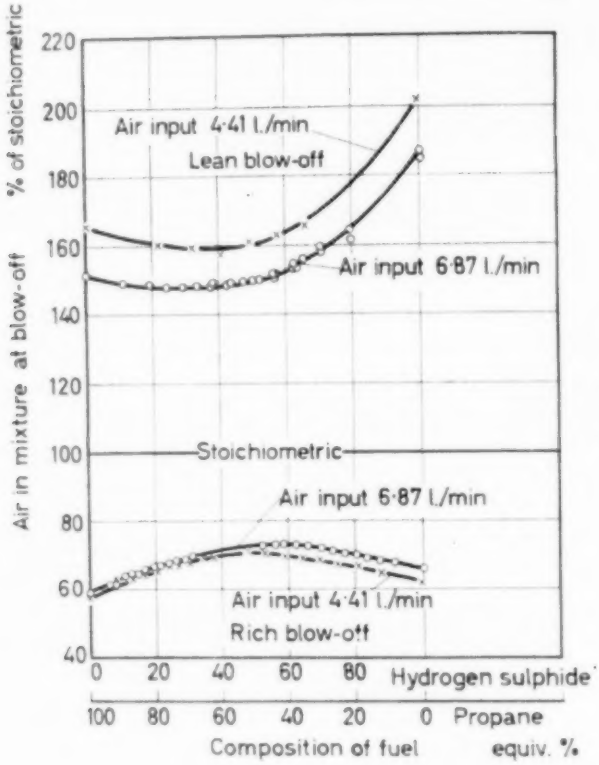

Figure 2. Relation between fuel composition and blow-off limits of lean and rich propane–hydrogen sulphide flames on an inverted burner

upon earlier work by H. LE CHATELIER[5] on flammability limits and by W. PAYMAN[6] and H. F. COWARD and H. P. GREENWALD[7] on flame speeds of fuel mixtures.

If $V_{C_3H_8}/V^*_{C_3H_8} + V_{H_2S}/V^*_{H_2S} \neq 1$, then the fuels are not compatible and either inhibition or promotion is occurring. It has been shown in *Figures 1* and *2* that with propane–hydrogen sulphide mixtures inhibition occurs.

Figure 3 shows that the relationship between $V_{C_3H_8}/V^*_{C_3H_8}$ and $V_{H_2S}/V^*_{H_2S}$ is non-linear at the lean blow-off limit. The upward bowing of the curve shows that the sum of the two ratios is greater than unity. Hence, either $V_{C_3H_8}$ or V_{H_2S} or both must be greater than would be predicted from experimental values of $V^*_{C_3H_8}$ and $V^*_{H_2S}$ based on the assumption that the two fuels are non-interfering.

Figure 4 shows that a non-linear relationship also exists between $V_{C_3H_8}/V^*_{C_3H_8}$ and $V_{H_2S}/V^*_{H_2S}$ at the rich blow-off limit. The downward bowing of the curve indicates that the sum of the two ratios is less than unity. Hence, either $V_{C_3H_8}$ or V_{H_2S} or both must be smaller than would be predicted from $V^*_{C_3H_8}$ and $V^*_{H_2S}$ on a non-interfering basis.

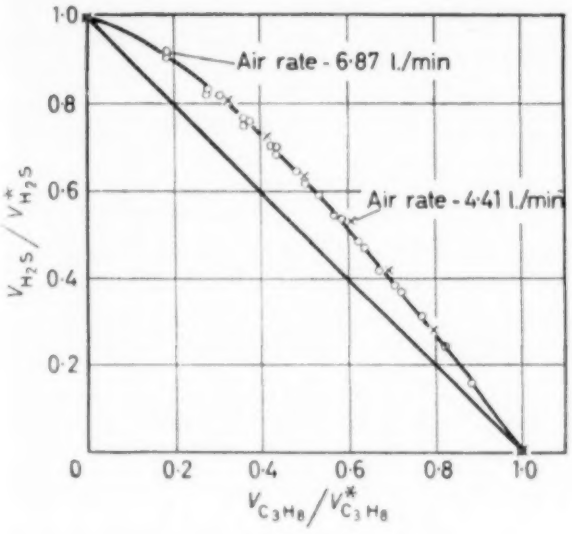

Figure 3. Non-linear relationship between $(V_{C_3H_8}/V^*_{C_3H_8})$ *and* $(V_{H_2S}/V^*_{H_2S})$ *showing inhibition in burning of lean propane–hydrogen sulphide mixtures at blow-off*

Figure 5 shows the relation between $V_{C_3H_8}/V^*_{C_3H_8}$ or $V_{H_2S}/V^*_{H_2S}$ and the composition of the fuel mixture expressed as equivalent per cent at lean blow-off. It is evident that $V_{C_3H_8}/V^*_{C_3H_8}$ varies linearly with changes in the fuel composition whereas the curve representing the hydrogen sulphide portion of the fuel departs substantially from linearity. This suggests that to obtain a barely stable flame more hydrogen sulphide must be present

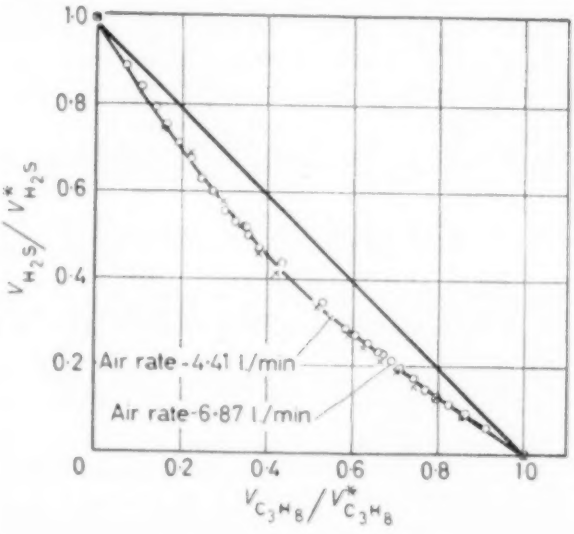

Figure 4. Non-linear relationship between $(V_{C_3H_8}/V^*_{C_3H_8})$ *and* $(V_{H_2S}/V^*_{H_2S})$ *showing inhibition in burning of rich propane–hydrogen sulphide mixtures at blow-off*

in the fuel mixture than would be predicted from the behaviour separately of propane and of hydrogen sulphide flames. Hence, in the presence of propane in lean flames, hydrogen sulphide is not able to contribute its proportionate share to the stability of the mixture, and it may be concluded that, in lean propane–hydrogen sulphide flames, the flame reactions of propane are essentially unaffected whereas those of hydrogen sulphide are inhibited significantly.

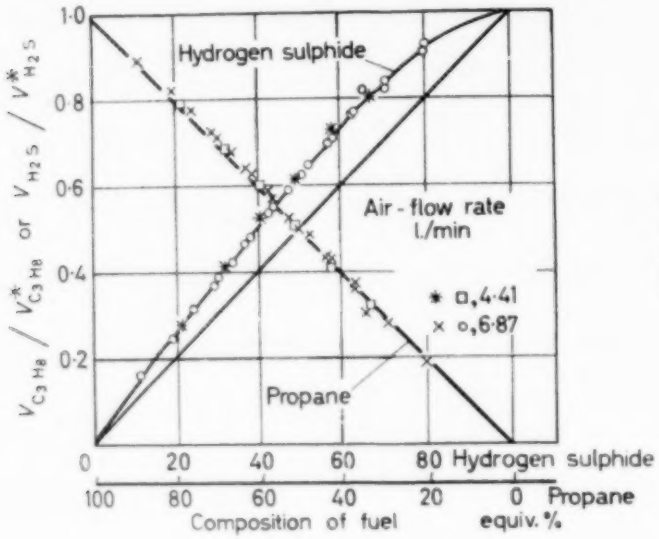

Figure 5. Predictable behaviour of propane and preferential inhibition of hydrogen sulphide combustion in lean mixtures at blow-off

Figure 6 shows the relationship between $V_{C_3H_8}/V^*_{C_3H_8}$ or $V_{H_2S}/V^*_{H_2S}$ and the fuel composition at rich blow-off. For values of $V_{H_2S}/V^*_{H_2S}$ between 0 and 0·25, $V_{H_2S}/V^*_{H_2S}$ varies linearly with changes in fuel composition. However, for values of $V_{H_2S}/V^*_{H_2S}$ greater than 0·25, the curve for hydrogen sulphide departs to a small extent from linearity. The curve for propane departs from linearity for all values of $V_{C_3H_8}/V^*_{C_3H_8}$ from 0 to 1·0. These data suggest that hydrogen sulphide contributes its proportionate share to the stability of the mixture when the fuel contains less than about 25 equivalent per cent (about 53 vol. per cent) of it. When more than about 25 equivalent per cent hydrogen sulphide is present in the mixture, the values of $V_{H_2S}/V^*_{H_2S}$ are less than would be predicted. Thus, in these

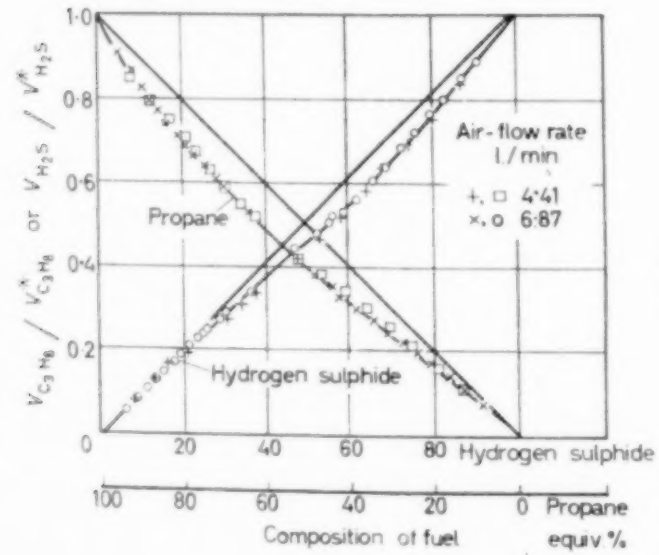

Figure 6. Mutual inhibition of propane and hydrogen sulphide in rich mixtures at blow-off

rich mixtures at blow-off, the burning of the hydrogen sulphide is inhibited. Likewise, the fact that $V_{c_3H_8}/V^*_{c_3H_8}$ is less than would be predicted from a knowledge of $V^*_{c_3H_8}$ suggests that the burning of propane is inhibited in all rich mixtures in which hydrogen sulphide is present. Furthermore, the brunt of the inhibition in rich mixtures appears to fall on propane.

This work was carried out under the sponsorship of the Chemistry Research Branch, Aeronautical Research Laboratory, Wright Air Development Center, Wright-Patterson Air Force Base, Ohio. The author wishes to express his thanks to Mr W. B. Thompson who assisted ably and faithfully in the experimental work and to Dr J. F. Byrne, Assistant Division Chief at the Battelle Memorial Institute, for his helpful interest.

Battelle Memorial Institute,
Columbus, Ohio

(Received December 1956)

REFERENCES

[1] SMITHELLS, A. and INGLE, H. *J. chem. Soc.* 61 (1892) 204
[2] KURZ, P. F. *Industr. Engng Chem. (Industr.)* 47 (1955) 121
[3] LEWIS, B. and VON ELBE, G. *J. chem. Phys.* 11 (1943) 75
[4] KURZ, P. F. *Industr. Engng Chem. (Industr.)* 45 (1953) 2072
[5] LE CHATELIER, H. *Ann. Min., Paris* 19 (1891) 388
[6] PAYMAN, W. *J. chem. Soc.* 115 (1919) 1436
[7] COWARD, H. F. and GREENWALD, H. P. *Tech. Pap. Bur. Min., Wash.* No. 427, 1928

An Investigation of the Behaviour and Reaction Mechanisms of Nitric Acid–Hydrocarbon Flames

M. H. BOYER* and P. E. FRIEBERTSHAUSER

Apparatus is described for producing nitric acid supported bunsen flames. Data are presented on the flame speed, flashback and blow-off limits, emission spectra, and analysis of the combustion products, for flames burning mixtures of nitric acid vapour and propane or butane. A possible interpretation in terms of the reaction sequence through the combustion wave is presented.

DEVELOPMENT over the past few years of interest in practical combustion devices employing fuming nitric acid and hydrocarbon materials as oxidizer and fuel respectively has led to recognition of a need for information about the basic combustion behaviour of this system. The research presented in this paper concerns a study of bunsen flames supported by mixtures of nitric acid and hydrocarbon vapours, undertaken as part of the development of such information. Since the study of oxidizers other than oxygen is a relatively new field of combustion research, the objective of the programme was to survey a broad area of behaviour. Consequently, the work is, to some extent, exploratory in nature. Data are presented on: (*1*) flashback and blow-off or extinction limits, (*2*) measurement of flame speeds, (*3*) investigation of the products of combustion, and (*4*) some details on the spectral distribution of emitted radiation. An interpretation of the findings in terms of a scheme for the combustion reaction is suggested.

EXPERIMENTAL

Burner apparatus

A block diagram of the bunsen burner apparatus is shown in *Figure 1*. Liquid nitric acid is metered from storage (A) by means of a capillary flowmeter (B). Flow rate is controlled by pressure applied to the storage flask through pressure regulator (C). The acid passes into the elevated end of a $\frac{1}{4}$ in. o.d. aluminium tube (D) around which is wound a resistance heater. The tube is inclined at a downward angle of about 20° so that the acid flows rapidly down in the form of a thin film over the hot inner surface, and is essentially flash vaporized. It was found that with this arrangement relatively smooth vapour flow with low liquid hold-up occurs, and response of the vapour flow to changes in liquid flow rate is very rapid. Furthermore, since the rate of decomposition of acid vapour is considerably lower than that of the liquid, the short heating and evaporation times involved minimized decomposition. The latter has been shown by condensation and analysis of nitric acid vapour which has passed through the system. Increases in the nitrogen dioxide and water content of less

*Now at Aeronutronic Systems Inc.

than 0·2 per cent were found. It should be noted in this connection that stainless steel surfaces have appeared to catalyse the vapour phase decomposition of nitric acid[1], and should not be used in the vaporizing system

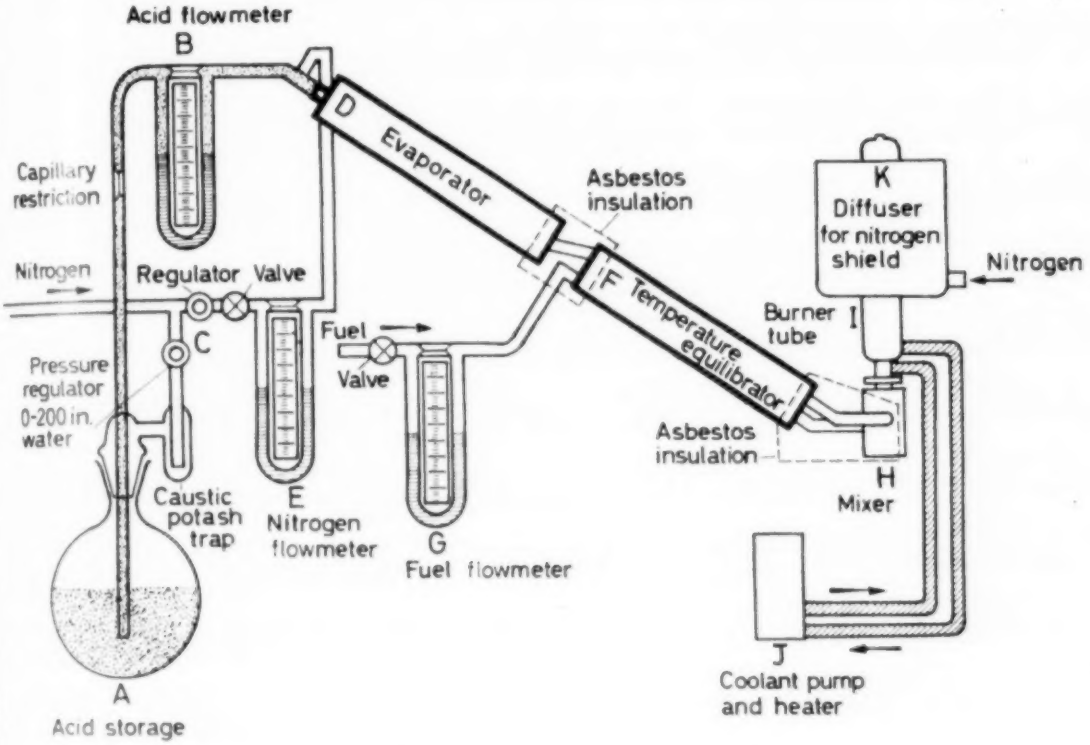

Figure 1. Diagram of bunsen burner apparatus

Nitrogen or other gases can be mixed with the acid vapour, as desired, by metering them into the evaporator via flowmeter E.

From the evaporator, the acid vapour mixture passes through one channel of a two-channel preheater (F). Fuel gas (propane or butane) is metered through the other channel from flowmeter G. The fuel and oxidizer streams emerge from the preheater at the same temperature and pass directly into the mixing block (H), thence up through the burner tube (I) to burn at the tip to provide the desired flame. The burner tube is jacketed and its temperature is controlled by means of circulating oil from a combination pump and heater (J). Only nominal temperature control is maintained on the evaporator, and considerable variation occurs during the operation. The temperature is not permitted to rise above 175°C, however. Close temperature control of the remainder of the system is maintained, with the preheater and mixing block a few degrees above the temperature of the burner tube. The latter is taken as the unburnt gas temperature. A diffusing chamber (K) surrounding the burner tube is used to provide a uniform gas blanket of desired composition around the flame.

Burner tubes of 0·177 in. and 0·420 in. i.d. fabricated from 18–8 stainless steel tubing have been used with the apparatus. These were chosen on

the basis of convenience since they are the inside diameters of stock $\frac{1}{4}$ in. and $\frac{1}{2}$ in. stainless steel tubing. It was not desirable to go to smaller sizes due to the probability of large consequent quenching errors. Data on flame stability limits and flame speeds were obtained with the 0·177 in. i.d. burner. The data on combustion products and emission spectra were obtained with the 0·420 in. i.d. burner.

The manometric fluid used in the flowmeters was fluorocarbon oil manufactured by the Hooker Chemical Company. It was found to be unreactive to liquid fuming nitric acid over long periods of time.

Flashback and blow-off limits

Flashback and blow-off limits were determined by setting up a predetermined acid flow rate, varying the fuel flow, and noting the points at which flashback and blow-off occurred. These points were passed several times from both directions without significant difference. The flame was surrounded by a nitrogen blanket in all cases for which data are reported. The presence of secondary air was found to affect the stability limits in the fuel-rich region but not in the oxidizer-rich region.

Flame speed

Observations of the primary combustion zone were made by spark shadowgraph photography. The usual technique was modified somewhat in that the flame shadow was cast directly on a ground glass plate and photographed with a standard Graphic camera employing a short-focus lens. Distance from the flame to the ground glass plate was $3\frac{1}{8}$ in. and from the spark to the flame was $15\frac{1}{4}$ in. No attempt was made to vary the flame to ground glass plate distance. Measurements were always made on the dark zone of the shadow cast by the combustion wave.

The cone area method of calculation was used to determine flame speed from the shadowgraphs under conditions where laminar flow existed. This method is not suitable for turbulent flow conditions. Since with the burner tube used, stability could not be maintained at certain mixture ratio conditions without operation in the turbulent region, no data are reported for these conditions. It is anticipated that in future work the region involved will be explored by means of a nozzle burner.

Combustion product analysis

Samples of the effluent gas from the primary combustion cone were obtained by surrounding the flame with a Smithells separator tube and aspirating off part of the effluent gas through a side arm. The aspirated gas passed first through a cold trap at 0 C to separate condensible material and thence into an evacuated bulb. The contents of the latter were analysed by standard Orsat methods. When no nitrogen dioxide was present, the carbon dioxide was removed in caustic potash solution, followed by the successive absorption of first, nitric oxide in ferrous sulphate solution; secondly, carbon monoxide in cuprous chloride solution; thirdly, partial absorption of unsaturates in mercurous sulphate–sulphuric acid solution[7];

fourthly, hydrogen by copper oxide combustion; and fifthly, total hydrocarbon by slow combustion. When nitrogen dioxide is present, there is interference with the carbon dioxide determination which cannot be resolved by any relatively simple procedure. However, since no residual combustible material was found to be present under the oxidizer-rich conditions for which nitrogen dioxide appeared, it was deemed satisfactory to assume that the theoretical concentration of carbon dioxide was present. This could be in error only as a result of retention of high boiling carbonaceous material in the ice trap, which was not found to be significant at these mixture ratios. It was then possible to determine the nitrogen dioxide by subtraction of the theoretical carbon dioxide from the total absorption in caustic potash, and the remaining constituents by the methods outlined above.

Weight concentrations of the constituents of the gaseous portion in terms of total sample weight were determined by weighing separately the non-condensible and the condensible fractions. It was then assumed that the mol fraction of each gaseous constituent was equal to its volume fraction, and since the total volume of the gas was known, the value of the corresponding weight concentration could be calculated. This method is subject to error due to gas imperfection which partly accounts for the fact that the weight percentages for the various analyses listed in *Table 1* do not add up to 100.

Study of the contents of the cold trap was carried out only for fuel-rich mixture ratios. Four main constituents were found which were determined by the following procedures:

Formaldehyde—

(1) Preparation of a 2, 4-dinitrophenyl hydrazone derivative from the unknown sample, and its separation into fractions corresponding to the original carbonyl compound by the method of paper chromatography[3].

(2) Determination of the melting point and mixed melting point of the hydrazone with a sample of a known hydrazone.

Nitromethane—

(1) Test for nitro groups consisting of hydrolysis in caustic potash and detection of resultant nitrous acid by means of Griess–Ilosvay reagent[4].

(2) Identification of the nitro derivative as nitromethane by methazonic acid formation[5].

(3) Determination of nitromethane colorimetrically with ferric chloride reagent[6].

(4) Absorption spectra of condensed phase material.

Cyanide or cyanogen—

(1) Formation of prussian blue upon addition of ferric and ferrous ions to the condensed phase material.

Water—

(1) Karl Fischer titration.

(2) Distillation.

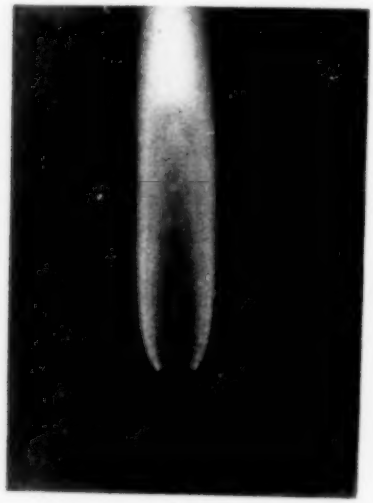

(a)

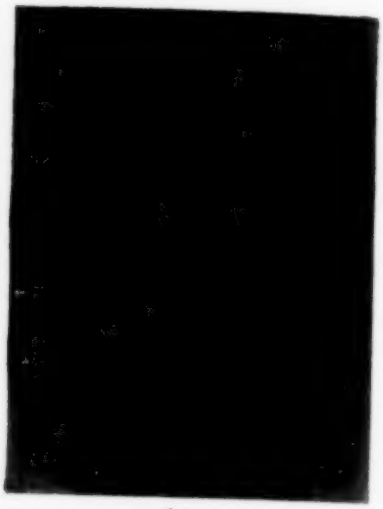

(b)

(c)

(d)

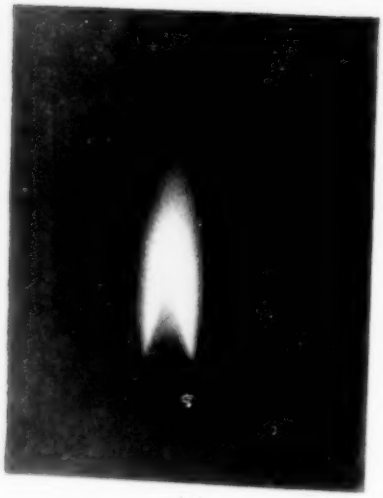

(e)

Figure 2(a). Primary and secondary reaction zones. $[O/(F+O)]\times 100 = 84{\cdot}5$. $N_2 = 10{\cdot}3$ wt %

Figure 2(b). With nitrogen shield. $[O/(F+O)]\times 100 = 80{\cdot}5$. $N_2 = 2{\cdot}0$ wt %

Figure 2(c). Doublet secondary reaction zone. $[O/(F+O)]\times 100 = 71{\cdot}7$. $N_2 = 4{\cdot}17$ wt %

Figure 2(d). Near stoichiometric. $[O/(F+O)]\times 100 = 93{\cdot}5$. $N_2 = 4{\cdot}3$ wt %

Figure 2(e). Acid - rich flame. $[O/(F+O)]\times 100 = 95{\cdot}0$. $N_2 = 3{\cdot}7$ wt %

Figure 2. Flame photographs

Flame emission spectra

Data were obtained with a Beckmann DK-2 recording spectrophotometer operated as a spectrometer. Light from the flame was gathered by a 6 in. concave first surface mirror of 12 in. radius of curvature and focused on the end of a $\frac{5}{8}$ in. o.d. aluminium tube with a polished inner surface. The tube gradually flattened toward the opposite end to form a slit about $\frac{1}{16}$ in. wide which was inserted into the spectrophotometer entrance tunnel so that emergent radiation fell directly upon the entrance slit. Spectral distribution of the radiation was determined for different mixture ratios and flame image positions over the range of 220 to 3000 millimicrons using photomultiplier and lead sulphide detectors.

MATERIALS

The fuming nitric acid used in the work reported herein was a commercial product with composition in the following range:

HNO_3	98·5 to 97 per cent
NO_2	0·5 to 1·0 per cent
H_2O	1·0 to 2·0 per cent

In all cases, the fuel was either propane or butane (as indicated) of 99 per cent purity (Phillips pure grade). This assay was verified by vapour phase chromatographic analysis.

RESULTS

Appearance of flames

Nitric acid flames exhibited considerable structure which was dependent upon mixture ratio and upon the presence or absence of secondary air. This is illustrated in *Figures* 2(a) to (e). With medium fuel-rich mixtures, i.e. $R = [O/(F + O)] \cdot 100 = 84{\cdot}5$, where O = wt flow of oxidizer and F = wt flow of fuel, and in the presence of secondary air, two reaction zones were observed at considerable separation [*Figure* 2(a)]. The innermost one had the typical shape of a bunsen cone and was assumed to be the zone of initial reaction. The outer had the appearance of a diffusion reaction zone and this, together with the fact that it disappeared when the flame was surrounded by a nitrogen shield [*Figure* 2(b)] led to the conclusion that it was derived from the diffusion of secondary air into the flame.

If the mixture ratio was made more fuel-rich, again in the presence of secondary air, the flames took on an appearance as shown by *Figure* 2(c). It is seen here that the outer diffusion cone was divided into a closely spaced doublet, and the primary reaction zone became invisible, although its continued presence was demonstrable by spark shadowgraph photography. The doublet was characterized by a yellow colour on the inner side, and a blue-grey colour on the outer side and appeared to be quite similar, both as to appearance and as to conditions for its existence, to a doublet reaction zone occurring with nitrogen dioxide supported flames[2,3]. Under spark shadowgraph photography, the secondary structure obtained in this as well as in the above case showed only a single, rather weak shadow, indicating that it did not include a region of high density gradient.

Exclusion of secondary air from the most fuel-rich flames always caused the outer structure to disappear leaving a thin, pale, magenta-coloured primary reaction zone of so low a luminosity that it was barely visible in a lighted room. This was surrounded by an outer mantle which was visible as a faint glow, only in a well darkened room. No evidence of solid carbon formation in the flame appeared at any mixture ratio.

Under more acid-rich conditions, it became necessary, even with the smaller burner tube (0·177 in.), to operate in the turbulent flow region in order to maintain stability. As a stoichiometric point was approached for the reaction

$$4HNO_3 + C_3H_8 \rightarrow 2N_2 + 6H_2O + 3CO_2 \qquad \ldots [1]$$

the outer reaction zones disappeared and there remained only the turbulent primary bunsen reaction zone and a pale blue-grey outer mantle which began visibly to persist in the absence of secondary air.

Further increase in the acid concentration to $R = 90$ brought about the appearance of a very interesting structure to the primary reaction zone. A sharp separation into two broad coloured regions occurred; the upstream side assuming a bright orange colour, the downstream side a light blue, suggestive of normal hydrocarbon–air flames. The orange colour of the flame had the appearance of leaking out around the base of the reaction zone into the outer mantle, which was grey, and giving it an orange colour around the edges. As will be discussed later, this flame was characteristic of the point at which maximum theoretical flame temperature occurred and at which excess fuel disappeared from the combustion products. It is shown in *Figure* 2(d), but unfortunately its rather striking appearance cannot be shown by black and white photography.

Finally, an increase of the acid concentration to the maximum possible value, $R = 95$, compatible with the maintenance of stability produced a structureless appearance as shown in *Figure* 2(e). The flame consisted of a diffuse orange mantle surrounding an inner dark conical area. Evolution of nitrogen dioxide was sometimes noted at these mixture ratios. In the range between this and the previous case, $R = 90$ to 95, little or no effect on the flame appearance resulted from the presence or absence of secondary air.

Flame stability parameters

Figure 3 shows the curves of critical velocity gradients for flashback and blow-off of the flames in the absence of secondary air plotted against the quantity $O/(F + O) \times 100$. Velocity gradients were calculated from the expressions[9]

$$g = (4/\pi)(V/R^3) \qquad \ldots [2]$$

for the laminar flow region [i.e. to Reynolds numbers (R_e) of 2000] and

$$g = 0{\cdot}023\,U^{1.8}\rho^{0.8}/(2R)^{0.2}\eta^{0.8} \qquad \ldots [3]$$

for the turbulent flow region (R_e greater than 3000) where:

g = velocity gradient (sec^{-1})
V = volume flow rate (cm^3/s)
$\bar{U}$ = average linear stream velocity (cm/s)
R = tube radius (cm)
ρ = density of combustible mixture (g/cm^3)
η = viscosity of combustible mixture (poise).

For the purpose of the calculations, the combustible mixture was assumed to be a perfect gas. No experimental information on the viscosity of nitric acid vapour is available. Consequently, a value was calculated based upon an assumed R_e of 2200 for the average flow rate at which the stream was first observed to become turbulent. This value (137 micropoise) is very close to the theoretical values of 132 micropoise calculated by the method of L. A. BROMLEY and C. R. WILKE[10], for which the values of the

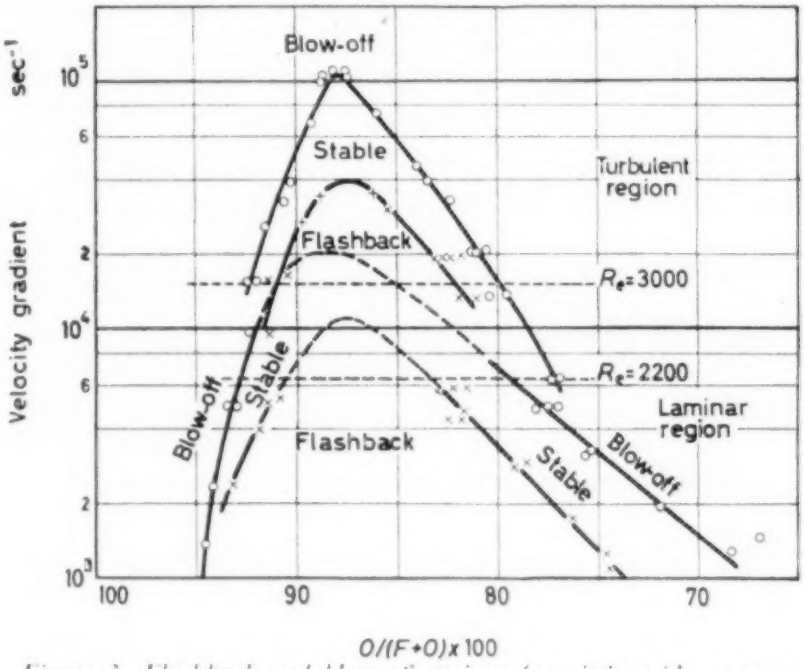

Figure 3. Flashback and blow-off regions for nitric acid—propane flames

critical temperature and volume were approximated by the numerous empirical equations which are available[11]. For the calculation of *Figure 3*, an average value of 135 micropoise was used.

The curves of *Figure 3* show a significant discontinuity and change of slope at R_e 2200, the value at which turbulence is generally assumed to appear first in the approach stream. It is apparent from the curves that if the velocity gradient interpretation of flashback and blow-off is assumed to have validity throughout the turbulent region, then the true values of the velocity gradient in the stream must be lower than the calculated values, i.e. from equation 2. A probable explanation of this behaviour is derived from the low flame speeds which suggest correspondingly large quenching

Table 1. Composition of combustion product gases from premixed nitric acid and butane flames

Constituents	*Fuel rich*						*Acid rich*	
	Concentration, wt % total sample						*Constituents*	*Concentration wt % total sample*
Unburnt gas							Unburnt gas	
1. HNO_3	73·7[b]	79·9	81·4	82·4	86·8	87·3	HNO_3	91·7 91·7
2. C_4H_{10}	22·9	17·0	16·2	15·4	11·7	10·6	C_4H_{10}	5·98 5·98
3. N_2	3·4	3·3	2·4	2·2	1·5	2·1	N_2	2·30 2·30
Burnt gas							Burnt gas	29·4 29·3
4. NO_2	26·9	35·6	34·8	32·3	32·5	32·2	NO	7·2 5·8
5. NO *(theor.)*	35·1	38·0	38·8	39·3	41·1	41·6	NO_2	18·2[c] 18·2[c]
6. CO_2	6·5	7·7	8·2	8·0	17·1	22·4	CO_2	*Nil Nil*
7. CO	19·5	19·7	18·8	16·9	13·0	8·8	CO	*Nil Nil*
8. H_2	0·18	0·50	0·37	0·46	0·39	0·51	H_2	*Nil Nil*
9. *Olefins*[a]	3·0	1·8	1·13	0·96	0·29	*Nil*	*Olefins*[a]	*Nil Nil*
10. *Sat.* H—C[a]	2·8	1·27	0·97	0·71	0·53	0·12	*Sat.* H—C[a]	8·9[d] 8·5[d]
11. N_2	5·78	1·38	3·0	6·1	7·7	5·36	N_2	31·1 29·9
12. *Condensed fraction*	29·8	29·2	30·7	29·4	26·8	23·2	*Condensed fraction*	43·6 43·6
							Theor. $NO + NO_2$[e]	34·1 33·1
							Actual $NO + NO_2$	

[a] Sat. H—C as methane, olefins as ethylene.
[b] These mixture ratios were outside the stability limit. Flames were not attached to burner tube.
[c] The theoretical value assuming all hydrocarbon completely oxidized.
[d] Includes some nitrogen added in sampling process.
[e] Assumes complete reduction of nitric acid to nitric oxide.

distances. The latter may very well be larger than the thickness of the laminar boundary layer of the stream in which case the velocity gradient interpretation would not apply. The observed behaviour would then be due to an increase in burning rate with the onset of turbulence. This has been discussed by K. WOHL[12]. Similar behaviour has also been observed with hydrogen–oxygen flames[13].

An additional point of clarification should be made concerning *Figure 3*. The accuracy is relatively poorer for points at the lowest velocity gradients because of the very low flowmeter settings required.

Flame speed

Data obtained on flame speed as a function of composition are shown on *Figure 4*(a). Calculations were made from spark shadowgraphs of the

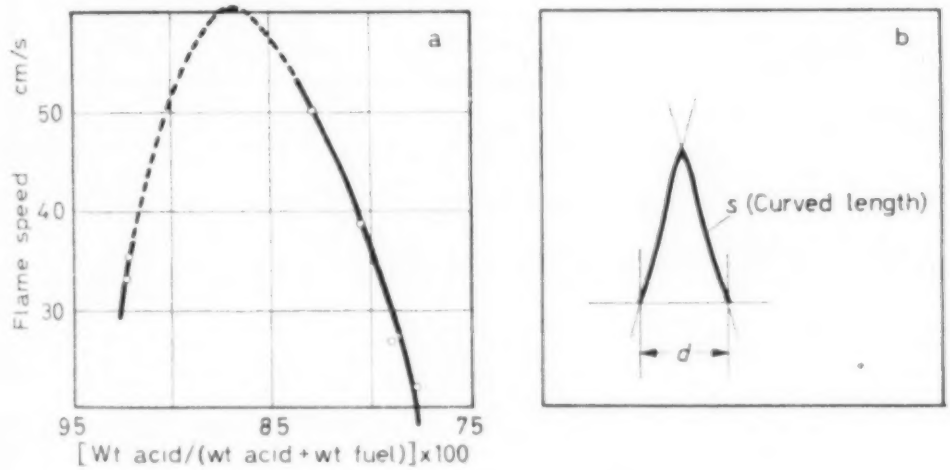

Figure 4. Flame speeds of nitric acid–propane supported flames—nitrogen 1·7% by weight

primary flame cone using the cone area method[7, 11, 13]. For conditions of laminar flow, the latter were very close to true geometric cones, and the flame front area was calculated using the relation

$$\text{Area} = \tfrac{1}{2}ds$$

where, for present purposes, d was taken as the base of the best geometric cone which could be drawn through the shadowgraph image, and s was the measured curved length of one side of the image. These definitions are indicated more clearly in *Figure 4*(b).

Combustion product analysis

Data obtained on the analysis of the non-condensable products of combustion are given in *Table 1* for several different unburnt gas mixtures. It will be noted that findings on the residual fuel components show nothing that is unexpected. It is, however, of considerable interest that large concentrations of nitric oxide appear, undoubtedly as a reduction product of nitric acid. Comparison of row 4 of the table with row 5 indicates that

the conversion of nitric acid to nitric oxide is nearly stoichiometric at all mixture ratios. This fact is more clearly brought out by *Figure 5*, in which the percentage of theoretical reduction of nitric acid to nitric oxide is plotted

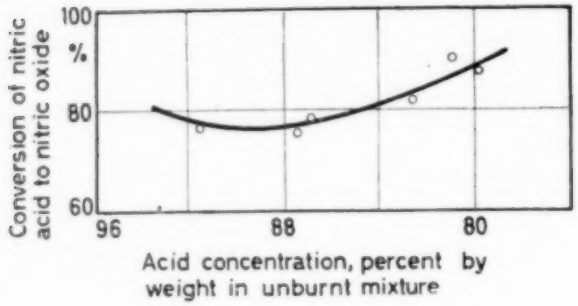

Figure 5. Conversion of fuming nitric acid to nitric oxide in white fuming nitric acid–supported butane flames—nitrogen concentration 1·5 to 3·5% by weight

against mixture composition. The ordinate in the plot represents the expression

$$\frac{\%\text{ nitric oxide in mixture} \times 100}{\text{theoretical \% nitric oxide for quantitative reduction of nitric acid to nitric oxide}}$$

The curve is seen to indicate a minimum of 78 per cent conversion at about 89 per cent acid in the unburnt gas mixture, which is quite close to the stoichiometric composition calculated for the reaction

$$26HNO_3 + 3C_4H_{10} \rightarrow 12CO_2 + 28H_2O + 26NO \qquad \ldots [4]$$

It will be shown in the following discussion that this is the mixture ratio at which maximum flame temperature is to be expected.

Analytical findings on the condensable products (at 0° C) of combustion at fuel-rich mixture ratios are shown in *Table 2*. They are of interest in

Table 2. Results of condensed-phase product analysis with details of composition of unburnt gas

Products	*Wt % approx.*	*Unburnt gas*	*Wt %*
Formaldehyde	1·5	*Nitric acid*	69·8
Nitromethane	0·3	*Propane*	28·8
Cyanide	0·15	*Nitrogen*	1·4
Nitro-olefins	1·5		
Nitroalcohols			
Water	95		

connection with the nature of the residues likely to be deposited within combustion chambers, as well as for the further insight which they may yield into the nature of the combustion reaction. The major constituent is water, as was to be expected. Formaldehyde is a common intermediate product of hydrocarbon oxidation. The nitromethane probably derives from reaction 11 below, and the cyanide (or cyanogen) is believed likely to result from its partial decomposition as has been demonstrated[16]. The presence of the nitro-olefins and their precursors, the nitroalcohols, has not

been demonstrated conclusively. Identification has been based upon rather diffuse absorption spectra data, and the qualitative observation of certain fractions of distillates from the combustion product mixture. However, the reactions which lead to them are well known[3]:

$$CH_2O + CH_3NO_2 \rightarrow CH_2OH{-}CH_2{-}NO_2 \quad \ldots . [5]$$
$$\rightarrow (CH_2OH)_2{=}CH{-}NO_2$$
$$\rightarrow (CH_2OH)_3{=}CNO_2$$

$$CH_2OH{-}CH_2{-}NO_2 \rightarrow CH_2{=}CH{-}NO_2 \quad \ldots . [6]$$

and the necessary reactants have been shown to be present.

Flame emission spectra

Spectrometer tracings which show the distribution of radiant energy from the flame are given in *Figure 6*, (a) to (e), for the region of 700 to 340 millimicrons. These curves are uncorrected for frequency response of the 1P28 detector tube so that the detector response, indicated vertically, is

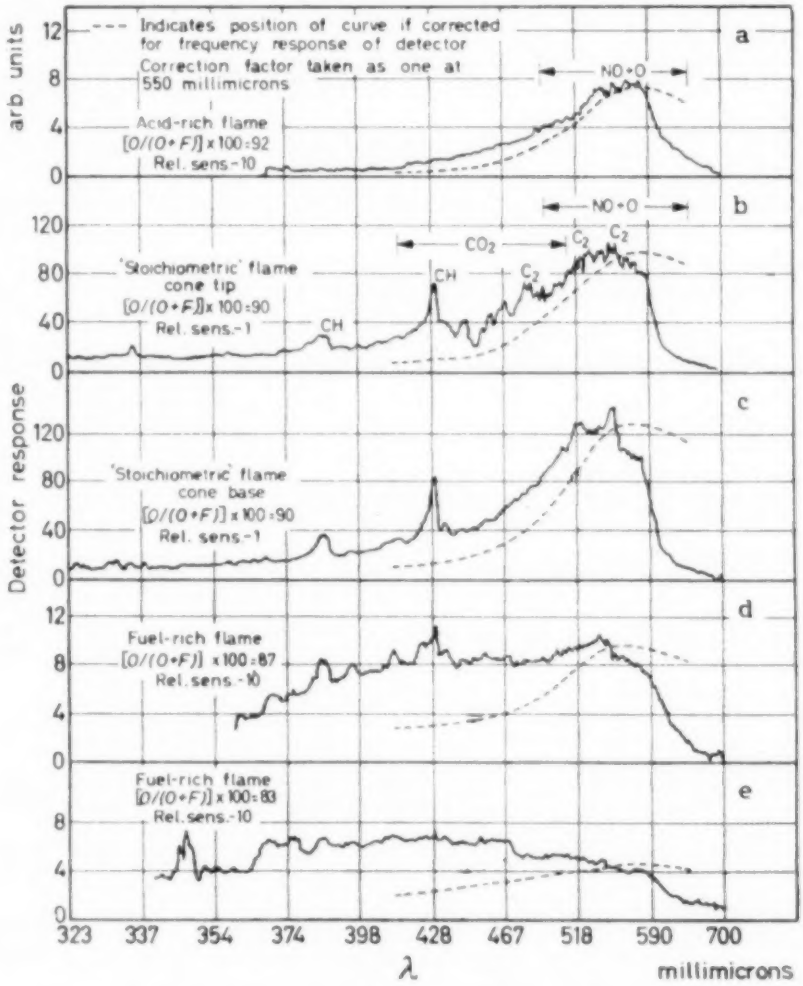
arb units
Detector response
Indicates position of curve if corrected for frequency response of detector
Correction factor taken as one at 550 millimicrons
Acid-rich flame [O/(O+F)] x 100=92 Rel. sens.=10
'Stoichiometric' flame cone tip [O/(O+F)] x 100=90 Rel. sens.=1
'Stoichiometric' flame cone base [O/(O+F)] x 100=90 Rel. sens.=1
Fuel-rich flame [O/(O+F)] x 100=87 Rel. sens.=10
Fuel-rich flame [O/(O+F)] x 100=83 Rel. sens.=10
NO+O
CO2
CH
C2
a
b
c
d
e
323 337 354 374 398 428 467 518 590 700
λ millimicrons

Figure 6. Emission spectra of propane–nitric acid supported flames

not a true indication of relative intensity. Corrected curves would take the general shape shown by the dotted line, with the peaks and valleys of the solid curve superimposed. It should also be noted that the intensity response of the spectrometer for curves (a), (d) and (e) is set for ten times that for curves (b) and (c). The rather considerable difference in intensity which is indicated for different unburnt gas mixture ratios is regarded as mainly due to differences in flame temperatures. This will be discussed more fully below.

Major interest in these curves centres about the nature of the orange emission observed primarily with acid-rich flames. Considering *Figure 6*(a), which is for $R = 92$, one sees that this consists of a continuum, peaking in the yellow and extending strongly into the red. The actual intensity at wavelengths longer than 630 mμ is not well known because of the low response of the detector beyond this point. Emission drops off rapidly from about 550 mμ toward shorter wavelengths and little or no typical hydrocarbon radiation is present.

As the acid concentration is reduced, the successive curves (b) to (e) of *Figure 6* are obtained with curves (b) and (c) both being for the stoichiometric mixture ratio as of reaction 3 but respectively from the tip and base of the bunsen cone. The flames are nitrogen shielded in all cases. One sees that considerable hydrocarbon radiation appears in these curves, with strong CH peaks at 430 and 386 mμ, C_2 peaks at 550, 518, and 480 mμ and what is probably some CO_2 emission in the region 520 to 446 mμ. However, this all appears to be superimposed upon the continuum shown in *Figure 6*(a), and no change occurs in the region between 600 and 700 mμ, where hydrocarbon radiation does not appear, except as to relative intensity. Since a distinct orange-blue colour separation appears in the primary reaction zone at this mixture ratio, it is believed that the hydrocarbon radiation originates at a different location in the flame than does the orange-yellow continuum. *Figure 6*(e) shows the emission curve for the most fuel-rich flame, and it is seen that although the radiation is weak and predominantly of a diffuse structure attributable to hydrocarbon flame bands, definite indications of the orange continuum remain. It is probably the radiation from this latter region which gives even these fuel-rich flames their distinctive magenta colour rather than the normal blue of hydrocarbon–oxygen flames. In many respects, the colour is suggestive of CN emission in the red. However, no indication of the typical CN bands appears in the region covered. A detailed examination of the region from 650 to 900 mμ would be desirable for clarification of this point.

A study of emission in the near infra-red from 900 to 3000 mμ has shown strong peaks attributable to water, together with some weaker structure. However, a detailed examination of this region has not been carried out.

DISCUSSION

Among the more interesting observations which have been made on acid-supported flames are those showing a close structural resemblance to

nitrogen dioxide-supported flames as reported by H. G. WOLFHARD and co-workers[7, 8, 17]. This structure, its dependence upon secondary air and seeming resemblance to a diffusion flame form together with the nearly stoichiometric evolution of nitric oxide from acid flames, all fit into a single coherent interpretation. The doublet reaction zone observed for nitrogen dioxide has been attributed to an initial decomposition of the nitrogen dioxide to produce oxygen and nitric oxide, followed by the combustion of these species with two different burning rates. Since the combustion of nitric oxide requires that it be preheated by the ignition source to a relatively high temperature, it could be said that the oxygen combustion initiates the combustion of nitric oxide which then occurs slightly downstream. One deduces that with acid flames the nitric oxide evolved from the first reaction zone burns as a result of ignition by the oxygen diffusion flame supported by ambient air. This accounts for both the structural resemblance to nitrogen dioxide flames and the diffusion flame shape.

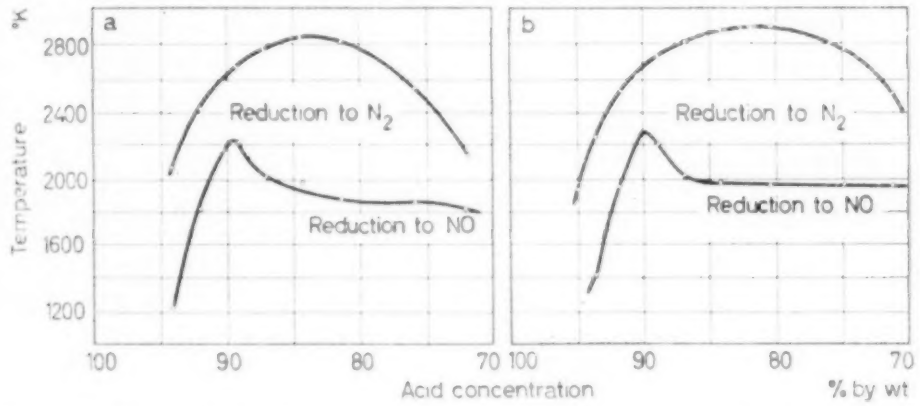

Figure 7. Theoretical temperatures of (a) *nitric acid–propane, and* (b) *red fuming nitric acid* ($HNO_3 + 15\% NO_2$)*–propane flames*

The question arises as to why the nitric oxide combustion step is not piloted by the initial phase of the nitric acid reaction. At the present time, this is uncertain. It may be that some species produced in the reaction of molecular oxygen, but not in its absence, is catalytic for the reduction of nitric oxide; i.e. that the ignition by the oxygen reaction is not strictly thermal. However, previous studies on the high ignition temperatures of nitric oxide-supported flames[7, 8, 17] indicate that the question might revolve around the temperature attained by the gases as a result of the initial phase of the nitric acid reaction.

In an attempt to provide some clarification of the situation, calculations were carried out for the theoretical flame temperatures of nitric acid–butane-supported flames for the two situations of reduction of the acid to nitric oxide and nitrogen, respectively. Results for white fuming nitric acid and red fuming nitric acid are shown in *Figure 7*. The significant point is the relation between the flame temperature for reduction of the acid to nitric oxide, and the ignition temperature for the subsequent reaction of the

nitric oxide. It will be noted from the curves that the maximum theoretical temperature for white fuming nitric acid reduced to nitric acid is 2225 K. For the small flames studied in this work, actual temperatures are probably lower by a few hundred degrees. Since temperatures as high as 1772 K have been observed[7] in nitrogen dioxide–hydrogen flames which fail to burn nitric oxide in the product gases, formation of nitric oxide in the present case is not inconsistent. That the temperature actually attained is close to that at which reduction of nitric oxide becomes rapid is, however, suggested by the close correlation between the mixture ratios of the lowest point of *Figure 5* and the maxima of *Figure 7*.

The reduction of nitric oxide, which has apparently been observed in nitrogen dioxide–hydrocarbon flames[7, 8, 17] can very likely be explained in terms of the fact that somewhat higher flame temperatures would be expected from the reaction

$$10NO_2(g) + C_3H_8(g) \rightarrow 10NO(g) + 3CO_2(g) + 4H_2O(g) \quad \ldots . [7]$$
$$\Delta H = -352 \text{ kcal}$$

than from the corresponding reaction with nitric acid ($\Delta H = -308$ kcal). The difference would be further increased by the approximately 5 per cent inert material (water, nitrogen) in the unburnt gas mixtures of the present study, as well as by any secondary effects of inhibition of the combustion process by the water.

Some interesting speculations concerning mechanisms of flame propagation can be based upon the foregoing temperature relationships. The values for flame speed shown in *Figure 4* are close to those reported for air–propane flames[9] and nitrogen dioxide–hydrocarbon flames[5]. Likewise, the theoretical flame temperatures shown in *Figure 7* for the reduction of acid to nitric oxide are quite close to the observed flame temperature for air–propane flames, and not greatly different from the theoretical temperatures expected for nitrogen dioxide flames. These facts suggest that flame propagation is facilitated by processes which are common to all of the three cases. That thermal transport may be involved is suggested by arguments, previously cited, that the initial reaction in nitrogen dioxide combustion is a thermal decomposition to nitric oxide and oxygen, and by arguments which will follow supporting the thesis that the initial reaction in nitric acid-supported combustion is also a thermal decomposition step. However, OH radical diffusion could also be important in the present case since it is capable of initiating attack on nitric acid in accordance with reaction 14 below. It is strongly suggested that with both nitrogen dioxide and nitric acid the only temperature gradient of significance to the transport of the combustion wave is that derived from oxidation processes which accompany initial steps leading to the formation of nitric oxide. Any heat release from the further reaction of nitric oxide lags too far behind to contribute materially to the transport process.

The primary steps by which nitric acid reacts with fuel in the combustion wave are believed to be the following:

$$HONO_2 \rightarrow HO + NO_2 \quad \ldots . [5]$$

$$NO_2 \rightarrow NO + O \quad \ldots.[9]$$

$$2NO_2 \rightarrow 2NO + O_2 \quad \ldots.[10]$$

$$NO_2 + C_3H_8 \rightarrow NO + \text{oxidation and nitration products} \quad \ldots.[11]$$

$$HO + C_3H_8 \rightarrow \text{Oxidation products and free radicals} \quad \ldots.[12]$$

$$O + C_3H_8 \rightarrow \text{Oxidation products and free radicals} \quad \ldots.[13]$$

$$HO + HNO_3 \rightarrow HOH + NO_3 \quad \ldots.[14]$$

$$NO_3 \rightarrow NO_2 + O \quad \ldots.[15]$$

Step 8 is fairly well documented. Studies on the thermal decomposition of nitric acid vapour at temperatures up to 600°C have shown that step 8 is the only initial reaction (other than surface reaction) which occurs[1, 18, 19]. Furthermore, extensive research over the past few years by Hass and co-workers on the vapour phase nitration of hydrocarbons by nitric acid in the region of 200°C has revealed that step 8 is the preliminary to all subsequent reaction processes. Although these temperature regions are considerably removed from flame conditions, it can be shown by simple kinetic reasoning that more complicated reactions should not become predominant at higher temperatures.

The evolution of nitric oxide from the primary combustion zone of the flame suggests either steps 9, 10 or 11. Step 11 is suggested by the work of P. Grey and A. D. Yoffe[20]. Evidence for steps 9 or 10, however, derives from the resemblance between acid flames and nitrogen dioxide flames, as has been discussed. In addition, the orange continuum shown in *Figures 6*(a) to *6*(e) appears to be identical to a continuum which has been observed in several instances where the reverse of reaction 9 is to be expected; i.e. where the simultaneous presence of nitric oxide and oxygen atoms is expected[21, 22]. Its intensity appears to be a direct function of the acid concentration and in a highly acid-rich mixture it is mainly responsible for the visible appearance of the flame. It is thus closely associated with acid decomposition, and reaction 9 is a possible source of oxygen atoms. However, a high temperature would be required in order for 9 to be significant with respect to the energetically much more favourable reaction[19]. A more acceptable source for oxygen atoms may be reactions 14 and 15. The species nitrogen trioxide is quite unstable and its decomposition, according to reaction 15, is reasonable under flame conditions. This interpretation also accounts for the sharp orange-blue colour separation in near-stoichiometric flames since reactions 14 and 15 would be expected to occur predominantly in the low temperature initial part of the combustion wave. They would be repressed at fuel-rich mixture ratios, however, by competition of the hydrocarbon for the O and OH radicals.

The blue reaction zone which follows the orange at stoichiometric mixture ratios is believed to represent a region in which decomposition of the acid is complete and oxidation of hydrocarbon is the primary process. This stage would be represented by reactions 11, 12 and 13 in which no attempt is made to designate a mechanism. The colour is presumably due to C_2 and CH radiation which is clearly shown in *Figures 6*(a) to *6*(e).

While the role of free radicals is not stressed in the above much simplified reaction scheme, it is clear that hydrocarbon radicals will be produced rather early in the combustion process by reaction 12 and may play an important part in the subsequent oxidation and nitration reactions. In particular, the nitrated products found in the analysis presumably result from reaction of nitrogen dioxide with such species. However, it is believed that these reactions are of less importance than the acid decomposition reactions in determining the unique character of nitric acid-supported flames.

This work was supported by the United States Air Force, Wright Air Development Center, under Contract AF 33(616)—329.

Rocketdyne Division,
North American Aviation Inc.,
Canoga Park, Calif.

(*Received November 1956*)

REFERENCES

[1] JOHNSTON, H. S., FOLRING, LOUISE and THOMPSON, R. *J. phys. Chem.* 57 (1953) 390
[2] WOLFROM, N. L. and KARABINOS, J. V. *J. Amer. chem. Soc.* 66 (1944) 909
[3] RICE, R. G., KELLER, G. J. and KIRCHNER, J. G. *Analyt. Chem.* 23 (1951) 194
[4] BOSE, P. K. *Analyst* 56 (1931) 504
[5] HASS, H. B. and RILEY, F. F. *Chem. Rev.* 32 (1943) 401
[6] SCOTT, E. W. and TREON, J. F. *Industr. Engng Chem. (Anal.)* 12 (1940) 189
[7] GAYDON, A. G. and WOLFHARD, H. G. *Flames, Their Structure, Radiation and Temperature* Chapman and Hall: London, 1953
[8] PARKER, W. G. and WOLFHARD, H. G. *Fourth Symposium (International) on Combustion* p. 420 Williams and Wilkins: Baltimore, 1953
[9] LEWIS, B. and VON ELBE, G. *Combustion, Flames and Explosions in Gases* Academic Press: New York, 1951
[10] BROMLEY, L. A. and WILKE, C. R. *Industr. Engng Chem. (Industr.)* 43 (1951) 1641
[11] PARTINGTON, J. R. *An Advanced Treatise on Physical Chemistry*, Vol. I. Longmans Grec.,: London, 1951
[12] WOHL, K. *Fourth Symposium (International) on Combustion* p. 82 Williams and Wilkins: Baltimore, 1953
[13] EDSE, R. *Studies on Burner Flames of Hydrogen Oxygen Mixtures at High Pressure. W.A.D.C. tech. Rep. No. 52-59*, Apr 1952
[14] GOUY, G. *Ann. Chim. (Phys.)* Ser. 5, 18 (1879) 27
[15] ECKE, E. *Physical Measurements in Gas Dynamics and Combustion* (Section K) Princeton University Press, 1954
[16] MUELLER, K. H. *J. Amer. chem. Soc.* 77 (1955) 3469
[17] WOLFHARD, H. G. and PARKER, W. G. *Fifth Symposium (International) on Combustion* Reinhold: New York, 1955
[18] JOHNSTON, H. S. *et al. J. Amer. chem. Soc.* 73 (1951) 2319, 4542 and 4782
[19] JOHNSTON, H. S., FOLRING, LOUISE and WHITE, J. R. *J. Amer. chem. Soc.* 77 (1955) 4208
[20] GREY, P. and YOFFE, A. D. *Chem. Rev.* 55 (1955) 1069
[21] GAYDON, A. G. *Spectroscopy and Combustion Theory* Chapman and Hall: London, 1948
[22] PEARSE, R. W. B. and GAYDON, A. G. *The Identification of Molecular Spectra* John Wiley: New York, 1950

Extraction of Ions from a Flame

J. DECKERS and A. VAN TIGGELEN

A complete study of ionization in flames involves solution of the problems: (1) identification of the ions (as yet nothing definite is known about their nature); (2) evaluation of the ion concentration (even now there is still some disagreement concerning the exact amount of ions in a flame); and (3) determination of the mechanism by which ions are formed in the flame. There seems to be no question about 'chemi-ionization'; not much, however, is known about the mechanism which can lead to ion formation. It is precisely in view of this that a new technique has been developed in the laboratory. It is based essentially on the extraction of the ions from the flame and their separation from the burnt gases. We have succeeded in producing the extracted ions in a vacuum of 10^{-5} mm of mercury and we hope to be able to identify them by a mass spectrometric method in a further development of our equipment. This paper describes the extraction apparatus and gives some indications concerning the concentration of the ions in a flame as measured by a completely new technique.

THE principle of a method of ion extraction has been published by L. VANREUSEL and J. M. DELFOSSE[1]; these authors kindly investigated the possibility of solving our extraction problem. Their extraction apparatus has now been completely adapted to the systematic investigation of the ionization in a flame as proposed above. The ions are extracted from the flame and brought into a high vacuum system where, after separation from the burnt gases, they can be accelerated and projected on to a narrow slit which can be used as the entrance slit of a mass spectrometer.

The data given below show how the identification of the ions will become a possibility in the near future. It is also possible to collect the ions as soon as they enter the extraction apparatus and, knowing the amounts of gases and collected ions, to calculate the ion concentration in the sample.

EXPERIMENTAL

Since a flame cannot be run at the very low working pressure (10^{-5} mm of mercury) of a mass spectrometer, a sample of the flame gases has to be expanded through a hole and behind the latter the burnt gases have to be pumped away while the ions are kept in a straight beam by means of an electrostatic field maintained by a system of electrodes. If the hole is too narrow most of the ions may lose their charge by collision with the walls, but if the hole is large enough no pumping installation would be sufficient to obtain a satisfactory vacuum. The equipment which we have built makes it possible to bring the ions from a flame burning at pressures from 3 to 10 cm of mercury into an intermediate region at 10^{-2} mm of mercury and from there into a vacuum of 10^{-5} mm of mercury. The passage in the intermediate region was made as short as possible in order to avoid a randomized redistribution of the initially nearly homogeneous ion velocities. *Figure 1* gives a schematic description of the apparatus. It consists of

three chambers: the combustion chamber I, the separation chamber II and the acceleration chamber III.

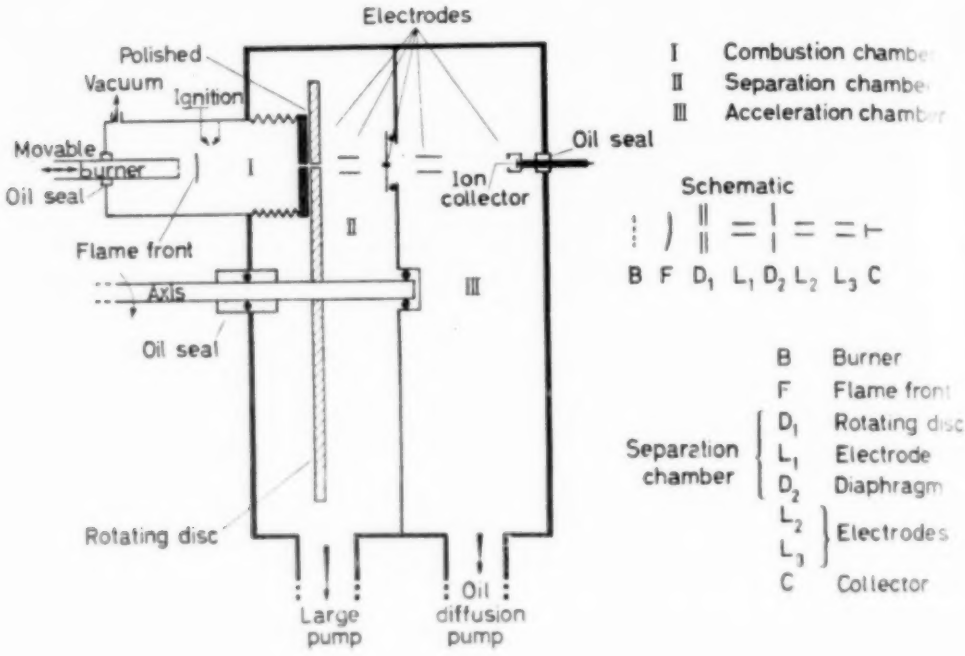

Figure 1. Schematic arrangement of apparatus

The Pyrex combustion chamber I (65 mm diameter) contains the burner; it is connected to a pump and has a side arm for the ignition system of the flame. The burner is a Pyrex tube (30 mm diameter) moving in the chamber through a 'simmer ring'. The polished 'lava' bottom of chamber I is pressed against the rotating disc by means of a flexible membrane. The separation chamber II is made of a steel cylinder (diameter 300 mm) closed by two steel plates with a rubber seal. A system of 'simmer ring' allows rotation of the disc while a vacuum of 10^{-2} mm of mercury is maintained in this chamber. Single holes in the lava bottom and in the rotating disc are 2 mm in diameter and at a distance of 70 mm from the central axis; the communication between I and II lasts 1/220 of a second, since the revolution speed is 6 rev/s. The communication between chambers II and III consists of a hole (of 2 mm diameter) in a copper plate, supported for insulation by Plexiglas and fitted with a rubber seal. A vacuum of 10^{-4} mm of mercury is obtained in the acceleration chamber by means of an oil diffusion pump. Behind this hole a mean current is measured by collecting the ions on a collector protected by an earthed shield. This collector is movable and allows measurement of the dispersion of the ion beam. As shown in *Figure 2* the disc and the insulated copper plate are used as electrodes and other electrodes are located in chambers II and III in order to keep the ions in a beam and to obtain a much greater mean ionic current strength. The electrostatic field was created by maintaining the various electrodes at a well defined electrostatic potential. The distribution

of that field had to be carefully checked since discharges between the lenses could occur in certain conditions.

Therefore a special feeding and control device was needed and is illustrated schematically in *Figure 2*. A brief description of it follows.

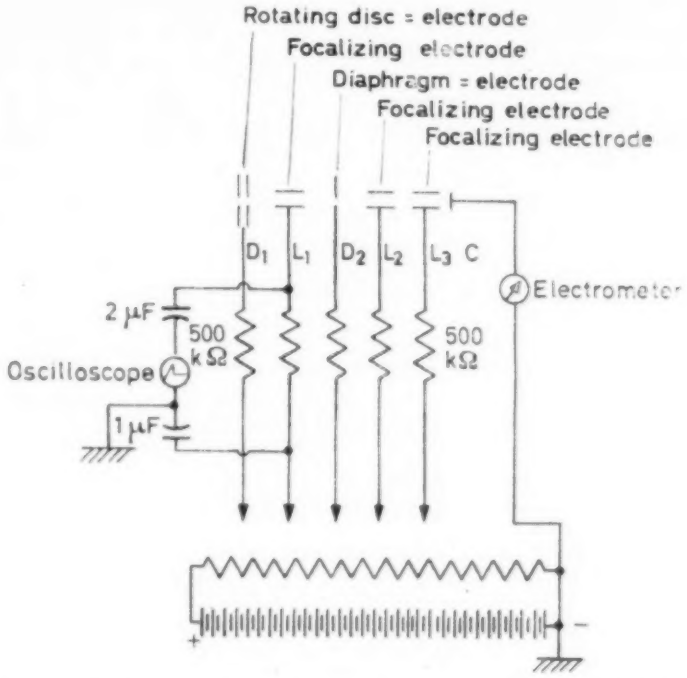

Figure 2. Electrode train and scheme for maintaining potential gradient along ionic beam

Each electrode is connected to a chosen output of the feeder potentiometer by means of a resistor of 500 kΩ. By varying the outputs connected to the electrodes it is possible to adjust the field distribution in order to have the most intense ionic current under safe operating conditions.

The terminals of the 500 kΩ resistors can be connected to an oscilloscope after suppression of the d.c. components by means of 2 μF condensers; any fluctuation of the potential on an electrode produces a voltage drop on the terminals of the connecting resistor and deflects the electronic beam of the oscilloscope.

Measurement of the ionic current, after acceleration of the ions, is done by drawing them to a collector. The time integrated mean ionic current is measured by means of a valve electrometer.

RESULTS

When a brass plate is placed directly behind the rotating disc, all ions entering the first chamber are collected and the value of the voltage drop on the connecting resistor ($r = 10^5\ \Omega$) can be measured on the oscilloscope through large condensers. The signal on the screen is the first derivative of the voltage drop as a function of time; this signal is approximately a triangular peak for the following reasons.

(*1*) The overlap of two identical circles, which are moving uniformly along the line joining their centres is a linear function of time with an approximation which is far better than the precision of our measurements.

(*2*) As is shown below, no critical orifice flow is observed: the flow is proportional to the pressure difference. Therefore Poiseuille's law is obeyed and the amount of ions passing in unit time through the hole is proportional to the square of its uncovered section.

(*3*) The addition of the large d.c. blocking capacitor does not have a time delay effect because of the very low capacity of the oscilloscope.

The base of the triangular signal is equal to the total opening duration (1/1300 sec) and its height (ΔV_{max}) to the first derivative of the voltage drop. Graphical integration leads to

$$\tfrac{1}{2}\Delta V_{max} = V_{mean}$$

Using Ohm's law

$$V_{mean} = rI_{mean}$$

I_{mean}, being the mean current intensity during one opening, is evidently proportional to the mean amount of ions (N_+') collected in unit time on the collector while connection is established. So we can write

$$\tfrac{1}{2}\Delta V_{max} = rI_{mean} = \varepsilon r N_+'$$

where ε = absolute value of the electron charge in coulombs. The total number of ions which are collected in one second is equal to $N^+ = ftN_+'$ where t = duration of one opening (1/1300 sec), and f = rotation frequency (6 rev/s).

Therefore

$$N^+ = \tfrac{1}{2}\Delta V_{max}\, tf/r\varepsilon$$

Introducing numerical values

$$N^+ = \Delta V_{max} \times 2{\cdot}9 \times 10^{19}$$

The total amount of gas per second entering chamber II can be calculated experimentally from the time which is necessary to reduce the pressure in the combustion chamber to a known fraction of its initial value while the disc is rotating and all other connections are kept closed. The total volume of combustion chamber I is equal to 975 cm³.

It has been found that at room temperature ($T = 293$ K) the time t needed for reducing the initial pressure p_0 to half its value in chamber I is independent of pressure and equal to 350 seconds. This proves that Poiseuille's law still holds; according to this and since pressure in chamber II is very small (10^{-3} mm of mercury) compared with the pressure p in chamber I, we have

$$-\mathrm{d}p/\mathrm{d}t = k_\eta p/T^{1/2}$$

The denominator on the right takes into account the fact that the viscosity of gases, appearing in Poiseuille's law, is proportional to the square root of the absolute temperature of the gases in chamber I. Integration gives

$$p = p_0 \exp(-k_\eta t/T^{1/2})$$

In particular

$$p/p_0 = 0{\cdot}5 = \exp(-k_\eta \cdot 350/T^{1/2})$$

This relation allows the calculation of the constant, $k_0 = 3{\cdot}38 \times 10^{-2}$. The number of molecules $\mathcal{N}$ entering chamber II per second, for any pressure p and temperature T in combustion chamber I, is now given by

$$\mathcal{N} = \frac{VN(\Delta p)/\text{sec}}{RT} = \frac{VNk_0 p}{RT^{3/2}}$$

where N = Avogadro's number $= 6{\cdot}06 \times 10^{23}$
R = gas constant $= 6{\cdot}24 \times 10^{4}$ (in cm^3, mm Hg)
V = volume of combustion chamber I $= 975$ cm^3
p = pressure in combustion chamber I (in mm Hg)
$k_0 = 3{\cdot}38 \times 10^{-2}$.

Finally we obtain

$$\mathcal{N} = (3{\cdot}2\, p/T^{3/2})10^{20}$$

The mole ratio of ions to the total amount of molecules in the sample will now be given by $N^+/\mathcal{N}$.

Some difficulty arises in the exact evaluation of the temperature T: the gases are probably cooling down a little during their passage through the periodically opened hole. However, in the examples given below, we have supposed that T is still practically equal to that of the flame T_f. Taking as an example of a stoichiometric flame the mixture ethylene–oxygen–nitrogen containing 60 per cent nitrogen: $T_f = 2570$ °K (as measured at atmospheric pressure); $\Delta V_{max} = 0{\cdot}12\,V$; $p = 52$ mm of mercury; V_0 (flame velocity) $= 182$ cm/s. Calculations give now:

$$N^+ = 3{\cdot}33 \times 10^{9} \qquad \mathcal{N} = 1{\cdot}28 \times 10^{17}$$

$$N^+/\mathcal{N} = 2{\cdot}61 \times 10^{-8}$$

The number of ions per cm^3 is equal to

$$\frac{N^+ \times 6{\cdot}06 \times 10^{23} \times 52 \times 273}{\mathcal{N} \times 2{\cdot}24 \times 10^{4} \times 760 \times 2570} = 0{\cdot}51 \times 10^{10}$$

This order of magnitude can be compared to some recent data[2] obtained by a different technique on flames burning at atmospheric pressure.

It should be kept in mind that the concentration which is calculated here corresponds to a flame which is burning as near as possible without extinction to the hole in the bottom of the burning chamber.

In *Table 1* some relative values of ion concentrations are given for a stoichiometric ethylene–oxygen flame at different degrees of dilution with nitrogen.

Table 1. Relative values of ion concentrations measured with stoichiometric ethylene–oxygen flame at different degrees of dilution with nitrogen

Nitrogen present %	*Flame velocity* V_0 cm/s	T_f °K *(At atmos. pressure)*	$N_+/\mathcal{N}$ *ions/cm^3 (arb. units*)*
60	182	2570	1·00
65	140	2450	0·83
70	100	2325	0·69
75	60	2150	0·53

*One arbitrary unit for $(N_+/\mathcal{N})$ corresponds approximately to $0{\cdot}5 \times 10^{10}$ ions/cm^3.

A few experiments have been made on a flame which could be expected to have a very low ion concentration: because of our equipment we needed a coloured flame and this is the reason why we chose the nitrous oxide–oxygen flame instead of the hydrogen–oxygen flame.

The sensitivity of our equipment was not sufficient to measure the ion concentration in this case but the real value certainly does not exceed 10^9 ions/cm^3; it most probably reaches the order of magnitude of 10^8 for a stoichiometric flame of nitrous oxide–hydrogen with 35 per cent nitrogen.

The authors express their thanks to the European Office of the Air Research and Development Command which has sponsored in part this research under Contract No. AF61(514)–1099 and also to the Fonds National de la Recherche Scientifique for financial support.

Laboratory of Inorganic Chemistry,
University of Louvain

(Received January 1957)

REFERENCES

[1] VANREUSEL, L. and DELFOSSE, J. M. *Ann. Soc. sci. Brux.* 70 (1956) 67
[2] CALCOTE, H. F. and KING, I. R. *Fifth Symposium (International) on Combustion* p. 423 Reinhold: New York, 1955

I. Predicting the Laminar Flame Speed in Gases with Temperature-explicit Reaction Rates

D. B. SPALDING

The rates of (a) *single-step reactions,* (*b*) *reactions satisfying the steady-state approximation,* (c) *'explosive' chain reactions, may be expressed as explicit functions of temperature, if the diffusion coefficients of reactants and heat are equal. The paper provides a simple method of predicting the laminar burning velocities in gaseous mixtures exhibiting these reactions. Examination of exact solutions shows that burning velocity can be calculated with 1 per cent accuracy by:*

(i) *Plotting a curve of R versus* τ,

$$\text{where } R \equiv \frac{\text{conductivity} \times \text{volumetric energy release rate}}{\text{the conductivity of the unburnt gas, } k_u \quad \text{temperature rise}}$$

$$\text{and } \tau \equiv \frac{}{\text{maximum temperature rise, } T_b - T_u}$$

(ii) *Evaluating area beneath the curve,* $\overline{R}$

(iii) *Evaluating horizontal position,* τ_c, *of centroid of area beneath R curve*

(iv) *Evaluating* λ, *from* $\lambda = 0{\cdot}5 - 0{\cdot}6604\,(1-\tau_c) - 0{\cdot}4283\,(1-\tau_c)^2$

(v) *Evaluating burning velocity* v_f, *from* $v_f = [k_u \overline{R} / \lambda (T_b - T_u) c^2 \rho^2_u]^{\frac{1}{2}}$ *where* ρ_u = *density of unburnt gas, and* c = *mean specific heat at constant pressure.*

Graphs are given which lead to the burning velocity when the diffusion coefficients of reactant or radical are not normal.

In calculating laminar flame velocities, it frequently occurs that the local rate of reaction per unit volume can be expressed as a function of local temperature, before the main calculation begins. Cases in which the reaction rate functions are explicit in this way are: (*i*) the single-step reaction, (*ii*) chain reactions obeying the steady-state approximation, (*iii*) simple chain-branching reactions. It is necessary that the diffusion coefficients of all components should be 'normal'*, and that the flames should be adiabatic.

Several methods exist by which the differential equations governing the flame can be solved. The present paper, however, is intended to enable flame velocities to be calculated without the necessity of solving a differential equation. The method is accurate to well within 1 per cent in most cases, and relies on a property of the flame equations discovered by examination of numerous exact solutions.

Although diffusion coefficients in flames are not accurately known, so that the assumption of 'normality' usually suffices, it is important to estimate

* I.e. equal to each other and to the thermal diffusivity. See below: 'Calculation of flame speed for non-normal reactant, and radical, diffusion'.

the effect of departures from normality on the flame velocity. This is made possible for a wide range of parameters by graphs presented below, which are valid for cases (*i*), (*ii*) and (*iii*) above, on the condition that the reaction rate is linear in temperature close to the hot boundary.

The present paper merely describes how to use the method, the theory being given in an accompanying paper referred to as II. First the evaluation of the reaction rate function with normal diffusion constants is discussed. It is then shown how the area and the centroid position of this curve can be used to give the flame velocity. The accuracy of the method, and its indebtedness to other work, are discussed in II.

EVALUATION OF REACTION RATE FUNCTION

An inescapable preliminary to the calculation of flame speed is the evaluation, from knowledge or assumptions about the reaction kinetics of the flame, of the dependence of volumetric reaction rate on temperature and gas composition. This is now discussed for the particular cases in which reaction rate can be shown to depend on temperature alone.

The single-step reaction

Suppose that the flame is dominated by a reaction comprising a single step, e.g. A + B→C. Then if attention is focused on one of the reactants, A, reaction kinetic assumptions make it possible to write the volumetric reaction rate at a point in the flame as

$$\dot{m}_A''' = f(z, \beta, T) \qquad \ldots [1]$$

where

$\dot{m}_A'''$ = mass of A being consumed per unit volume and time (g/cm^3 sec)

$z = \dfrac{\text{mass of A per unit mass of local mixture}}{\text{(mass of A per unit mass of mixture in unburnt material)}}$ (dimensionless)

$\beta = \dfrac{\text{mass of B per unit mass of local mixture}}{r\,\text{(mass of A per unit mass of mixture in unburnt material)}}$ (dimensionless)

T = local absolute temperature (°K)

r = mass of B combining chemically with unit mass of A.

Common possibilities for equation 1 are:

Monomolecular reaction: $\dot{m}_A''' = Z_1 z \rho \exp(-E_1/RT)$ ....[2]

Bimolecular reaction: $\dot{m}_A''' = Z_2 z \beta \rho^2 \exp(-E_2/RT)$ ....[3]

where

ρ = local gas density (g/cm^3)

Z_1 = a constant of the monomolecular reaction (sec^{-1})

E_1 = a constant of the monomolecular reaction (cal/mole)

Z_2 = a constant of the bimolecular reaction (cm^3/g sec)

E_2 = a constant of the bimolecular reaction (cal/mole)

R = universal gas constant (1·985 cal/mole °K).

In equations 2 and 3, the gas density depends on T and perhaps on z and β, while in some cases it may be considered worthwhile to take

account of the variation of Z with temperature. These matters are the province of reaction kinetics and will not be further discussed here.

Energy conservation—It is shown in II that, with normal values of the diffusion constants and an adiabatic flame, z is related to T by energy conservation. The relation is

$$zm_{A_u}H + cT = \text{const.}$$
$$= m_{A_u}H + cT_u \qquad \ldots . [4]$$

where m_j = mass of component j in unit mass of mixture
H = heat of reaction of A at standard temperature (cal/g), and
c = specific heat at constant pressure (cal/g °C).
suffix A refers to the main reactant
suffix u refers to the unburnt state far upstream.

It is usually sufficiently accurate to treat c as a constant given by

$$c = m_{A_u}H/(T_b - T_u) \qquad \ldots . [5]$$

where suffix b refers to the burnt gas, in which it is assumed that the A concentration is zero. In this case equation 4 leads to

$$z = 1 - (T - T_u)/(T_b - T_u)$$
$$= 1 - \tau, \quad \text{say} \qquad \ldots . [6]$$

which defines the dimensionless temperature rise τ, sometimes called the reactedness. Clearly τ is zero in the unburnt gas and unity in the burnt gas.

Mass conservation—It remains to relate the concentration β of the second reactant, if present, to temperature. This is done by way of the stoichiometric relation. If the reaction is

$$1\text{g A} + r\text{g B} \rightarrow (1 + r)\text{g products}$$

then, provided that A and B have equal diffusion coefficients, it is shown in II that

$$z - \beta = 1 - \beta_u \qquad \ldots . [7]$$

Equations 6 and 7 can be used to relate β to τ.

Reaction rate—Since now both reactant concentrations can be expressed in terms of temperature, the volumetric reaction rate of equation 1 can be written as

$$\dot{m}_A''' = f(\tau) \qquad \ldots . [8]$$

where the function $f(\tau)$ depends on the chemical constants of the reaction, the thermodynamic constants of the reactants, and the composition and temperature of the unburnt gas.

The reaction rate function—In the theory of the one-dimensional laminar flame we need, not $\dot{m}_A'''$ directly, but this quantity multiplied by the local thermal conductivity k of the gas. It is therefore convenient to introduce a function R, defined by

$$R = (k/k_u) H \dot{m}_A''' \qquad \ldots [9]$$

This has the units of cal/cm³ sec.

The thermal conductivity of a gas depends on its temperature and composition in a way that can be estimated with some precision. It is therefore possible to express (k/k_u) as a function of the reactedness τ. Combination with equations 8 and 9 therefore leads to

$$R = R(\tau) \qquad \ldots [10]$$

where $R(\tau)$ is a function which can be evaluated from the reaction kinetic, thermodynamic, stoichiometric, transport property, and initial data of the problem.

Evaluation of $R(\tau)$, which will be termed the reaction rate function, usually leads to a graph of the form indicated in *Figure 1*. The shape near

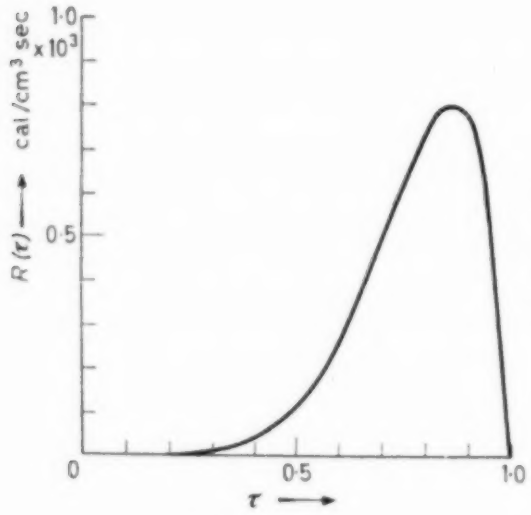

Figure 1. Typical relation of volumetric reaction rate to dimensionless temperature: monomolecular reaction, or reaction with excess of one reactant

the upper temperature limit $\tau = 1$ is typical of monomolecular reactions; bimolecular reactions may have a horizontal tangent at that point. Always, however, $R = 0$ at $\tau = 0$* and $\tau = 1$, and usually R only has appreciable values at the higher τ values.

Chain reactions obeying the 'steady-state approximation'

T. VON KÁRMÁN and S. PENNER[1] have introduced the idea that flames involving complex chain reactions can be treated as single-step flames if the local radical concentration is determined only by opposed production and destruction reactions. Although this assumption is invalid when the

*Strictly speaking R is merely very small at $\tau = 0$. This is not practically significant.

radical destruction rate is low[2], J. C. GIDDINGS and J. O. HIRSCHFELDER[3] have shown that, under some circumstances, this 'steady-state approximation' can give very good results. We now discuss how it may be used to yield a temperature-explicit reaction rate function.

Consider the reaction scheme

$$A \rightarrow 2C \qquad \text{radical-generating} \qquad \ldots.[11]$$

$$A + C \rightarrow sC + D \qquad \text{chain reaction} \qquad \ldots.[12]$$

$$tC \rightarrow D \qquad \text{chain-breaking} \qquad \ldots.[13]$$

Here A is the original reactant, C is an intermediate radical, and D is the product of combustion.

The mass rate of destruction of radical C per unit time and volume is given by

$$\dot{m}_c''' = Z_b \gamma^t \rho^t f_b(T) - Z_g z \rho f_g(T) - (s-1) z \gamma \rho^2 Z_c f_c(T) \qquad \ldots.[14]$$

where γ is the dimensionless radical concentration, suffixes b, g and c stand for the breaking, generating and chain reactions respectively, and the Z's and f's are properties of the reactions.

In general $\dot{m}_c'''$ is equal to the sum of the rates of diffusion and convection of radicals into the element of volume, but these rates become very small if the breaking reaction is fast enough to keep the radical concentration low. The steady-state approximation neglects the diffusion and convection terms, putting $\dot{m}_c''' = 0$. This enables equation 14 to be solved for γ, as for example:

$$t = 1 : \gamma = \frac{Z_g f_g z}{Z_b f_b - (s-1) z \rho Z_c f_c} \qquad \ldots.[15]$$

$$t = 2,\ s > 1 : \gamma = \frac{(s-1) Z_c f_c z}{Z_b f_b} \quad \begin{pmatrix} \text{if generation} \\ \text{term negligible} \end{pmatrix} \qquad \ldots.[16]$$

These equations, together with the earlier discussion concerning z, show that γ can be expressed by the steady-state approximation as a function of temperature alone. In general the energy equation must be modified to account for the presence of β. Now the rate of consumption of A per unit volume depends only on z, γ and T

$$\dot{m}_A''' = Z_g z \rho f_g(T) + (M_A / M_C) z \gamma \rho^2 Z_c f_c(T) \qquad \ldots.[17]$$

where M_A / M_C = molecular weight ratio, A : C. Substituting the appropriate functions of T for z and γ, we obtain once more

$$\dot{m}_A''' = f(\tau) \qquad \ldots.[18]$$

as for single-step reactions.

Examination of equation 15 indicates that if $s > 1$ (branching chain reaction) there is the possibility of γ becoming infinite or negative when the second term of the denominator is large. This occurrence means that the steady-state approximation has ceased to be valid (γ no longer small) and the method of the present section breaks down. Nevertheless, as

has been pointed out[2], it is still possible to reduce the problem approximately to that of a single-step flame; this will be dicussed in the next section.

'Explosive' chain-branching reactions

When $s=2$, for example, and the temperature level of the flame is such that the chain reaction is very fast compared both with the radical-generating and the chain-breaking reactions, very nearly one molecule of C is produced for each molecule of A which disappears. A simple material balance therefore leads to

$$\alpha+\gamma=1 \qquad \ldots.[19]$$

where γ is suitably defined.

If the reactant diffusion coefficients are once more assumed equal to the thermal diffusivity, the constant enthalpy condition applies. It follows that

$$\alpha H_A+\gamma H_C+cT=\text{const.} \qquad \ldots.[20]$$

where H_A and H_C are the negative heats of formation of A and C to a base of products at absolute zero.

As before the volumetric combustion rate of the main reactant depends on the local values of α, γ and τ in a way determined by the reaction kinetic constants. But equations 19 and 20 enable α and γ to be expressed in terms of τ. For this reaction scheme also, therefore, a function $R(\tau)$ can be determined purely from reaction kinetic and thermodynamic data.

DETERMINATION OF FLAME SPEED

Having determined the reaction rate function the next step is normally to solve a differential equation. There are numerous ways of doing this, exactly or approximately. In the present method, however, this step is avoided.

Dimensionless reaction rate: the eigenvalue λ

Given $R(\tau)$, the average value of R, $\overline{R}$, is easily evaluated from the quadrature

$$\overline{R}=\int_0^1 R(\tau)\,\mathrm{d}\tau \qquad \ldots.[21]$$

It is shown in II that the flame velocity v_f, measured relative to the unburnt gas, is given by

$$v_f=\left[\frac{1}{\lambda}\frac{k_u\overline{R}}{(T_b-T_u)c^2\rho_u{}^2}\right]^{\frac{1}{2}} \qquad \ldots.[22]$$

where ρ_u is the density of the unburnt gas, and λ is a constant. Formulation of the problem in this way ensures that λ, the so-called eigenvalue, is always somewhat less than $\frac{1}{2}$. The determination of its exact magnitude is the main problem in solving the flame equations.

Determination of λ: the centroid rule

In II it is shown that, for normal diffusion, the value of λ can be determined within about 1 per cent accuracy from the formula

$$\lambda=\tfrac{1}{2}-0{\cdot}6604\,(1-\tau_c)-0{\cdot}4283\,(1-\tau_c)^2 \qquad \ldots.[23]$$

where τ_e is the value of τ corresponding to the centroid of the area beneath the reaction rate function, and thus is defined by

$$\tau_e = \int_0^1 \tau R \, d\tau / \overline{R} \qquad \ldots . [24]$$

Given R, τ_e is easily evaluated by quadrature or other means.

The centroid rule of formula 23 is valid for $0{\cdot}6 \leqslant \tau_e \leqslant 1$ which covers most practical cases.

Calculation of flame speed with normal diffusion

The procedure for calculating the flame speed of a mixture thus becomes: (*i*) from reaction kinetic and other data establish the reaction rate function $R(\tau)$; (*ii*) hence evaluate $\overline{R}$ and τ_e by quadrature; (*iii*) evaluate formula 23 to get λ; and (*iv*) substitute λ in equation 22 and evaluate v_l.

Calculation of flame speed for non-normal reactant diffusion

If δ_A is defined as $D_A \rho c / k$ where D_A is the diffusion coefficient of the main reactant A, the 'normal diffusion' case is characterized by $\delta_A = 1$. If A is a very light molecule, however, δ_A may be greater than unity (about 3·3 for hydrogen in air); if A is a heavy molecule, δ_A will be less than unity (about 0·49 for propane in air).

The diffusion parameter δ_A affects the eigenvalue and therefore the flame speed also. Provided that the reaction rate function is linear in temperature close to the hot boundary, λ now must be obtained from *Figure 2* instead of from equation 23. The determination of $\overline{R}$ and τ_e is not changed, however. The asterisk on τ_e indicates this.

Inspection of *Figure 2* shows that when $\tau_e{}^\star$ is close to 1 (reactions with steep temperature dependence), the effect of δ_A is greatest. For this case $\lambda = \frac{1}{2}\delta_A$. A large δ_A increases λ, and so decreases the flame velocity.

Figure 2 has been constructed by approximations disclosed in II. The inaccuracy is not, however, serious in view of the uncertainty attaching to diffusion data. *Figure 2* is valid for reactions in which A is the sole reactant or in which the other reactant is in excess. It is not valid for stoichiometric bimolecular reactions, for which a suitable approximation procedure has not so far been derived.

Calculation of flame speed for non-normal radical diffusion

Radicals take no part in single-step reactions. In reactions for which the steady-state assumption is valid, radicals are present but their diffusion coefficients are by hypothesis without influence on the flame velocity. Explosive chain-branching reactions on the other hand are influenced by radical diffusion. Defining δ_c as $D_c \rho c / k$, where D_c is the radical diffusion coefficient, λ may be found as a function of $\tau_e{}^\star$ and δ_c in *Figure 3*, which is to be used instead of equation 23 when $\delta_c \neq 1$. Once again the asterisk superscribed on τ_e indicates that the $\delta_c = 1$ value is to be used.

Inspection of *Figure 3* shows that an increase in δ_c above unity increases the flame speed, though the effect is limited. Very small values of δ_c,

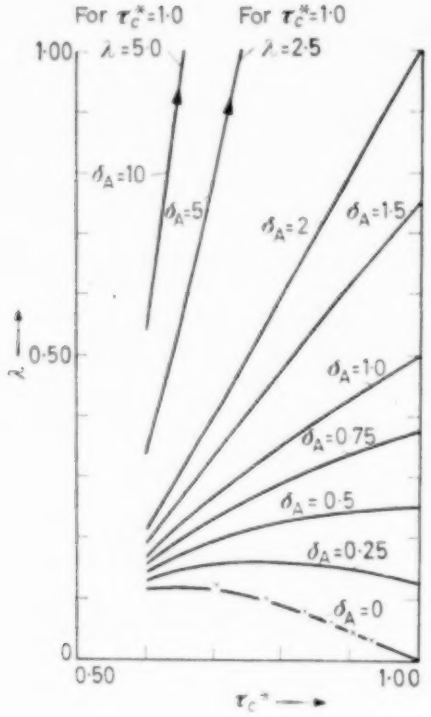

Figure 2. Effect of reactant diffusion parameter δ_A *on the eigenvalue* $\lambda[\propto 1/(\textit{flame speed})^2]$*; monomolecular reactions, or bimolecular reactions with excess of the other reactant. × signifies exact calculation of* R. FRIEDMAN *and* E. BURKEY[4]

however, can greatly decrease the flame speed. Since radicals are of low molecular weight, the values of δ_C greater than unity are of chief practical interest. II discloses how *Figure 3* has been prepared.

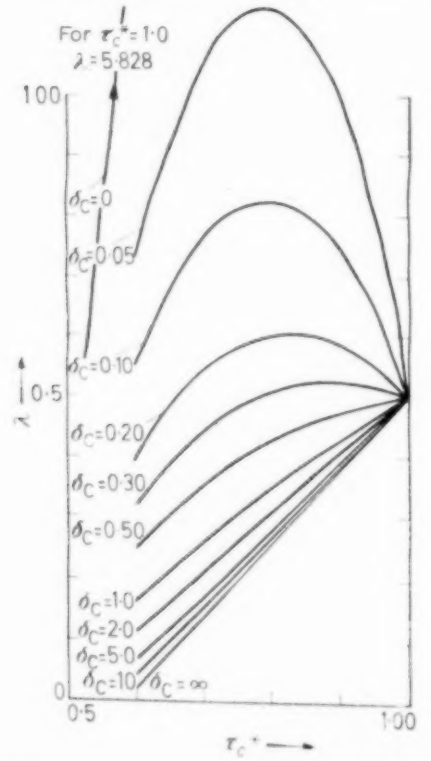

Figure 3. Effect of radical diffusion parameter δ_C *on eigenvalue* λ

DISCUSSION

Accuracy of flame speed predictions

It has been stated that the main difficulty in one-dimensional flame theory is the determination of λ, which is always in the neighbourhood of $\frac{1}{2}$. For normal diffusion the whole practical range of λ's is between $\frac{1}{2}$ and $\frac{1}{6}$. This corresponds to only a 1·73 : 1 range of flame speed.

The approximate theory of Y. B. ZELDOVICH and D. A. FRANK-KAMENETSKY[5], as quoted by N. N. SEMENOV[6], simply assumes that $\lambda = \frac{1}{2}$. In a typical case this causes a 25 per cent underestimate of the flame speed. It may be thought illuminating that, on the one hand, much effort has been expended to develop methods which reduce the error to, say, 10 per cent, whereas on the other hand the uncertainties in experimental reaction kinetic, transport, and even flame speed data are usually of a higher order.

Effect of flame temperature on flame speed

The variation of flame speed with burnt gas temperature is often required, both in prediction and in interpretation of experiments. Examination of equation 22 shows that v_f may be influenced by T_b directly, via $\bar{R}$, or via λ. Of these the second is usually overwhelmingly more important, for $(T_b - T_u)$ changes little in practical problems while λ depends only on τ_c which is also insensitive to T_b. With particular assumptions for R, it is often possible to obtain analytical relationships between v_f and T_b.

Department of Mechanical Engineering,
Imperial College of Science and Technology

(*Received March 1957*)

REFERENCES

[1] VON KÁRMÁN, T. and PENNER, S. *Selected Combustion Problems, p* 5. Butterworths: London, 1954
[2] SPALDING, D. B. *Phil. Trans. A* 249 (1956) 1
[3] GIDDINGS, J. C. and HIRSCHFELDER, J. O. *Rep. Nos. SQUID 5 and 6.* University of Wisconsin, 1956
[4] FRIEDMAN, R. and BURKE, E. *J. chem. Phys.* 25 (1953) 710
[5] ZELDOVICH, Y. B. and FRANK-KAMENETSKY, D. A. *Zh. fiz. Khim., Mosk.* 12 (1938) 100
[6] SEMENOV, N. N. *Tech. Memor. Nat. Adv. Comm. Aero., Wash, No. 1026,* 1942

II. One-dimensional Laminar Flame Theory for Temperature-explicit Reaction Rates

D. B. SPALDING

Several exact solutions are given for flames with normal diffusion and with reaction rate explicit in temperature. It is shown that, when the eigenvalue is defined in terms of the temperature-mean reaction rate, its value depends only on the position of the centroid of the reaction rate function. Various approximate theories are reviewed and it is shown that they may be arranged in order of merit: Wilde (best), Adams, Kármán-Penner, Zeldovich-Frank-Kamenetsky, Corner. The Wilde approximate method is developed to provide general relations for the effect of reactant and radical diffusion coefficients on the flame velocity. The few checks possible show good agreement with exact solutions. No theory has been developed for diffusion with bimolecular reactions in stoichiometric mixtures.

THIS paper provides the theory for the foregoing one which will be referred to as I. First the equations are set up and results concerning normal diffusion are obtained. Then the equations are put in non-dimensional first-order form, exact solutions are given for various cases of normal diffusion, and the relation of the eigenvalue to the centroid of the reaction rate curve is noted. Finally the effects of the reactant and radical diffusion coefficients are examined for the reaction schemes which have reaction rate falling linearly to zero as the temperature approaches its maximum value.

The fundamental equations have of course been derived previously by many authors (e.g. J. O. HIRSCHFELDER and C. F. CURTISS[1]). They are given here for easy reference and for consistency of notation. The numerical method of solution adopted for some of the flames is due to G. KLEIN[2], and the whole paper is written in the light of work done by the Wisconsin school. Other borrowings will be noted as they are made. The author is not aware that the centroid rule or the general results relating the eigenvalue to the diffusion parameters have been established before. The theory of 'explosive' chain-branching reactions is also believed to be novel, as are the various analytical solutions.

EQUATIONS

We consider a one-dimensional, steady, laminar, adiabatic flow at constant pressure (negligible kinetic energy). Dealing first with the single-step reaction, the conservation equations run:

Energy:

$$\frac{\mathrm{d}}{\mathrm{d}x}\left(k\frac{\mathrm{d}T}{\mathrm{d}x}\right)+H\frac{\mathrm{d}}{\mathrm{d}x}\left(D_{sp}\frac{\mathrm{d}m_s}{\mathrm{d}x}\right)+\frac{\mathrm{d}}{\mathrm{d}x}\left(T\sum_j c_j D_{jp}\frac{\mathrm{d}m_j}{\mathrm{d}x}\right)-G\frac{\mathrm{d}}{\mathrm{d}x}\left(T\sum_j c_j m_j+m_s H\right)=0 \qquad \ldots\ldots[1]$$

A: $$\frac{\mathrm{d}}{\mathrm{d}x}\left(D_{\mathrm{A}}\rho\frac{\mathrm{d}m_{\mathrm{A}}}{\mathrm{d}x}\right)-G\frac{\mathrm{d}m_{\mathrm{A}}}{\mathrm{d}x}=\dot{m}_{\mathrm{A}}''' \qquad \ldots.[2]$$

and, if a second reactant B is present,

B: $$\frac{\mathrm{d}}{\mathrm{d}x}\left(D_{\mathrm{B}}\rho\frac{\mathrm{d}m_{\mathrm{B}}}{\mathrm{d}x}\right)-G\frac{\mathrm{d}m_{\mathrm{B}}}{\mathrm{d}x}=r\dot{m}_{\mathrm{A}}''' \qquad \ldots.[3]$$

where x = distance in stream direction (cm)
k = local thermal conductivity (cal/cm sec °C)
T = absolute temperature (°K)
G = mass flow rate per unit area (g/cm² sec)
c_j = mean specific heat at constant pressure of component j over temperature range from T to base temperature (cal/g °C)
m_j = mass of component j per unit mass of mixture
H = standard heat of reaction of main reactant A (cal/g of A)
$\dot{m}_{\mathrm{A}}'''$ = mass of A consumed by chemical reaction per unit volume per unit time (g/cm³ sec)
$\sum_j$ = signifies summation over all gas components j
m_j = fractional mass concentration of component j (g/g)
D = diffusion coefficient (cm²/sec)
ρ = local gas density (g/cm³ sec)
r = mass of B reacting with unit mass of A (g/g).

The boundary conditions are:

$$x=-\infty: T=T_u,\ m_{\mathrm{A}}=m_{\mathrm{A}_u},\ m_{\mathrm{B}}=m_{\mathrm{B}_u} \qquad \ldots.[4]$$

$$x=+\infty: T=T_b,\ m_{\mathrm{A}}=m_{\mathrm{A}_b}(\text{usually}=0),\ m_{\mathrm{B}}=m_{\mathrm{B}_b} \qquad \ldots.[5]$$

where subscripts u and b refer to the unburnt and burnt states respectively.

By adding equations 1 and 2 a more usual form of the energy equation is obtained, namely

$$\frac{\mathrm{d}}{\mathrm{d}x}\left(k\frac{\mathrm{d}T}{\mathrm{d}x}\right)+\frac{\mathrm{d}}{\mathrm{d}x}\left(T\sum_j c_j D_j\rho\frac{\mathrm{d}m_j}{\mathrm{d}x}\right)-G\frac{\mathrm{d}}{\mathrm{d}x}\left(T\sum_j c_j m_j\right)=-H\dot{m}_{\mathrm{A}}''' \qquad \ldots.[6]$$

Here k, c_j and m_j vary with temperature in a way which is supposed to be known. The last two variations can be accounted for with some difficulty. For most purposes, however, it suffices to suppose

$$c_j=\text{const.}=c=H(m_{\mathrm{A}_u}-m_{\mathrm{A}_b})/(T_b-T_u) \qquad \ldots.[7]$$

where c = average specific heat at constant pressure in cal/g °C. This will be done below. The second term of equation 6 then disappears, because there is no net diffusion flux by definition, while the third term can be simplified.

Relations between dependent variables for normal diffusion

Introducing

$$\delta_{\mathrm{A}}=D_{\mathrm{A}}\rho c/k,\ \delta_{\mathrm{B}}=D_{\mathrm{B}}\rho c/k \qquad \ldots.[8]$$

and assuming $\delta_A = \delta_B = 1$, equations 2 and 6 may be combined and integrated to give

$$m_A H + cT = m_{A_u} H + cT_u \quad \ldots [9]$$

In terms of the non-dimensional variables

$$z = m_A / m_{A_u} \quad \ldots [10]$$

$$\tau = (T - T_u)/(T_b - T_u) \quad \ldots [11]$$

Equation 9 may be written

$$z + \tau = 1 \quad \ldots [12]$$

Combination and integration of equations 2 and 3 on the other hand yields

$$z - \beta = 1 - \beta_u \quad \ldots [13]$$

where β is defined as

$$\beta = m_B / r m_{A_u} \quad \ldots [14]$$

The results 12 and 13, first noted by Y. B. ZELDOVICH and D. A. FRANK-KAMENETSKY[3], were used in I and enable $\dot{m}_A'''$ to be written as a function of τ alone.

Dimensionless equations

On introduction of the following substitutions:

$$dy = cG\,dx/k \quad \ldots [15]$$

$$\tau = (T - T_u)/(T_b - T_u) \quad \ldots [16]$$

$$R(z, \beta, \tau) = kH\dot{m}_A'''/k_u \quad \ldots [17]$$

$$\bar{R} = \int_0^1 R(\tau)\, d\tau \text{ evaluated for } \delta_A = \delta_B = 1 \quad \ldots [18]$$

$$\Phi(z, \beta, \tau) = R(z, \beta, \tau)/\bar{R} \quad \ldots [19]$$

$$\lambda = k_u \bar{R}/(T_b - T_u)c^2 G^2 \quad \ldots [20]$$

equations 2, 3 and 6 reduce to

$$\frac{d^2\tau}{dy^2} - \frac{d\tau}{dy} = -\lambda\Phi(z, \beta, \tau) \quad \ldots [21]$$

$$\delta_A \frac{d^2 z}{dy^2} - \frac{dz}{dy} = \lambda\Phi(z, \beta, \tau) \quad \ldots [22]$$

$$\delta_B \frac{d^2\beta}{dy^2} - \frac{d\beta}{dy} = \lambda\Phi(z, \beta, \tau) \quad \ldots [23]$$

in which it has been supposed that δ_A and δ_B are constants.

With normal diffusion ($\delta_A = \delta_B = 1$), these equations become identical in content and may be represented by the single equation

$$\frac{d^2\tau}{dy^2} - \frac{d\tau}{dy} = -\lambda\Phi(\tau) \quad \ldots [24]$$

This equation can be reduced in order by using the temperature gradient p as the dependent variable and τ as the independent. For with

$$p \equiv \mathrm{d}\tau/\mathrm{d}y \qquad \ldots.[25]$$

equation 24 becomes

$$p\,\mathrm{d}p/\mathrm{d}\tau - p = -\lambda\Phi(\tau) \qquad \ldots.[26]$$

The boundary conditions are:

$$\begin{aligned} \tau = 0 &: p = 0 \\ \tau = 1 &: p = 0 \end{aligned} \qquad \ldots.[27]$$

SOLUTIONS FOR NORMAL DIFFUSION

In this section some exact solutions of equation 26 are presented. Consideration of the results enables the centroid rule to be deduced.

Solutions by the Klein method

Equation 26 can be integrated as

$$\tfrac{1}{2}p^2 - \int_0^\tau p\,\mathrm{d}\tau = -\lambda \int_0^\tau \Phi(\tau)\mathrm{d}\tau \qquad \ldots.[28]$$

Since $\Phi(\tau)$ is defined so that $\int_0^1 \Phi(\tau)\mathrm{d}\tau = 1$, equation 28 yields

$$\lambda = \int_0^1 p\,\mathrm{d}\tau \qquad \ldots.[29]$$

Figure 1 exemplifies how p varies with τ. At low τ, $p = \tau$. When the reaction rate function is finite the p curve droops downwards, eventually passing through the point (1, 0). Equation 29 shows that λ is equal to the area under the p curve, and therefore λ is always somewhat less than $\frac{1}{2}$.

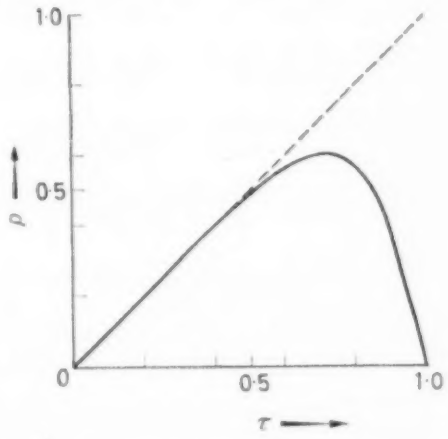

Figure 1. Typical variation of p with τ

Klein[2] determines p as a function of τ by using equation 28 as an iteration formula in the form

$$p_{(k+1)} = \left[2\left\{\int_0^\tau p_{(k)}\mathrm{d}\tau - \left(\int_0^1 p_{(k)}\mathrm{d}\tau\right)\left(\int_0^\tau \Phi(\tau)\mathrm{d}\tau\right)\right\}\right]^{\frac{1}{2}} \qquad \ldots.[30]$$

in which $p_{(k)}$ is a guessed value and $p_{(k+1)}$ is a better approximation.

This method has been used in the present investigation to determine λ for the two families of reaction rate functions:

(*i*): $$\Phi = (n+1)(n+2)(1-\tau)\tau^n \quad \ldots\ldots[31]$$

and

(*ii*): $$\Phi = \tfrac{1}{2}(n+1)(n+2)(n+3)(1-\tau)^2\tau^n \quad \ldots\ldots[32]$$

These expressions have been chosen as representing, respectively, flames with excess of one reactant, and flames in stoichiometric mixtures. They are plotted in *Figures 2* and *3*.

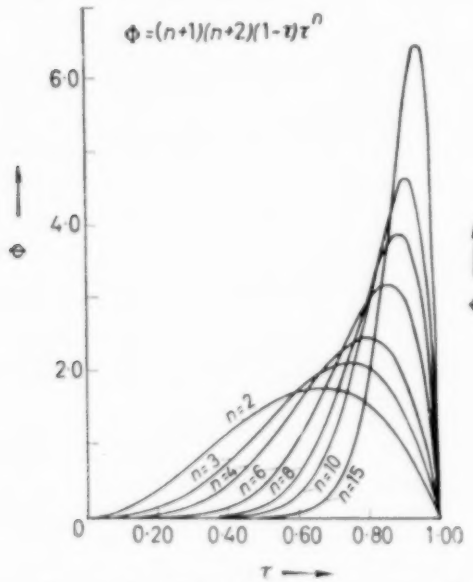

Figure 2. Reaction rate curves of family (i)

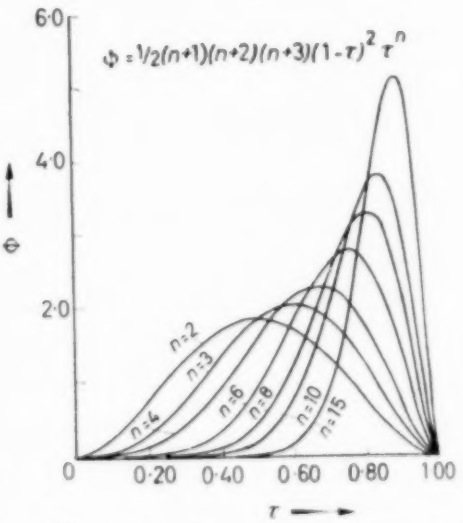

Figure 3. Reaction rate curves of family (ii)

The results of the calculations are presented in *Figure 4* as respectively a curve and a set of points, marked (*i*) and (*ii*), on a graph of λ versus the horizontal position τ_c of the centroid of the appropriate reaction rate expression, evaluated from the formulae:

(*i*): $$\tau_c = (n+1)/(n+3) \quad \ldots\ldots[33]$$

(*ii*): $$\tau_c = (n+1)/(n+4) \quad \ldots\ldots[34]$$

Analytical solutions

The flame equation 26 has analytical solutions when the reaction rate function has either of the forms:

(*iii*): $$\Phi(\tau) = [2n(n+1)/(n-1)] \cdot \tau^n(1-\tau^{n-1}) \quad \ldots\ldots[35]$$

(*iv*): $$\Phi(\tau) = (2/n^2)(n+1)(n+2)\{2(n+1)\tau^{n+1} - (6n+5)\tau^{2n+1} + 2(3n+2)\tau^{3n+1} - (2n+1)\tau^{4n+1}\} \quad \ldots\ldots[36]$$

Representative members of these families are plotted in *Figures 5* and *6*. They exhibit once more the characteristics respectively of 'weak' and of stoichiometric mixtures.

The analytical solutions are:

(*iii*): $$\lambda = (1/\tau_c)\{-1 + (1-\tau_c+9\tau_c^2/4)^{\frac{1}{2}}\} \quad \ldots\ldots[37]$$

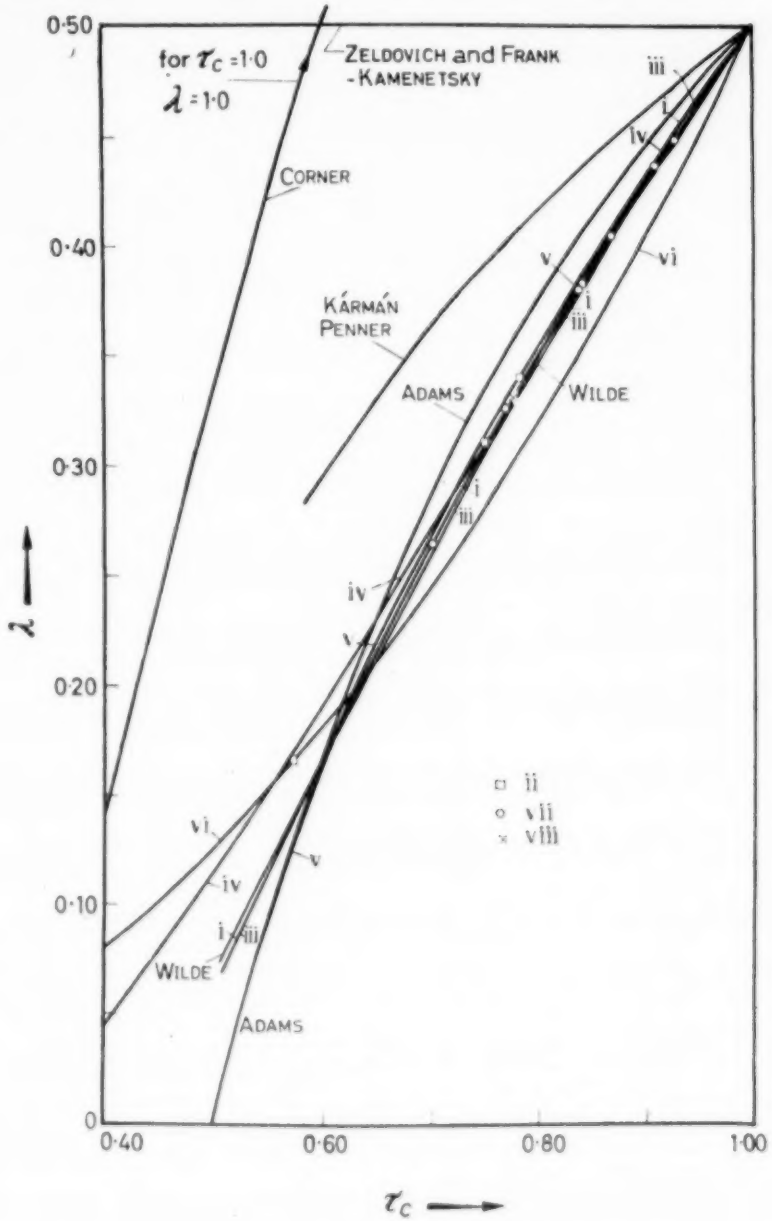

Figure 4. Exact solutions [(i) to (viii)] and approximate solutions (indicated by authors' names) of the flame equation for explicit reaction functions with normal diffusion

where

$$\tau_c = 2n(n+1)/(2n+1)(n+2) \quad \ldots\ldots [38]$$

and (*iv*):

$$\lambda = n^2/2(n+2)(n+1) \quad \ldots\ldots [39]$$

with

$$\tau_c = \frac{2(n+1)(n+2)}{n^2}\left\{\frac{1}{2} - \frac{4}{n+3} + \frac{4}{2n+3} - \frac{2}{3(n+1)} + \frac{1}{2(4n+3)}\right\} \quad \ldots\ldots [40]$$

These solutions are also plotted on *Figure 4*.

Analytical solutions may also be derived for somewhat more 'artificial' reaction rate functions, namely:

(*v*): $\Phi = 0$ for $0 \leqq \tau \leqq \tau_i$
$\Phi = 1/(1-\tau_i)$ for $\tau_i < \tau < 1$ .... [41]

and (*vi*): $\Phi = 0$ for $0 \leqq \tau < \tau_e$ and $\tau_e + h < \tau \leqq 1$
$\Phi = 1/h$ for $\tau_e \leqq \tau \leqq \tau_e + h$ .... [42]

where $h \to 0$. These represent respectively 'step-function' and 'concentrated' reaction rate expressions.

The solutions are:

(*v*): $$\frac{\lambda}{1-\tau_i} = \frac{1}{\ln\{\lambda/(\lambda - \tau_i + \tau_i^2)\}} \quad \ldots [43]$$

$$\tau_e = (1+\tau_i)/2 \quad \ldots [44]$$

and (*vi*): $$\lambda = \tfrac{1}{2}\tau_e^2 \quad \ldots [45]$$

These solutions are also plotted on *Figure 4*.

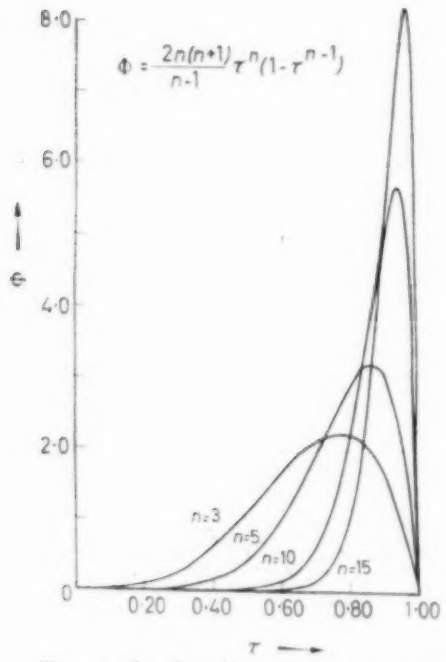

Figure 5. Reaction rate curves of family (iii)

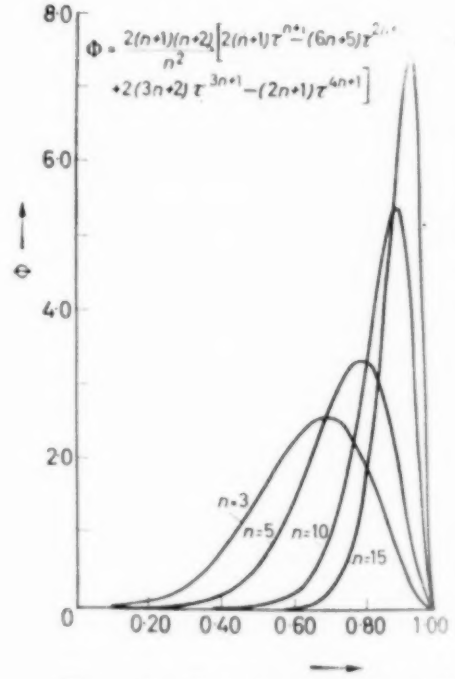

Figure 6. Reaction rate curves of family (iv)

Solutions obtained by other workers

Numerous particular exact solutions have been obtained by other workers. Often, however, the results have been presented as actual values of flame velocity with insufficient auxiliary data to permit comparison with the present work. However, R. FRIEDMAN and E. BURKE[4] have examined reaction rate functions of the form

(*vii*): $$R = (1-\tau)\exp(-\varepsilon/\tau) \quad \ldots [56]$$

where ε is a constant indicative of the steepness of the temperature dependence of the reaction. Their results have been put in the form of the present paper and are plotted in *Figure 4*.

An example of a reversible first-order reaction has been studied by Klein[2]. His result is marked (*viii*) in *Figure 4*.

The centroid rule

Examination of *Figure 4* shows that, with the exception of the unrealistic case (*vi*), all the results lie close together, provided that τ_c is greater than about 0·6. For this reason it suffices to assume that all the results obey the empirical relation obtained by analysing the data of reaction rate family (*i*), namely

$$\lambda = \tfrac{1}{2} - 0{\cdot}6604(1-\tau_c) - 0{\cdot}4283(1-\tau_c)^2 \qquad \ldots.[57]$$

This formula is correct to within 1 per cent for reaction rate curves with finite gradients at $\tau = 1$. The accuracy is slightly poorer for reaction rate curves with zero gradient at $\tau = 1$ (stoichiometric mixtures), but better values for these may be obtained from *Figure 4* directly. Since the reaction rate functions represented in *Figure 4* are rather varied in shape, it does not seem likely that any practical reaction rate function will be found which gives results markedly different from that of equation 57.

Critical review of approximate theories: normal diffusion

The opportunity will be taken to compare the exact results of *Figure 4* with the predictions of some approximate theories.

Zeldovich and Frank-Kamenetsky[3]—This theory, giving $\lambda = \frac{1}{2}$, has already been discussed. It is plotted as a horizontal line in *Figure 4*.

Corner—J. CORNER[5] uses equation 26 in the form

$$\frac{\mathrm{d}g}{\mathrm{d}\tau} = \lambda \frac{\Phi(\tau)}{\tau - g} \qquad \ldots.[58]$$

where

$$g \equiv \tau - p \qquad \ldots.[59]$$

Consideration will be restricted to the reaction rate function (*i*). Corner makes the RHS of equation 58 integrable by substituting in it

$$g = \tau - a(1-\tau) \qquad \ldots.[60]$$

where a is to be determined by its value close to $\tau = 1$, at which point

$$\frac{\mathrm{d}g}{\mathrm{d}\tau} = 1 + a = \lambda \frac{(n+1)(n+2)(1-\tau)\tau^n}{\tau - \tau + a(1-\tau)}$$

$$= \lambda(n+1)(n+2)/a \qquad \ldots.[61]$$

Integration of equation 58 with substitution from conditions 60 and 61 leads to:

$$g = \tau^{\lambda} \qquad \ldots.[62]$$

$$\lambda = n/(n+2) \qquad \ldots.[63]$$

The result of equation 63 is plotted in *Figure 4*. It is obviously a very poor approximation. However, a better approximation is possible by substituting the new expression 62 for g in equation 58 and integrating again, in general numerically.

Adams—E. N. ADAMS[6] assumes $g=\tau^{n+1}$, and so carries out what is very nearly the Corner second approximation, by transferring the denominator of equation 58 to the LHS before integration; thus

$$\int_0^1 \tau \mathrm{d}g - \int_0^1 g \mathrm{d}g = \lambda \int_0^1 \Phi \mathrm{d}\tau \qquad \ldots.[64]$$

i.e.

$$\left[\tau g\right]_0^1 - \int_0^1 g \mathrm{d}\tau - \left[\tfrac{1}{2}g^2\right]_0^1 = \lambda \qquad \ldots.[65]$$

Substitution of $g=\tau^{n+1}$ and insertion of the boundary conditions leads to

$$\lambda = (n-1)/2(n+1) \qquad \ldots.[66]$$

This expression is plotted in *Figure 4*. It is seen to give a maximum error, for the reaction functions of family (*i*), of just over 7 per cent.

Wilde—K. A. WILDE[7] assumes

$$g=\tau^{(1+a)} \qquad \ldots.[67]$$

where a is chosen to satisfy equation 61 close to $\tau=1$, so that

$$a(1+a) = \lambda(n+1)(n+2) \qquad \ldots.[61]$$

Combining this with condition 67 substituted in expression 65, we obtain

$$\lambda = \tfrac{1}{2}\left[1 - \frac{4}{1+\{1+2(n+1)(n+2)\}^{\frac{1}{2}}}\right] \qquad \ldots.[68]$$

Equation 68 gives results which agree with the exact values for family (*i*) within 1 per cent. It is plotted in *Figure 4*. The Wilde approximation is generalized below to deal with the cases of non-normal diffusion.

Kármán-Penner—T. VON KÁRMÁN and S. PENNER[8] assume in effect that, in evaluating expression 65, g is to be regarded as consisting of two straight lines: $g=0$ at low values of τ, and equation 60 at high values. This leads, in the present formulation, to

$$\lambda = \tfrac{1}{2} - 1/\{2(n+1)(n+2)\}^{\frac{1}{2}} \qquad \ldots.[69]$$

Equation 69 is plotted in *Figure 4*. It is evident that the approximation is considerably poorer than that of Adams. Its inaccuracy derives from the cruder assumption as to g.

APPROXIMATE SOLUTIONS FOR NON-NORMAL DIFFUSION

Effect of reactant diffusion coefficient

A reaction will be considered for which equations 21 and 22 reduce to

$$\frac{d^2\tau}{dy^2} - \frac{d\tau}{dy} = -\lambda(n+1)(n+2)z\tau^n \quad \ldots.[70]$$

$$\delta_A \frac{d^2z}{dy^2} - \frac{dz}{dy} = \lambda(n+1)(n+2)z\tau^n \quad \ldots.[71]$$

Such reactions are: (*a*) single-step with large excess of one reactant, (*b*) 'steady-state assumption' chain reaction with same condition, (*c*) 'explosive' branching reaction with normal radical diffusion. An exponent n can usually be found which expresses adequately the temperature dependent part of Φ. The factor $(n+1)(n+2)$ appears in order that the average dimensionless reaction rate should be unity when diffusion is normal.

We now suppose that the fuel concentration is given by

$$z = 1 - \tau^b \quad \ldots.[72]$$

where b is to be determined by the slope condition at $\tau = 1$. This leads to

$$b = (1+a)/(1+\delta_A a) \quad \ldots.[73]$$

where a has the same significance as in the Wilde approximation, being given this time as

$$a(1+\delta_A a) = \lambda(n+1)(n+2) \quad \ldots.[74]$$

Combination of expressions 25, 70 and 72, and integration, leads to

$$\lambda = \frac{(n+b+1)}{b(n+2)} \int_0^1 p\,d\tau \quad \ldots.[75]$$

Now $\int_0^1 p\,d\tau$ is given by the centroid rule as a function of τ_c. In the present case the centroid position is

$$\tau_c = \frac{(n+1)(n+1+b)}{(n+2)(n+2+b)} \quad \ldots.[76]$$

The simultaneous equations 57 and 73–76 have been solved by iteration for various values of δ_A and n. The results are plotted in *Figure 2* of I as λ versus τ_c^*, the latter signifying the centroid position for the reaction rate function with $\delta_A = 1$, not the actual τ_c given by equation 76.

Also plotted in *Figure 2* of I are a few exact calculations of Friedman and Burke[1] for $\delta_A = 0$. The agreement with the present results is good even though these authors used an exponential reaction rate function. The present author believes the results to be reliable to within a few per cent for all reaction rate functions which are directly proportional to fuel concentration.

The solutions for stoichiometric mixtures (rate proportional to z^2) may be expected to show a trend similar to that of *Figure 2* of I, but no

suitable approximation procedure has been found for this case. The difficulty lies in the fact that the gradients of p and Φ at $\tau = 1$ are zero and cannot be used in the choice of z function.

It will be noted that for $\tau_c^* = 1$ and $\delta_A = 0$, we have $\lambda = 0$. This does not, however, correspond to an infinite flame speed because simultaneously the absolute value of the mean reaction rate tends to zero. For any given τ_c^*, however, flame speed increases as δ_A decreases, the effect being most marked at large values of τ_c^*.

The effect of radical diffusion coefficient in 'explosive' chain-branching reactions

The equations for this case can be put in the form:

$$\frac{d^2\tau}{dy^2} - \frac{d\tau}{dy} = -\lambda(n+1)(n+2)z\gamma\tau^n \qquad \ldots.[77]$$

$$\delta_A \frac{d^2z}{dy^2} - \frac{dz}{dy} = \lambda(n+1)(n+2)z\gamma\tau^n \qquad \ldots.[78]$$

$$\delta_C \frac{d^2\gamma}{dy^2} - \frac{d\gamma}{dy} = -\lambda(n+1)(n+2)z\gamma\tau^n \qquad \ldots.[79]$$

where γ is the dimensionless radical concentration. We now assume that z has the form 72 and γ is related to τ by

$$\gamma = \tau^c \qquad \ldots.[80]$$

in which a, b and c are to be determined from the slope conditions at $\tau = 1$. These conditions lead to:

$$a(a+1) = \lambda b(n+1)(n+2) \qquad \ldots.[81]$$

$$b = (a+1)/(a\delta_A + 1) \qquad \ldots.[82]$$

$$c = (a+1)/(a\delta_C + 1) \qquad \ldots.[83]$$

In addition, integration of equation 77 leads to

$$\lambda = \frac{(n+c+1)(n+b+c+1)}{b(n+2)(n+3)} \int_0^1 p\,d\tau \qquad \ldots.[84]$$

in which the integral can be evaluated from the centroid rule, τ_c being given by

$$\tau_c = \frac{(n+c+1)(n+b+c+1)}{(n+c+2)(n+b+c+2)} \qquad \ldots.[85]$$

These simultaneous equations have been solved to give λ versus τ_c^* with δ_C as parameter with $\delta_A = 1$. τ_c^* is the centroid position for normal diffusion and in this case is given by $(n+2)/(n+4)$. The results are shown in *Figure 3* of I.

The author knows of no exact solutions to this problem against which the present results could be checked.

CONCLUSIONS

(*a*) The centroid rule gives as good accuracy as is needed for many applications of flame theory, and makes possible the determination of flame speeds without the necessity of solving a differential equation.

(*b*) Of the various approximate solutions to the flame equations which have been developed, that due to Wilde is the best.

(*c*) Definition of the eigenvalue in terms of the temperature-mean reaction rate is convenient for comparison of theories, and also reduces the eigenvalue to a small and easily recognized magnitude.

(*d*) Whereas an increased reactant diffusivity lowers the flame velocity, an increased radical diffusivity raises it. An approximate but probably reliable general theory of these effects has been presented.

(*e*) A general theory is still needed for the effects of non-normal diffusion in stoichiometric mixtures.

The computations have been performed by Miss M. P. Steele. The author is grateful to Mr G. K. Adams for many enlightening discussions on flame theory.

Department of Mechanical Engineering,
Imperial College of Science and Technology

(*Received March 1957*)

REFERENCES

[1] HIRSCHFELDER, J. O. and CURTISS, C. F. *Third Symposium (International) on Combustion* Williams and Wilkins: Baltimore, 1949
[2] KLEIN, G. *Rep. No. SQUID 1* University of Wisconsin, 1955; also *Phil. Trans. A* 249 (1957) 389
[3] ZELDOVICH, Y. B. and FRANK-KAMENETSKY, D. A. *J. phys. Chem. Moscow* 12 (1938) 100
[4] FRIEDMAN, R. and BURKE, E. *J. chem. Phys.* 21 (1953) 710
[5] CORNER, J. *Proc. Roy. Soc. A* 198 (1949) 388
[6] ADAMS, E. N. Quoted by HENKEL, M. J., SPAULDING, W. P. and HIRSCHFELDER, J. O. *Third Symposium (International) on Combustion* Williams and Wilkins: Baltimore, 1949
[7] WILDE, K. A. *J. chem. Phys.* 22 (1954) 1788
[8] VON KÁRMÁN, T. and PENNER, S. *Selected Combustion Problems*, Vol. I. AGARD; Butterworths: London, 1954

Flame Decomposition of the Propyl Nitrates

J. POWLING and W. A. W. SMITH

Decomposition flames of iso*propyl nitrate and* n*-propyl nitrate have been stabilized upon their liquid surfaces at atmospheric pressure. Temperature distributions and reaction product distributions have been measured through the flame zones. Suggestions have been made concerning the earliest degradation reactions giving rise to the many products observed in the flame front. The type of mechanism previously proposed for the ethyl nitrate flame degradation will describe quite adequately the appearance of practically all of the many observed ingredients of the propyl nitrate flames. The nitric ester is attacked by nitrogen dioxide and nitrous acid which abstract a methyl group or a hydrogen atom, leaving an unstable residue which breaks down spontaneously, with frequent regeneration of these active species to continue the chain.*

THIS study of the combustion of the propyl nitrates is part of a programme of work on the effect of molecular structure on the mode of degradation of nitric esters in their decomposition flames. The results of earlier work on ethyl nitrate[1] led the authors to postulate that, in flames, this nitric ester did not decompose mainly in a unimolecular fashion (the usual conclusion from thermal decompositions conducted at temperatures around 200° C), but was destroyed by nitrogen dioxide and nitrous acid in a chain process. It was therefore of interest to investigate the chemical processes occurring in the decomposition flames of the propyl nitrates, particularly to determine whether a similar type of reaction could account for the analytical results.

Decomposition flames of normal and *iso*propyl nitrates have been stabilized at atmospheric pressure to give flat reaction zones suitable for the determination of the distribution of reaction intermediates and products and of temperature. The aim has been to obtain complete quantitative analyses of the combustion products at several intervals through the flame zones. All the significant ingredients are believed to have been identified, but some of these could be only roughly quantitatively estimated in the complex mixtures obtained. It is considered that the accuracy is, however, quite adequate to provide evidence of the nature and extent of the reactions postulated.

EXPERIMENTAL

The experimental arrangements of the burner and the reaction product sampling system were essentially the same as in the ethyl nitrate study[1] and will not be given again here. A diagram of the burner is given in *Figure 1*. The burning liquid surface was 3·3 cm in diameter and was maintained at a fixed level by an external constant-head device. Decomposition flames of the liquid propyl nitrates are stabilized only with difficulty at atmospheric pressure; heat losses through the burner and turbulence in the gases

cause extinction of the flames. For reasonable stability it was necessary to supply a little extra heat to the liquid surface by allowing the combustion products of the decomposition flame to burn in a nitrogen–air mixture as a diffusion flame around the outside of the burner.

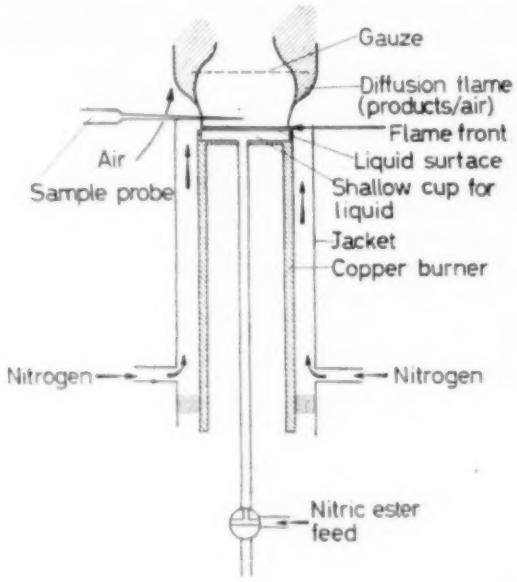

Figure 1. Burner

Gas samples were removed from horizontal elements of the flames with fine silica probes and analysed as completely as was compatible with a reasonable rate of progress. Fairly complete analyses of the complex mixtures could, in fact, be achieved by making full use of infra-red (i.r.) analytical methods; these were supplemented by chemical methods. The gases withdrawn slowly from the flame were passed directly into a trap at about −130° C. The gases passing through this trap, consisting essentially of carbon monoxide, nitric oxide, methane, hydrogen and nitrogen, were subjected to quantitative i.r. analysis and to chemical analysis. The trap was allowed to warm to room temperature and the fraction evaporating between these temperatures was analysed by its i.r. spectrum. With *iso*propyl nitrate this fraction contained mainly CH_3CHO, CH_3NO_2, CH_3ONO, CH_3OH, $(CH_3)_2CO$, CO_2 and N_2O, and with *n*-propyl nitrate the mixture was qualitatively similar except that CH_3OH was not detected and C_2H_4, $C_2H_5NO_2$, C_2H_5ONO were found additionally. Analysis of the liquid remaining in the trap was always difficult because of its nature and the quantities available (usually $\sim 0{\cdot}2$ g); the accuracy of this analysis is consequently limited.

The liquid fraction from *iso*propyl nitrate combustion consisted essentially of CH_3NO_2, CH_3OH, CH_3CHO, H_2CO, H_2O and $(CH_3)_2CO$. For analysis it was divided into several parts. The water, methanol and nitromethane content of the liquids was determined from the i.r. spectrum of a solution in acetonitrile. Empirical relationships between the optical densities of selected bands of each of the components and their concentrations were previously determined in synthetic mixtures of composition similar to those

to be encountered. A second part of the liquid fraction was vaporized in a heated i.r. cell (described previously[2]) and its spectrum recorded. The spectrum of the vapours of the materials found in the liquids is more detailed and characteristic than that of the condensed phase, because of the association and polymerization occurring in the latter. The vapour spectrum provided a check on the relative amounts of methanol and nitromethane and was used to estimate the acetone remaining in the liquid fraction. The spectra of synthetic mixtures could be matched with the observed spectra (for example *Figure 2b*). The aldehydes were determined separately—total aldehyde content of the liquids by the sodium sulphite

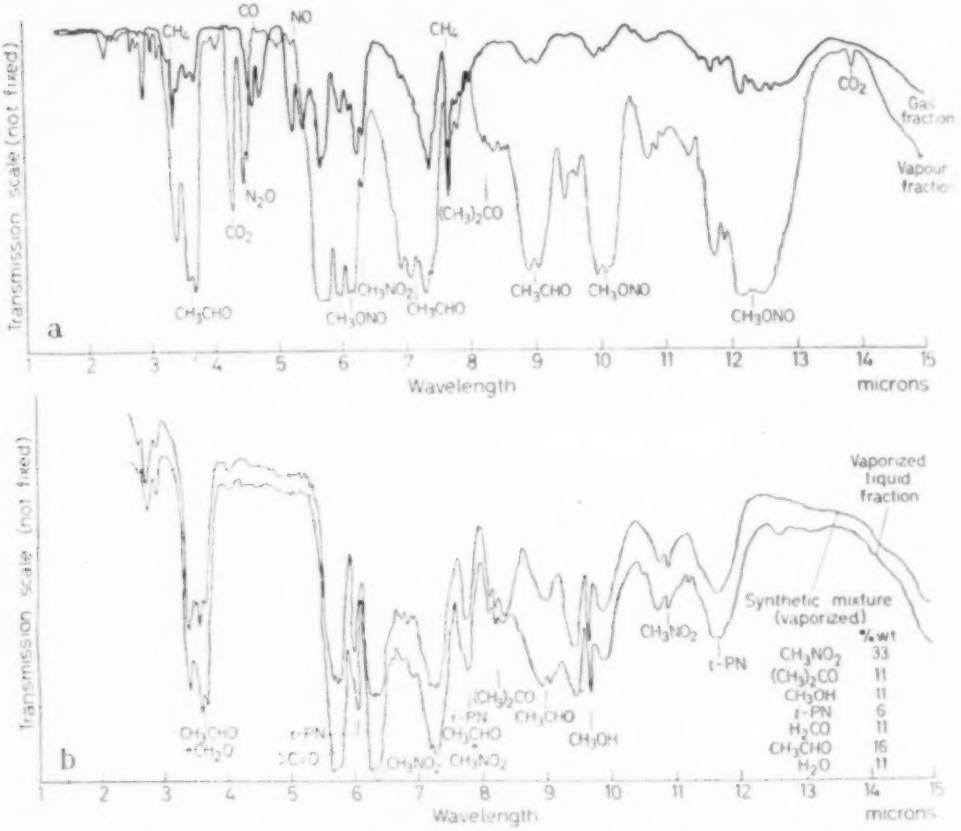

Figure 2. Infra-red spectra of combustion products of (a) isopropyl nitrate (gases) and (b) isopropyl nitrate (liquids)

method and the formaldehyde by the method of Deniges[3]. [In this colorimetric test the absorption at 5950 Å was measured, after allowing a fixed time interval for the colour to develop, using a Unicam SP 500 spectrophotometer. It was advisable to calibrate with standards each time.] The difference between the total aldehydes and the formaldehyde was taken to be acetaldehyde; this was the only other aldehyde detectable from the spectrum of the vaporized liquids.

The treatment of the liquid fraction from *n*-propyl nitrate combustions was similar. The ingredients were H_2CO, H_2O, $C_2H_5NO_2$, CH_3NO_2, CH_3CHO, (C_2H_5CHO?), and acids. The nitro compounds were mostly

nitroethane and a semiquantitative estimate only could be made of the sum of the two nitro compounds. There was some indication of the presence of propionaldehyde in addition to formaldehyde and acetaldehyde. The amount was quite small, however, and was estimated as acetaldehyde. These limitations should be borne in mind when considering the results for the *n*-propyl nitrate. A further restriction, which applies to both systems, is that the data obtained for gaseous nitrogen are probably spurious. Material balances indicated that the nitrogen values were high by an amount approximately equivalent to the gaseous nitrogen. It was probable that, because of the occasional instability of the flames, nitrogen from the jacket surrounding the burner had entered the stream of combustion products. To test this, a tracer (carbon tetrachloride) was mixed with the nitrogen and a gas sample was taken in the usual manner. The i.r. spectrum of this sample showed a weak absorption at 794 cm^{-1}, the frequency of the C—Cl stretching vibration. Some penetration of nitrogen from the surrounding nitrogen stream had, in fact, taken place. If the gaseous nitrogen values are subtracted, the atom balances for the *iso*propyl nitrate system are quite good, considering the complexity of the gas mixtures. The balances for the more difficult *n*-propyl nitrate system are still poor, however. It was not considered worth while devoting a great deal more time to improvement of the analytical method, since good indications of the course of reaction can be obtained from the results.

RESULTS AND DISCUSSION

The distributions of combustion products and of temperature in the flames are given in *Tables 1* and *2*; they are quoted as moles of product per 100 moles of nitric ester from which they were generated, the balance being derived from the total number of carbon atoms. An atom balance using the total nitrogen data, which are usually more reliable, could not be used here because of the penetration of external nitrogen into the flame gases, probably due to occasional instability of the flame front upon the liquid surface. The temperature and analytical data for the *iso*propyl nitrate flame are related graphically in *Figure 3*.

Sample i.r. spectra of the combustion products are shown in *Figure 2*. *Figure 2a* gives the spectra of the more volatile fractions from *iso*propyl nitrate, the heavy line showing the more permanent gases. *Figure 2b* shows the spectrum of the vaporized liquid fraction, together with a synthetic mixture made up to the same composition as that estimated in this particular analysis. The transmission scale is shifted for each spectrum, for clarity in presentation. *In situ* i.r. absorption and emission of a flame 10 cm wide did not prove to be of any use for quantitative work. Visible and u.v. absorption of the *iso*propyl nitrate flame revealed the presence of H_2CO, NO and a trace of NO_2.

Approximate flame temperatures have been calculated from the composition of the products of *iso*propyl nitrate using the carbon balance and taking the heat of formation of the liquid propyl nitrate to be 48 kcal/mole. The calculated temperatures are about 100°C higher than the measured values. No positive explanation of this is known, but it may well be due

Table 1. Combustion products from isopropyl nitrate

Distance from liquid surface mm	0	0·3	1·1	3·4	5·0
Component	*Moles per 100 moles* isopropyl nitrate				
CH_3CHO		52·8	62·5	51·7	38·7
NO		41·5	51	49	68
CH_3NO_2		35·3	30·4	27·6	26·2
CH_3OH		23·8	26	31·8	44·3
H_2CO		23·5	22·5	27·7	24·4
CO		21·5	23·5	30	48·5
CH_4		17·4	20·7	23·4	43·7
$(CH_3)_2CO$		14·0	11·2	15·6	7·8
CH_3ONO		12·8	6·6	1·8	2·0
N_2		(9·5)	(12·2)	(14·8)	(16)
CO_2		7·2	7·1	8·2	9·8
H_2O		7·1	13·1	9·5	(35·2)
$C_3H_7ONO_2$		3·5	1·3	0	0
H_2		2·1	2·0	3·8	9·0
N_2O		2·0	3·4	1·7	1·6
Flame temperatures calculated from products °C		480	530	590	820
Measured flame temperature °C	~100	260	420	450	520

Table 2. Combustion products from n-*propyl nitrate*

Distance from liquid surface mm	0	0·4	0·5 ±0·3	1·1	2·5	3·7
Component	*Moles per 100 moles* n-*propyl nitrate**					
H_2CO		87·6	78·3	48·5	66	77
H_2O		71	77	81	93	99
NO		53	73	77·6	62·8	68·7
CO		34·2	66·2	80·4	64·2	64·5
$C_2H_5NO_2$ $(+CH_3NO_2)$†		38·5	21·7	27·2	35·4	36·3
CH_3CHO‡		28·4	(11·4)	18·4	22·5	11·7
H_2		12·4	12·8	27·2	19·4	18·0
CH_4		11·5	24·2	31·2	28·6	20·2
C_2H_4		10·1	17	20·7	12	14·6
CH_3ONO		4·9	2·1	1·6	0·8	2·3
CO_2		3·8	4·2	3·8	3·9	9·3
C_2H_5ONO		3·6	0·9	—	1·1	0·6
N_2O		2·0	1·7	2·2	1·9	1·9
C_2H_2		0·04	0·13	0·1	0·07	0·15
(N_2)		(20·8)	(24·4)	(21·9)	(52·6)	(38·9)
Acids (as HCOOH)		—	4·2	1·7	—	1·7
Measured flame temperature °C	110	250	270	350	~470	~560

*Approximate †Mostly $C_2H_5NO_2$ ‡May include small amount of propionaldehyde.

to heat lost through the liquid. Analyses for the *n*-propyl nitrate are not sufficiently accurate for the calculation of useful temperatures.

The influence of the secondary diffusion flame of the products in the nitrogen–air mixture is noticed in *Figure 3* beyond 3 or 4 mm from the liquid surface.

The interpretation of the results for both nitric esters is basically the same but, to avoid confusion, the two systems will be discussed under separate headings.

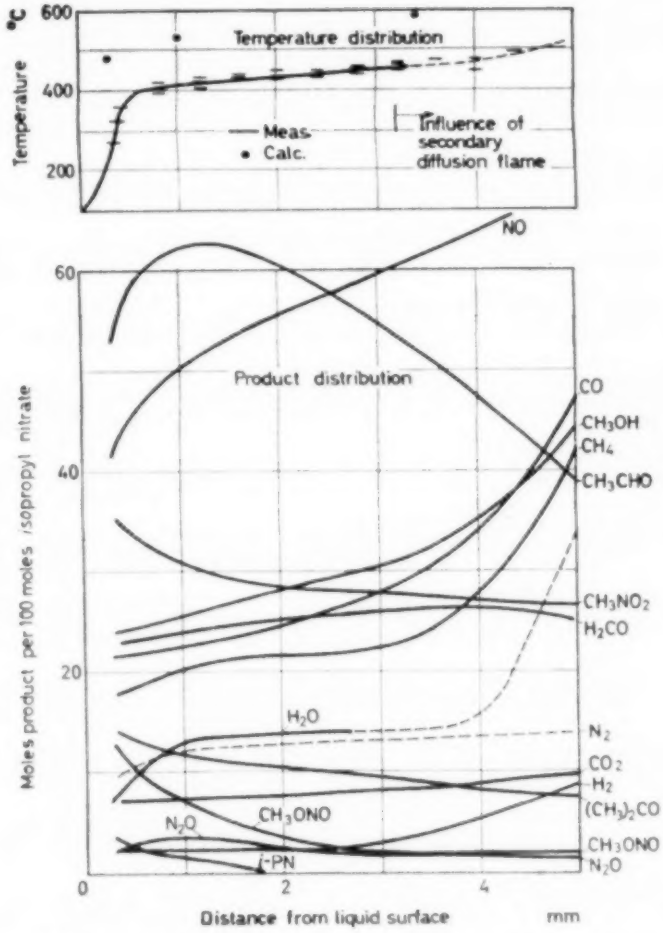

Figure 3. Distribution of temperature and reaction products in iso*propyl nitrate flame*

iso*Propyl nitrate*

The principal first-stage products of degradation of this ester are seen to be CH_3CHO, NO, CH_3NO_2, CH_3OH, H_2CO, CO and CH_4, in order of magnitude of concentration (*Table 1*). Of these, CH_3CHO and CH_3NO_2 are of major importance and the trends of the curves in *Figure 3* show that CH_3ONO, and perhaps $(CH_3)_2CO$, may well be present in the very earliest stages of the flame in higher concentrations than the first analysis shows. Practically all the *iso*propyl nitrate has decomposed to the above products at a distance of less than $\sim 0{\cdot}5$ mm from the liquid surface.

Beyond this distance, reactions in the flame are mostly concerned with the decomposition of CH_3CHO, CH_3NO_2 and CH_3ONO. The changes in concentration of CO and CH_4 'reflect' those of CH_3CHO and indicate that the former products are derived entirely from the latter. It seems most probable that CH_3ONO is generated in an amount approximately equal to that of CH_3NO_2, but the nitrite decomposes more rapidly than the nitro compound. Methyl nitrite itself is known to sustain a self-decomposition flame and the combustion products[4] are initially CH_3OH, H_2CO and NO. (The nitric oxide is subsequently reduced to nitrogen, providing the heat for propagation of the flame.) The curves for CH_3OH and H_2CO indicate that their main source is CH_3ONO; the H_2CO would be slowly decomposing to hydrogen and carbon monoxide. It seems likely, then, that the equal amounts of CH_3OH and H_2CO found in the earliest sample ($\sim 0{\cdot}3$ mm) are also derived from CH_3ONO produced at an even earlier stage, in which case roughly equal amounts of CH_3NO_2 and CH_3ONO are initially produced, namely, ~ 35 moles of each per 100 moles of the *iso*propyl nitrate.

With the ethyl nitrate flame it was suggested that reactions of the ethyl nitrate molecule with NO_2 and HONO were the important reactions taking place in the flame. The same type of chain reaction scheme will describe the observed products for the *iso*propyl and *n*-propyl nitrates, according to the mechanism below. There is, of course, no evidence from this work concerning the initiating step, but for the *iso*propyl nitrate decomposition it is probably reaction 1 and could be followed by reaction 2:

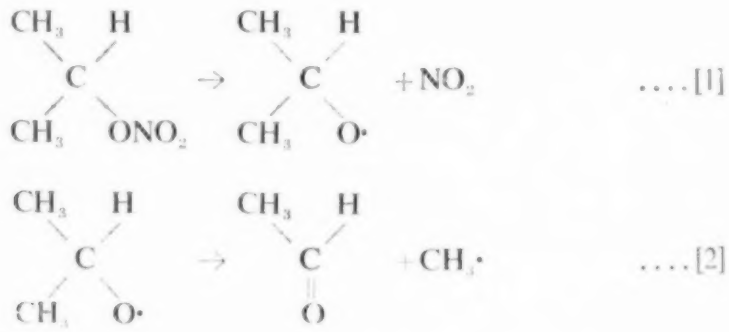

It is suggested that the reaction is then continued by the following main reactions:

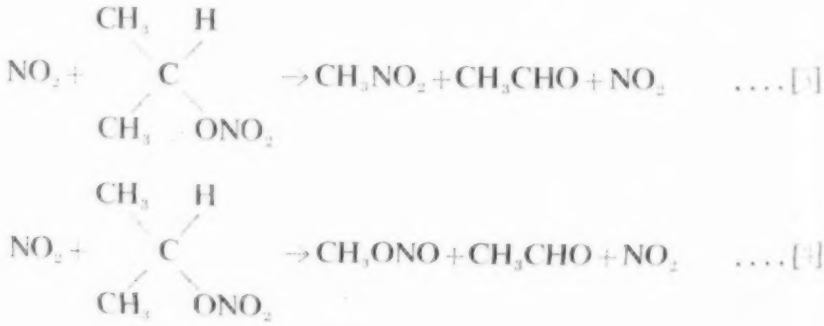

These reactions are analogous to the hydrogen-stripping reactions which were postulated for the ethyl nitrate reaction. With *iso*propyl nitrate it appears that removal of a methyl group is favoured. Hydrogen may, however, be stripped off by the nitrogen dioxide to give the observed acetone, according to reaction 5:

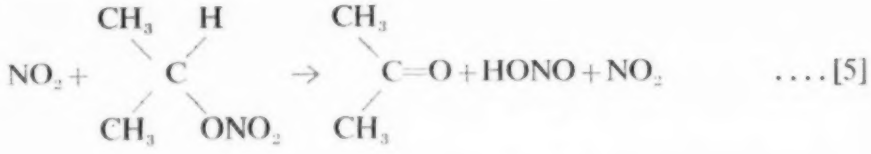

.....[5]

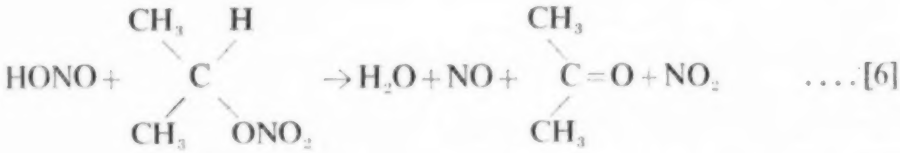

.....[6]

Following the scheme for ethyl nitrate, HONO would be expected to give H_2O and NO as the next step, according to the overall reaction 6. Since the hydrogen-stripping reactions of NO_2 do not seem to occur as extensively as in ethyl nitrate the amount of H_2O would not be expected to be as large. This is found to be so; the amounts of both $(CH_3)_2CO$ and water are about 13 moles per 100 moles *iso*propyl nitrate at ~ 1 mm from the liquid surface.

The main reactions occurring in the early stages, then, are probably 3 and 4 in which either the nitrite or nitro compound is produced according to the orientation of the NO_2 attack; CH_3CHO and another molecule of NO_2 are produced in both cases.

Reaction 5 occurs to a limited extent. According to reactions 3 and 4, the sum of the CH_3NO_2 and the estimated original CH_3ONO ($CH_3ONO + CH_3OH$ or H_2CO, see above) molecules should equal the estimated amount of CH_3CHO ($CH_3CHO + CO$ or CH_4). The number of moles of $CH_3NO_2 + CH_3ONO$ is 70, and of CH_3CHO is 71, per 100 moles nitric ester. About 14 moles of the nitric ester degrade to $(CH_3)_2CO$, about 4 remain undecomposed in the first sample, leaving about 11 moles which have been so completely broken down that there is no evidence of the mechanism.

Reactions 3 to 6 describe adequately the observed degradation products. Alternative mechanisms might, however, be expected to follow the initiating reactions 1 and 2. The *iso*propoxy radical from reaction 1 might be expected to produce *iso*propyl alcohol in its reactions with, for example, *iso*propyl nitrate or another *iso*propoxy radical. About 20 moles per cent of the alcohol is produced from the reactions of *iso*propoxy radicals in *cyclo*hexene solution[7]. No *iso*propyl alcohol has been observed in the flame products; it is more likely that, at higher temperatures, $C_3H_7O\cdot$ breaks down into CH_3CHO and $CH_3\cdot$ (reaction 2). The $CH_3\cdot$ radical could possibly give rise to a chain degradation of the *iso*propyl nitrate in a fashion similar to that given above, in which NO_2 is a chain carrier; for example, according to reactions 7 and 8:

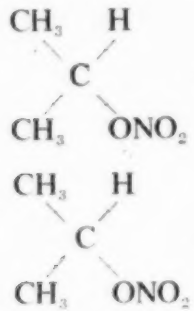

$$+ CH_3\cdot \rightarrow CH_3ONO + CH_3CHO + CH_3\cdot \; * \quad \ldots [7]$$

$$+ CH_3\cdot \rightarrow C_2H_6 + CH_3CHO + NO_2 \quad \ldots [8]$$

However, if reaction 7 or 1+2 occurred extensively, the presence of some ethane would be expected from recombination of $CH_3\cdot$ radicals and from reaction 8; yet no ethane has been observed. It is considered that the mechanism involving NO_2 and, to a limited extent, HONO as chain carriers describes the observations more completely and is supported by similar observations in ethyl nitrate[1] and *n*-propyl nitrate. It may be that reactions involving $CH_3\cdot$ radicals are rapidly quenched (reaction 9) by the NO generated early in nitric ester flames, whereas those continued by NO_2 are unaffected by NO and are favoured. There is some doubt whether this reaction will occur at elevated temperatures, however (see later).

$$CH_3\cdot + NO \rightarrow CH_3\cdot NO \rightarrow CH_2NOH \rightarrow HCN + H_2O \quad \ldots [9]$$

Not a great deal need be said about the overall reactions occurring beyond ~ 1 mm from the liquid surface; the inferences from *Figure 3* and *Table 2* are straightforward. Most of the energy release that will occur at atmospheric pressure has by then taken place to heat the products to 425° C. CH_3CHO, CH_3ONO, CH_3NO_2 and $(CH_3)_2CO$ are decomposing with relatively little heat release, producing NO, CO, CH_3OH, CH_4 and H_2. H_2CO may be produced and at the same time degraded to CO and H_2; its concentration remains approximately constant from 1 to 5 mm.

CH_3ONO might be expected to degrade in the manner believed to occur in its decomposition flame[1] (i.e. according to reactions 10 and 11), except that reaction 11 would become less probable as the concentration of CH_3ONO became smaller:

$$CH_3ONO \rightarrow CH_3O\cdot + NO \quad \ldots [10]$$

$$CH_3O\cdot + CH_3ONO \rightarrow CH_3OH + H_2CO + NO \quad \ldots [11]$$

It is, in fact, observed that, whereas CH_3OH increases continually as CH_3ONO decomposes, H_2CO does not. This would be expected if reactions of $CH_3O\cdot$ similar to 11 were taking place but were not involving CH_3ONO, e.g. the reaction

$$CH_3O\cdot + RH \rightarrow CH_3OH + R\cdot \quad \ldots [12]$$

CH_3NO_2 decomposes relatively slowly and there is no distinct evidence of its mechanism of decomposition from this work. T. L. Cottrell, T. E. Graham and T. J. Reid[2] have investigated the thermal decomposition

*Note added in proof. $CH_3\cdot$ radicals have been shown[3] to abstract NO from nitrites in the liquid phase in a reaction analogous to 7.

of CH_3NO_2 at temperatures almost as high as those reached in the flame and conclude that the degradation is by a non-chain radical process producing, as the main final products, NO, CH_4, CO and H_2O.

A small quantity of CO_2 is produced in the flame front, where reactions involving NO_2 (e.g. 3 and 4) are taking place. CO_2 is the product of more direct oxidation of organic fragments by NO_2 and could be a chain-terminating step. Production of CO_2 after the disappearance of the *iso*propyl nitrate is very small and is not associated in any obvious way with the degradation of CH_3ONO or CH_3NO_2. N_2O is also produced in the flame front as a minor product.

n-Propyl nitrate

The flame of this ester was more difficult to stabilise at atmospheric pressure. The initial temperature gradient is smaller than that for *iso*propyl nitrate.

Difficulties were encountered in obtaining compositions of reaction products which showed logical changes with respect to distance through the flame. This fact, coupled with the detection of fairly large amounts of nitrogen in the products, especially at the larger distances from the liquid surface, leads to the belief that some turbulence may occasionally be present in the flame. This reduces the usefulness of the determination of the distribution of products. Moreover, the special complexity of the combustion products from this ester has reduced the accuracy of the results, and certain ambiguities remain. For instance, nitroethane is an important product but the data quoted include a small, but unknown, amount of nitromethane, and there is some evidence that the value quoted for acetaldehyde may include a small amount of propionaldehyde. Nevertheless, the analytical results may be regarded as good semiquantitative data and adequately provide the necessary information regarding the identity, and approximate amounts, of the early-stage reaction products. With the above limitations in mind, atom balances have been made and the results given in *Table 2* are quoted as the number of moles of product per 100 moles of the nitric ester (carbon balance).

The results support a degradation scheme essentially similar to that postulated for ethyl nitrate and *iso*propyl nitrate. Any postulated mechanism must account for the rapid production of H_2CO, H_2O, NO, CO, $C_2H_5NO_2$, CH_3CHO, CH_4 and C_2H_4 (and other minor components shown in *Table 2*), and for the absence in any significant amounts of certain other substances such as NO_2, *n*-propyl alcohol and C_2H_6. It is considered that the scheme below affords the simplest description of the products of flame decomposition. Initiation (only) is probably reaction 13 and may be followed by 14:

$$CH_3CH_2CH_2ONO_2 \rightarrow CH_3CH_2CH_2O^{\cdot} + NO_2 \quad \ldots.[13]$$

$$CH_3CH_2CH_2O^{\cdot} \rightarrow CH_3CH_2^{\cdot} + H_2CO \quad \ldots.[14]$$

J. B. LEVY and F. J. ADRIAN[8] believe that 13 is the controlling reaction in the thermal decomposition at 191 °C and 20 mm initial pressure. Intramolecular rearrangement might also be a possible initiating step, thus

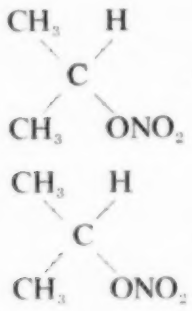

$$+ CH_3\cdot \rightarrow CH_3ONO + CH_3CHO + CH_3\cdot \; * \qquad \ldots [7]$$

$$+ CH_3\cdot \rightarrow C_2H_6 + CH_3CHO + NO_2 \qquad \ldots [8]$$

However, if reaction 7 or 1+2 occurred extensively, the presence of some ethane would be expected from recombination of $CH_3\cdot$ radicals and from reaction 8; yet no ethane has been observed. It is considered that the mechanism involving NO_2 and, to a limited extent, HONO as chain carriers describes the observations more completely and is supported by similar observations in ethyl nitrate[1] and *n*-propyl nitrate. It may be that reactions involving $CH_3\cdot$ radicals are rapidly quenched (reaction 9) by the NO generated early in nitric ester flames, whereas those continued by NO_2 are unaffected by NO and are favoured. There is some doubt whether this reaction will occur at elevated temperatures, however (see later).

$$CH_3\cdot + NO \rightarrow CH_3\cdot NO \rightarrow CH_2NOH \rightarrow HCN + H_2O \qquad \ldots [9]$$

Not a great deal need be said about the overall reactions occurring beyond ~ 1 mm from the liquid surface; the inferences from *Figure 3* and *Table 2* are straightforward. Most of the energy release that will occur at atmospheric pressure has by then taken place to heat the products to 425° C. CH_3CHO, CH_3ONO, CH_3NO_2 and $(CH_3)_2CO$ are decomposing with relatively little heat release, producing NO, CO, CH_3OH, CH_4 and H_2. H_2CO may be produced and at the same time degraded to CO and H_2; its concentration remains approximately constant from 1 to 5 mm.

CH_3ONO might be expected to degrade in the manner believed to occur in its decomposition flame[1] (i.e. according to reactions 10 and 11), except that reaction 11 would become less probable as the concentration of CH_3ONO became smaller:

$$CH_3ONO \rightarrow CH_3O\cdot + NO \qquad \ldots [10]$$

$$CH_3O\cdot + CH_3ONO \rightarrow CH_3OH + H_2CO + NO \qquad \ldots [11]$$

It is, in fact, observed that, whereas CH_3OH increases continually as CH_3ONO decomposes, H_2CO does not. This would be expected if reactions of $CH_3O\cdot$ similar to 11 were taking place but were not involving CH_3ONO, e.g. the reaction

$$CH_3O\cdot + RH \rightarrow CH_3OH + R\cdot \qquad \ldots [12]$$

CH_3NO_2 decomposes relatively slowly and there is no distinct evidence of its mechanism of decomposition from this work. T. L. Cottrell, T. E. Graham and T. J. Reid[2] have investigated the thermal decomposition

*Note added in proof.—CH_3 radicals have been shown[3] to abstract NO from nitrites in the liquid phase in a reaction analogous to 7.

of CH_3NO_2 at temperatures almost as high as those reached in the flame and conclude that the degradation is by a non-chain radical process producing, as the main final products, NO, CH_4, CO and H_2O.

A small quantity of CO_2 is produced in the flame front, where reactions involving NO_2 (e.g. 3 and 4) are taking place. CO_2 is the product of more direct oxidation of organic fragments by NO_2 and could be a chain-terminating step. Production of CO_2 after the disappearance of the *iso*propyl nitrate is very small and is not associated in any obvious way with the degradation of CH_3ONO or CH_3NO_2. N_2O is also produced in the flame front as a minor product.

n-Propyl nitrate

The flame of this ester was more difficult to stabilise at atmospheric pressure. The initial temperature gradient is smaller than that for *iso*propyl nitrate.

Difficulties were encountered in obtaining compositions of reaction products which showed logical changes with respect to distance through the flame. This fact, coupled with the detection of fairly large amounts of nitrogen in the products, especially at the larger distances from the liquid surface, leads to the belief that some turbulence may occasionally be present in the flame. This reduces the usefulness of the determination of the distribution of products. Moreover, the special complexity of the combustion products from this ester has reduced the accuracy of the results, and certain ambiguities remain. For instance, nitroethane is an important product but the data quoted include a small, but unknown, amount of nitromethane, and there is some evidence that the value quoted for acetaldehyde may include a small amount of propionaldehyde. Nevertheless, the analytical results may be regarded as good semiquantitative data and adequately provide the necessary information regarding the identity, and approximate amounts, of the early-stage reaction products. With the above limitations in mind, atom balances have been made and the results given in *Table 2* are quoted as the number of moles of product per 100 moles of the nitric ester (carbon balance).

The results support a degradation scheme essentially similar to that postulated for ethyl nitrate and *iso*propyl nitrate. Any postulated mechanism must account for the rapid production of H_2CO, H_2O, NO, CO, $C_2H_5NO_2$, CH_3CHO, CH_4 and C_2H_4 (and other minor components shown in *Table 2*), and for the absence in any significant amounts of certain other substances such as NO_2, *n*-propyl alcohol and C_2H_6. It is considered that the scheme below affords the simplest description of the products of flame decomposition. Initiation (only) is probably reaction 13 and may be followed by 14:

$$CH_3CH_2CH_2ONO_2 \rightarrow CH_3CH_2CH_2O^{\cdot} + NO_2 \quad \ldots . [13]$$

$$CH_3CH_2CH_2O^{\cdot} \rightarrow CH_3CH_2^{\cdot} + H_2CO \quad \ldots . [14]$$

J. B. LEVY and F. J. ADRIAN[5] believe that 13 is the controlling reaction in the thermal decomposition at 191°C and 20 mm initial pressure. Intramolecular rearrangement might also be a possible initiating step, thus

$$CH_3CH_2CH_2ONO_2 \rightarrow [\cdot CH_2CH_2CH_2O\cdot] + HONO \quad \ldots [15]$$
$$\downarrow$$
$$CH_2{=}CH_2 + H_2CO$$

Further reaction of NO_2 or HONO could give rise to an exothermic chain reaction which regenerates NO_2 or HONO (but not C_3H_7O):

$$NO_2 + CH_3CH_2CH_2ONO_2 \rightarrow [\dot{C}H_2CH_2CH_2ONO_2] + HONO$$
$$\downarrow$$
$$CH_2{=}CH_2 + H_2CO + NO_2 \quad \ldots [16]$$

$$NO_2 + CH_3CH_2CH_2ONO_2 \rightarrow [CH_3\dot{C}HCH_2ONO_2] + HONO$$
$$\downarrow$$
$$CH_3CHO + H_2CO + NO \quad \ldots [17]$$

$$NO_2 + CH_3CH_2CH_2ONO_2 \rightarrow [CH_3CH_2\dot{C}HONO_2] + HONO$$
$$\downarrow$$
$$CH_3CH_2CHO + NO_2 \quad \ldots [18]$$

Reactions 16 to 18 are the different hydrogen-stripping reactions possible; the rearrangement of the residual $\dot{C}_3H_6ONO_2$ is always a simple one, to satisfy the free valency on the appropriate carbon atom and form stable products. About 10 to 20 per cent of the molecules of the ester appear to degrade according to reaction 16 and 30 to 40 per cent by 17 (if the CH_4 observed early in the reaction is derived from CH_3CHO, as the trends of the data indicate). Little reaction according to 18 seems to take place, since propionaldehyde has not been observed with any certainty, although there are indications that small quantities may be present.

Removal of an ethyl group from the nitric ester by NO_2 seems to occur as readily as hydrogen removal, and about 35 per cent is degraded by reaction 19

$$NO_2 + CH_3CH_2CH_2ONO_2 \rightarrow CH_3CH_2NO_2 + H_2CO + NO_2 \quad \ldots [19]$$

Several reactions analogous to 19 appear to take place to a much smaller extent. Thus CH_3CH_2ONO may be produced instead of $CH_3CH_2NO_2$, and CH_3NO_2 or CH_2ONO may arise from reactions such as

$$(CH_3ONO)$$
$$NO_2 + CH_3CH_2CH_2ONO_2 \rightarrow CH_3NO_2 + [\dot{C}H_2CH_2ONO_2]$$
$$\downarrow$$
$$2H_2CO + NO \quad \ldots [20]$$

The hydrogen-stripping reactions of HONO are very similar to those of NO_2 in 16 to 18, except that H_2O and NO are among the products. Only one example need be given—it is analogous to 17

$$HONO + CH_3CH_2CH_2ONO_2 \rightarrow H_2O + NO + [CH_3\dot{C}HCH_2ONO_2]$$
$$\downarrow$$
$$CH_3CHO + H_2CO + NO \quad \ldots [21]$$

All the main reactions, 16, 17, 19 and 21, give one molecule of H_2CO per molecule of nitric ester consumed, and all reactions of HONO produce H_2O. These are major initial products.

The above reactions are suggested for the early phases of ignition. As the concentration of the ester falls, reactions of NO_2 and HONO with other products of reaction will predominate over those with *n*-propyl nitrate. NO is the main nitrogenous product of these reactions; a little N_2O is produced, but there is no reliable information regarding the amount of nitrogen because of diffusion of this gas from the outside into the flame. Hydrogen, carbon monoxide and carbon dioxide are produced by decomposition or oxidation of aldehydes, etc.

The nitrites formed decompose rapidly in the hot products, but the nitro compounds and aldehydes do so relatively slowly. There is evidence[6] that $CH_3CH_2NO_2$ decomposes at about 400°C according to the reaction

$$CH_3CH_2NO_2 \rightarrow CH_2{=}CH_2 + HONO \qquad \ldots . [22]$$

This would provide an explanation, alternative to reaction 16, of the early production of $CH_2{=}CH_2$ and infer that more $CH_3CH_2NO_2$ is produced (19) than is observed. Since the decomposition of this material is slow in the hotter gases behind the flame front, this possibility is unlikely.

CONCLUSION

In conclusion, the following points should be mentioned. The data presented here show that the mechanism suggested for the degradation of ethyl nitrate can be applied to the propyl nitrates. The same basic reactions, i.e. attack of the ester by NO_2 and HONO, seem to take place. The mechanisms suggested are adequate in that they account for the many observed major products without involving numerous reaction steps and they are chain mechanisms. P. GRAY and A. D. YOFFE[9] have shown that the ignitions of methyl and ethyl nitrates are 'chain thermal' processes. The burning velocities of these esters are much greater than those of certain aliphatic dinitrates[10] of the same heat of explosion in which, it seems[11], unimolecular decomposition takes place. The mechanism given here cannot account for the differences in the rates of burning found by R. STEINBERGER *et al.*[13] for the different deuterated *iso*propyl nitrates.

It is possible to formulate a somewhat similar mechanism in which alkyl radicals continue the chain and which will also describe the appearance of most of the products. Such reactions seem less probable to the authors because of the above mentioned absence of certain of the expected reaction products of the alkyl radicals. Alternatively, it may be said that extensive degradation of the nitric ester may take place to alkyl radical, aldehyde and NO_2, according to the reactions 1 and 2 (*iso*propyl nitrate) and 13 and 14 (*n*-propyl nitrate). The observed nitro alkyls and the alkyl nitrites could then be formed by the subsequent recombination of the alkyl radical and NO_2. There is no evidence, however, that alkyl radicals and NO_2 or, for that matter, alkyl radicals and NO, will, in fact, recombine in flames at these temperatures. It seems a little unlikely, for example, that CH_3· and NO_2 would give CH_3ONO at a temperature of 450°C when the heat of reaction is 59 kcal/mol and the activation energy for CH_3ONO decomposition is 36 kcal/mol[12]. Some flame experiments have been performed to gain information on this point. An upper-limit flame of

CH_3CHO–NO_2 with a temperature of about 570°C gave no nitromethane or methyl nitrite in its products although extensive thermal degradation of excess CH_3CHO to CH_4 and CO occurred. It is presumed that this degradation proceeds by way of a methyl radical chain[14]. In the hot products of this flame, decomposition continues in the presence of large amounts of NO, yet no CH_3NO nor significant amounts of its degradation products $H_2C{:}NOH$, HCN, NH_3 could be found (0·1 per cent HCN was detected). In the ethyl nitrate flame CH_3CHO is decomposing at about 900°C in the presence of excess NO but no $H_2C{:}NOH$ and only very small amounts of HCN can be found. Dilution of the *iso*propyl nitrate flame with excess NO yielded no such products either.

A mixture of equal volumes of ethylene oxide and NO_2 was made up and sufficient CO_2 added so that a relatively cool flame was obtained on ignition, here again the presence of methyl radicals might be expected[15] but no CH_3NO_2 or CH_3ONO was detectable in the products. Excessive dilution of the ethylene oxide decomposition flame with NO failed to show any evidence of the reaction $CH_3\cdot + NO$. Many other such experiments were performed with similar conclusions.

In the mixture *t*-butyl nitrite–50 per cent NO_2, however, CH_3NO_2 and CH_3ONO can both be detected in the flame products but then direct attack of NO_2 on the nitrite is possible, without the initial production of $CH_3\cdot$ radicals. In this flame, in fact, there was no evidence that $CH_3\cdot$ had recombined with NO either, although this occurs extensively in the relatively low temperature thermal decomposition[16].

It was concluded that in the propyl nitrate flames a mechanism involving extensive decomposition of the ester according to reactions 1 and 2 or 13 and 14 and subsequent recombination of alkyl radicals and NO_2 at elevated temperatures was less probable than the chain reaction scheme analogous to that given for ethyl nitrate.

REFERENCES

[1] Denston, Miss E. J., Needham, D. P. and Powling, J. *Proc. Roy. Soc. A* 232 (1955) 337
[2] Bernstein, H. J. *J. chem. Phys.* 18 (6) (1950) 897
[3] Walker, J. F. *Formaldehyde* p. 244 Reinhold: New York, 1944
[4] Arden, E. A. and Powling, J. *Sixth Symposium (International) on Combustion* Yale, 1956. In press
[5] Cottrell, T. L., Graham, T. E. and Reid, T. J. *Trans. Faraday Soc.* 47 (1951) 584
[6] Cottrell, T. L., Graham, T. E. and Reid, T. J. *Trans. Faraday Soc.* 47 (1951) 1089
[7] Rust, F. F., Seubold, F. H. and Vaughan, W. E. *J. Amer. chem. Soc.* 72 (1950) 338
[8] Levy, J. B. and Adrian, F. J. *J. Amer. chem. Soc.* 77 (1955) 2015
[9] Gray, P. and Yoffe, A. D. *Proc. Roy. Soc. A* 200 (1949) 114
[10] Adams, G. K. and Wiseman, L. A. *Selected Combustion Problems* Vol. I, p. 277 AGARD; Butterworths: London, 1954
[11] Powling, J. and Smith, W. A. W. To be published
[12] Steacie, E. W. R. and Shaw, G. T. *Proc. Roy. Soc. A* 146 (1934) 388
[13] Steinberger, R., Orlick, C. A. and Schaaf, V. P. *J. Amer. chem. Soc.* 77 (1955) 4748
[14] Steacie, E. W. R. *Atomic and Free Radical Reactions* pp. 206 to 215 Reinhold: New York, 1954
[15] Steacie, E. W. R. *Atomic and Free Radical Reactions* pp. 229 to 232 Reinhold: New York, 1954
[16] Yoffe, A. D. *Research, Lond.* 7 (1954) S44
[17] Kharasch, M. S., Meltzer, T. H. and Nudenberg, W. *J. org. Chem.* 22 (1957) 17

*Detonations in Gaseous Fuming Nitric Acid–Hydrocarbon Mixtures**

D. H. WAYMAN and R. L. POTTER

Detonation velocities in gaseous mixtures of fuming nitric acid with three hydrocarbons, n-heptane, methylcyclopentane, and toluene, were measured and their detonatable composition ranges determined. Detonation velocities and detonatability limits of fuming nitric acid–n-heptane mixtures diluted with up to 60 volume per cent nitrogen were also obtained. Comparison with velocities calculated by the Chapman–Jouguet hypothesis show excellent agreement except for toluene. For the latter, it is suggested that reaction prior to initiation occurred and that the detonation took place in a medium of acid and toluene, plus reaction products. The run distance with fuming nitric acid and n-heptane was found to be of the order of 8 to 13 centimetres at an initial pressure of one atmosphere.

THE propagation of a steady, plane detonation wave through an explosive medium has been discussed theoretically by a number of investigators[1]. The rule for the selection of the detonation process from all those satisfying the conservation laws of mass, momentum, and energy is known as the Chapman–Jouguet hypothesis. This hypothesis has now been put on an especially satisfactory basis by J. G. KIRKWOOD and W. W. WOOD[2]. The present state of the theory makes it possible, in principle, to calculate all the parameters of a plane detonation wave propagating through a homogeneous explosive medium. If the explosive mixture is gaseous, and at moderate pressure, then it suffices to assume that the burnt gas equation of state is given by the ideal gas law in order to obtain an excellent prediction of the detonation parameters. If the measured velocity agrees closely with the predicted one for a given detonatable mixture, then the calculated temperature and pressure parameters associated with the wave can confidently be assumed correct. Unfortunately, at present, it is impossible to predict what mixtures will support steady detonations and so experimental determinations of the detonatability of the mixtures in question must be available before the theoretical calculations are useful.

A gaseous detonation in a medium capable of supporting one can arise either from a flame initially propagating subsonically, or from a shock impinging on the mixture. The theoretical problem of transitions from flame to detonation has hardly been touched upon[3]; however, G. B. KISTIAKOWSKY *et al.* have studied experimentally[4] the initiation of gaseous detonations by shock waves.

The present paper describes experiments that outline the detonatable regions of fuming nitric acid and three hydrocarbon fuels in the gas phase, and the detonatable regions of one of these mixtures diluted with nitrogen. In order to attain steady waves, shock initiation was resorted to. The results of some preliminary experiments to determine the run distance required for a subsonic flame to jump to a detonation in nitric

*Work was conducted under the sponsorship of the USAF, ARDC under Contract No. W 33(038)-ac-14169.

acid–*n*-heptane mixtures are also reported. Curves of the detonation parameters are included for two of these combustible mixtures.

EXPERIMENTAL PROCEDURE

The apparatus used, the general experimental technique employed, and some preliminary test results were presented at the Sixth International Combustion Symposium[5]. Additional experiments have since extended and refined the previous results at one atmosphere initial pressure and 400 K.

The hydrocarbons used (*n*-heptane, methyl*cyclo*pentane, and toluene) were purchased from Phillips Petroleum Company at a stated purity of 99 mole per cent. The fuming nitric acid was purchased from Allied Chemical and Dye Corporation according to *MIL–N–7254B(USAF), Type I* (97·5 weight per cent nitric acid minimum). During calibration of the flowmeters, the acid appeared to decompose. Condensed samples of the hot acid vapours were analysed with the following results, expressed as mole fractions: HNO_3, 0·563; NO_2, 0·314; H_2O, 0·044 and O_2, 0·079, the latter being found by a material balance. Since check runs revealed these values to be reproducible, this acid composition was used in making the theoretical calculations.

Fischer and Porter Triflat Flowrator tubes were used for monitoring the propellant flows. A sapphire ball float was used in the acid and nitrogen meters and a stainless steel float in the hydrocarbon meter.

Two methods of ignition were employed to initiate reaction in the combustible mixtures. In one, a wire wrapped on ceramic was used as a glow plug. This could be heated in a fraction of a second to temperatures sufficient to start a flame in the mixtures. The other consisted of a shock arising from the detonation of an equimolar oxygen–acetylene mixture at one atmosphere initial pressure. This mixture was ignited by an electric spark. A 15 cm section of stainless steel tube with an aluminium disc at each end was used as a buffer between the oxygen–acetylene mixture and the reaction tube proper. This section was normally filled with air and served to separate the detonatable mixtures in the igniter and the reaction tube, and especially to permit the entire ignition tube to be at room temperature.

Wave velocities were measured by recording the signal from five small improved ionization probes set into the walls of the reaction tube. The signals from these probes were displayed as blanking pulses on a spiral sweep of 1040 microseconds (μsec) duration and 380 cm long. The display of the sweep on a DuMont Type 250AH oscilloscope was recorded with a DuMont Type 297 Polaroid Land Camera. The signal from the first probe started the sweep, which has a 40 μsec period divided into eight 5 μsec intervals. A standard quartz oscillator fixed the time basis to an accuracy of 5 parts per 10^5. The 5 μsec timing marks and signal pulses are displayed as blanking intervals by intensity modulation. The discharge time of the thyratron attached to each probe also affects the signal from the probes. Interchange of the thyratron circuits resulted in a shift of the time intervals between signal pulses in the sweep although the total elapsed

time for the wave to traverse the five probes remained constant. A wave was considered steady if the elapsed time between successive probe stations did not vary more than the known variance of the thyratron firing times. The results reported represent an average velocity obtained by dividing the total length of the probe intervals by the total elapsed time.

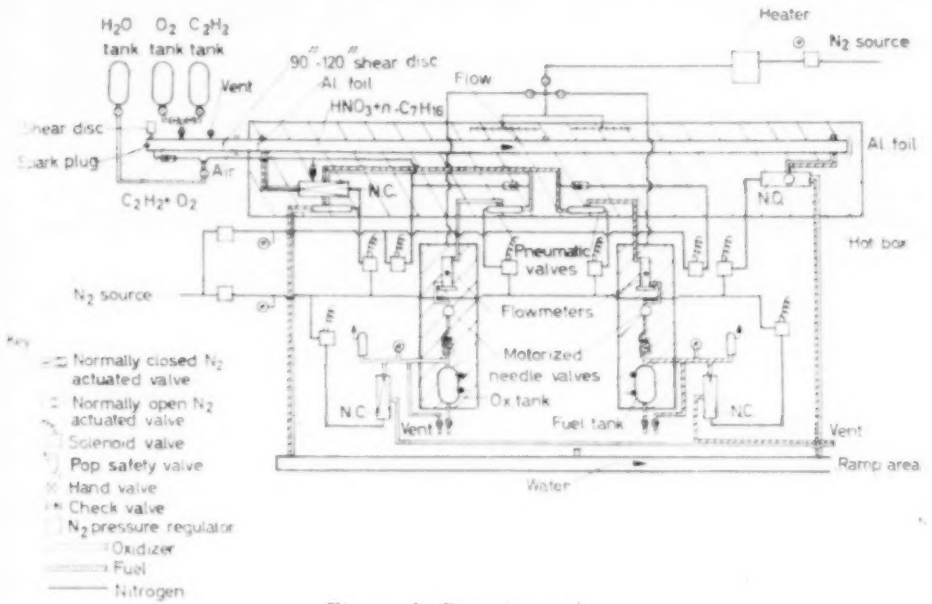

Figure 1. Reaction tube

A schematic diagram of the shock tube apparatus is shown in *Figure 1*. The first experimental step was to heat the propellants, reaction tube, and associated equipment to 400 K with hot nitrogen. Propellant flows were then established by flowing the acid–hydrocarbon vapours into a by-pass line, which also served to premix them, and then they were dumped overboard into a stream of water. When the desired mixture was established, the mixed vapours were diverted through the reaction tube until all the air had been swept out. Finally, the mixture was trapped in the reaction tube and the igniter was fired immediately. In the experiments with nitrogen added as diluent, the same procedure was employed except that hot nitrogen was also metered into the by-pass line.

An error analysis is rather difficult to make. The error in each individual flow measurement was estimated to be ± 3 per cent which should produce about 1 per cent uncertainty in the expected detonation velocity. The initial temperature variations of ± 8°C could yield 0·02 per cent uncertainty in the velocity. Uniformity of the mixture in the tube was not directly checked, but the detonation velocity is not too sensitive to small variations in mixture strength. Including the errors in probe spacings, reading the photographs of the spiral sweep display, crystal time standard, thyratron firing delays, and acid composition, together with the sources of error mentioned above, the velocity can be expected to be accurate to ± 2 per

cent. Since only one tube size (3·75 cm i.d.) was used, correction for finite tube size was impossible. The tube was filled at the prevailing atmospheric pressure; calculations showed a negligible effect on the velocity arising from the daily barometric pressure fluctuations.

The theoretical curves were calculated on an IBM 650 digital computer. The programme included tests for sixteen combustion products including solid carbon. The Bureau of Standards tabulation of thermodynamic properties of gases provided most of the thermochemical data[6]. Other information was taken from G. B. KISTIAKOWSKY *et al.*[7] and H. L. JOHNSTON *et al.*[8]. Allowance was made for the dissociation of nitric acid as mentioned earlier. It is estimated that the calculated parameters are good to about 0·25 per cent. The burnt gases were assumed ideal; a check revealed the gas imperfection correction to be less than 0·1 per cent. The initial temperature dependence was checked and calculated to be of the order of 0·05 metres per second per degree. The computations were made assuming frozen composition sound speed at the Chapman–Jouguet plane. The detonation temperatures and pressures are high: the high pressures arising in large part from the increase in number of moles upon combustion.

RESULTS

The results of the experiments with acid and *n*-heptane are shown in *Figure 2a* in which the detonation velocity is plotted versus mole fraction

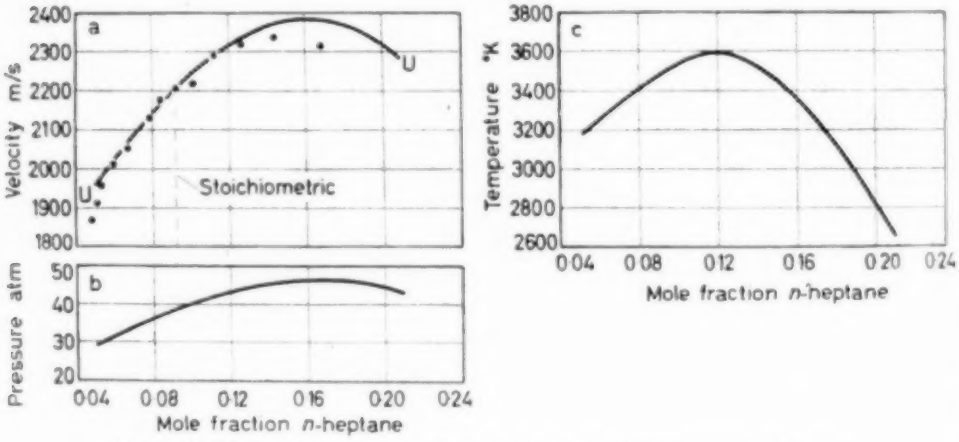

Figure 2. Detonation parameters for nitric acid–n-heptane mixtures.
$p_0 = 1$ atm. $T_0 = 400°$K

of fuel in the mixture. The solid line is the theoretical curve, while the points are experimental values. The 'U' denotes a detonatable region for which unstable velocity values were obtained. No detonations were obtained in mixtures having compositions farther from stoichiometric than these unstable regions. The agreement is within the error expected for these experiments. In order to check the efficiency of mixing the gases in the reaction tube, several experiments were carried out in which the total flow rate was varied at a fixed gas composition. These results are shown in *Figure 3*. The contact time in the tube varied by a factor of two and yet

there was no significant change in the detonation velocity. This is considered evidence that the mixing was good. The agreement between theory and experiment is also considered proof that negligible reaction occurred in the explosive medium before initiation.

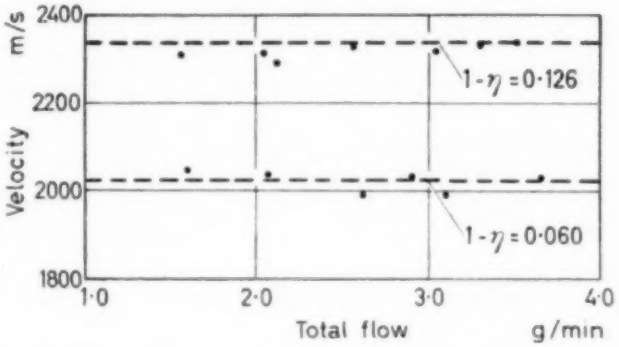

Figure 3. Effect of total flow on detonation velocity of nitric acid–n-heptane gas mixtures. p_0=1 atm. T_0=400°K. 1−η=mole fraction fuel. ● O_2–C_2H_2 ignition. ------ Theoretical velocity

The observed detonation velocities followed the theoretical curve toward the rich and lean limits until a mixture was reached in which the velocity was so low that it failed to record on the spiral sweep, although the sweep was triggered. In order to trigger the sweep and still not record at subsequent ionization probes during the remainder of the sweep, the wave velocity must be less than 300 m/s. The composition at which this abrupt drop in velocity occurred was taken to be the detonatability limit as determined in our apparatus. In the mixtures studied, a limiting detonatable composition was obtained rather than a composition region in which the velocity faded. As the limits were approached, the detonations seemed to become unsteady, but this is attributed to the dimensions of the reaction tube, not to the mixture itself. The theoretical temperatures and pressures for detonations in these mixtures are shown in *Figures 2b* and *2c* as a function of the composition.

Many tests were performed using a glow plug igniter. As has been reported before[9], detonations arising in this manner often have velocities higher than the steady values at start and our experiments showed the same behaviour. Frequently there was strong evidence of multiple ignitions ahead of the flame front in the pre-compression shock. Several tests showed that the run distance required for a flame to jump to a detonation was between 8 and 13 cm when the initial pressure was atmospheric. In general, the detonation velocities were not as steady when ignition was by glow plug as when ignition was by shock.

The fuel, methyl*cyclo*pentane, behaved very similarly to *n*-heptane. The detonation velocities are shown in *Figure 4a*; the dots represent shock-initiated runs and the diamonds glow wire-initiated runs. The points farthest from stoichiometric represent the limits of detonatability as found in our apparatus. On the oxidizer-rich side there is good agreement with theory for both types of initiation; as the fuel-rich side is approached, the detonation velocities resulting from glow wire initiation are significantly higher, indicating again that our tube was not long enough for the detonation wave to catch up to the front of the pre-compression shock. As with

n-heptane, the experimental velocity also showed no apparent dependence on total flow rate of the combustible mixtures through the tube. The theoretical temperatures and pressures for nitric acid and methyl*cyclo*pentane detonations are plotted in *Figures 4b* and *4c*.

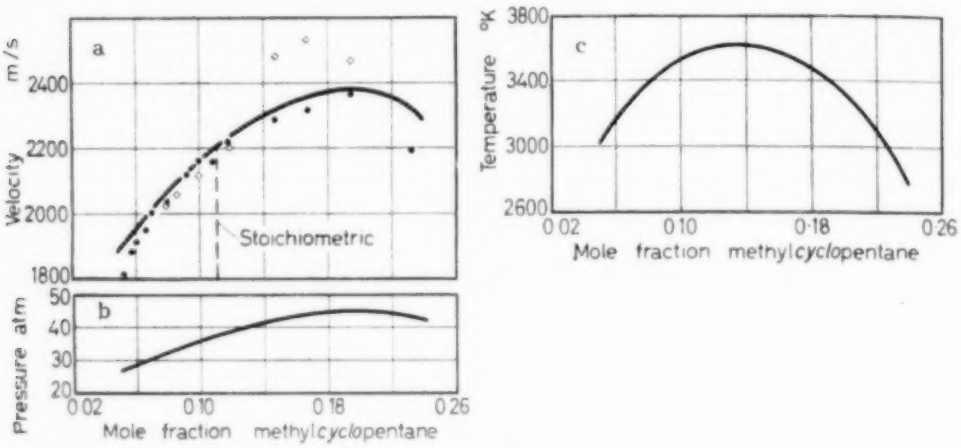

Figure 4. Detonation parameters for nitric acid–methylcyclopentane gas mixtures. $p_0 = 1$ atm. $T_0 = 400$ K. ● O_2–C_2H_2 ignition. ◇ glow plug ignition

In contrast, toluene did not give as consistently reproducible results as the other two hydrocarbons. The velocities for fixed composition and varying total flow are shown in *Figure 5*. The experiments were made over a period of five months, with different lengths of by-pass line, and with definite sequences of varying flow rates avoided. All these runs were shock-initiated. The average velocity of these runs as shown by the chain-dotted line is 190 m/s slower than the theoretical. The detonation velocity

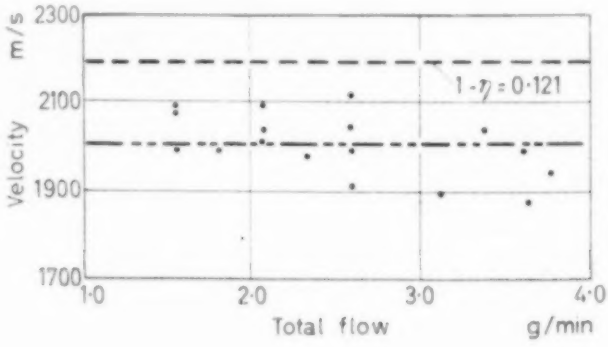

Figure 5. Effect of total flow on detonation velocity of nitric acid–toluene gas mixtures. $p_0 = 1$ atm. $T_0 = 400$ K. $1-\eta$ = mole fraction fuel. ● O_2–C_2H_2 ignition. ------ Theoretical velocity. — · — · — Average experimental velocity

as a function of mixture composition is shown in *Figure 6*. The points shown represent velocities that are steady according to our criteria. Again, the points farthest from stoichiometric represent the limits of detonatability as found in our apparatus.

The chemical activity of toluene with nitric acid suggests that gas phase reactions occurred prior to initiation and that the wave progressed through

a medium made up of acid, toluene and reaction products of these. J. L. BULLOCK and E. T. MITCHELL[10] have reported that the vapour phase nitration of toluene by nitric acid–water mixtures is fast under conditions roughly comparable to those in our shock tube, the principal products being

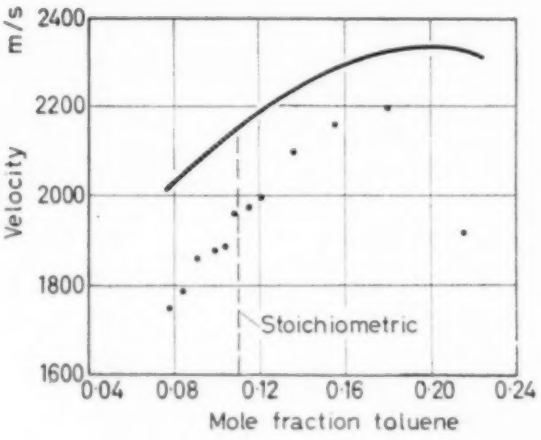

Figure 6. Detonation velocity versus composition for nitric acid–toluene gas mixtures. $p_0 =$ 1 atm. $T_0 = 400°K$

mononitrotoluenes. In order to test this hypothesis, the mixed gases of toluene and nitric acid were passed through the tube and either condensed directly or quenched in methylene chloride. These mixtures were subjected to i.r. and qualitative organic analysis and they showed the presence of oxidation and nitration products of toluene. Those products identified were *p*-nitrobenzoic acid and *p*-nitrobenzyl alcohol.

The discrepancy between the observed results and the theoretical ones for acid and toluene and the definite evidence of the reactivity of these mixtures makes it probable that the wave is indeed passing through a partially reacted medium, and if the composition of this mixture were used to formulate the detonation problem, then agreement between the experimental and calculated velocity would be satisfactory. It is our intention to try to verify this hypothesis with a new shock tube now under construction. This shock tube has windows let into the sides so that spectrographic observation of the mixture in the tube prior to initiation will be possible.

In the last series of experiments, nitrogen was added to the nitric acid and *n*-heptane mixtures in order to find the detonatability envelope of this three-component system. An important experimental verification of the Chapman–Jouguet hypothesis was produced by B. LEWIS and J. B. FRIAUF[11] and recently repeated by D. J. BERETS, E. F. GREENE and G. B. KISTIAKOWSKY[12] using hydrogen–oxygen mixtures diluted with inert gases. Our tests, performed to determine how much nitrogen dilution nitric acid and *n*-heptane mixtures can stand and still remain detonatable, also confirm the Chapman–Jouguet hypothesis over a wide range of mixture compositions and dilutions by nitrogen. The detonation velocities as a function of combustible gas composition and at several mole fractions of nitrogen diluent are shown in *Figure 7*, the solid lines being the theoretical values. The experiments were complicated by the necessity of metering nitrogen into

the by-pass line; however, the agreement between the observed and calculated velocities is very satisfactory and constitutes a confirmation of the

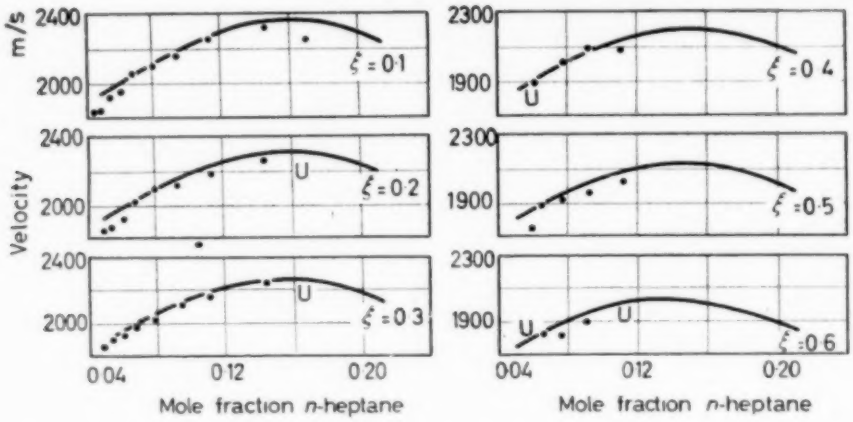

Figure 7. Detonation velocity versus mole fraction for nitrogen-diluted nitric acid–n-heptane gas mixtures. $p_0 = 1$ atm. $T_0 = 400°$K. ξ = *mole fraction nitrogen.* ● O_2–C_2H_2 *ignition.* U—*Detonation, but unstable*

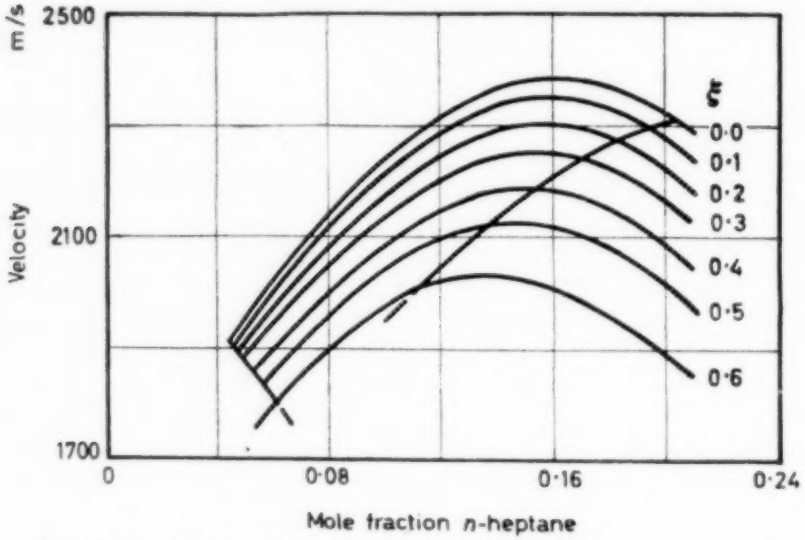

Figure 8. Detonatability limits of WFNA–n-heptane–nitrogen gas mixtures. $p_0 = 1$ atm. $T_0 = 400°$K. ξ = *mole fraction nitrogen. Oxygen–acetylene ignition. Detonatable mixtures are bounded by the heavy lines*

Chapman–Jouguet hypothesis on a new combustible mixture. *Figure 8* summarizes the calculated detonation velocities and the experimentally determined detonatability limits in the nitrogen-diluted mixtures.

(Received February 1957)

Bell Aircraft Corpn.,
Post Office Box One,
Buffalo 5, N.Y.

REFERENCES

[1] CHAPMAN, D. L. *Phil. Mag.* 47 (1889) 90
JOUGET, E. *C.R. Acad. Sci., Paris* 132 (1900) 573; 144 (1907) 415
ZELDOVICH, Y. B. *J. exp. theor. Phys. Moscow* 10 (1940) 542
VON NEUMANN, J. *U.S. Atomic En. Comm. Rep. No. OSRD–549* (1942)
DOERING, W. *Ann. Phys., Lpz.* 43 (1943) 421
[2] KIRKWOOD, J. G. and WOOD, W. W. *J. chem. Phys. 22* (1954) 1915, see also BRINKLEY, S. R., Jr and RICHARDSON, J. M. *Fourth Symposium (International) on Combustion* p. 450 Williams and Wilkins: Baltimore, 1953
[3] ZELDOVICH, Y. B. *J. tech. Phys. (U.S.S.R.)* 17 (1947) 3
[4] BERETS, D. J., GREENE, E. F. and KISTIAKOWSKY, G. B. *J. Amer. chem Soc.* 72 (1950) 1086
[5] SCHOLL, J. R., BYINGTON, H. W. and POTTER, R. L. *Sixth Symposium (International) on Combustion.* To be published
[6] ROSSINI, F. E. *et al. Circ. U.S. Bur. Stand. Nos. C461, 500* and *Series III. Washington*
[7] KISTIAKOWSKY, G. B., KNIGHT, H. T. and MALIN, M. E. *J. chem. Phys.* 20 (1952) 876
[8] JOHNSTON, H. L., BELZER, J. and SAVEDOFF, L. Ohio State University Research Foundation, Columbus 10, Ohio, *TR 316–7*, 1 May 1950
[9] BONE, W. A., FRASER, R. P. and WHEELER, W. H. *Trans. Roy. Soc.* A 235 (1936) 29
[10] BULLOCK, J. L. and MITCHELL, E. T. *J. Amer. chem. Soc.* 63 (1941) 3230; 65 (1943) 2428
[11] LEWIS, B. and FRIAUF, J. B. *J. Amer. chem. Soc.* 52 (1930) 3905
[12] BERETS, D. J., GREENE, E. F. and KISTIAKOWSKY, G. B. *J. Amer. chem. Soc.* 72 (1950) 1080

A Method for Determining Minimum Ignition Energies: Results for a Neo-pentane–Air Mixture

I. W. Wolf and V. T. Burkett

A technique employing repeated pulsed arcs having near-square wave form is reported. Details of circuitry, electrodes and fuel system are given. The effect of pulse width and of pulse repetition rate are discussed in the light of the results obtained and surprisingly good agreement is claimed between results using the technique described and those obtained with capacitor discharge measurements.

Previous determinations of ignition energies have involved the use of capacitance discharge arcs or continuous arcs. The latter is a minimum power measurement rather than an energy measurement—the distinction being that for an energy measurement the total time of energy input must be small compared to the thermal diffusion time from the arc. The results from the former suffer in accuracy because a shock wave is formed after the first instant of discharge. The power dissipated at the instant after this arc formation is much larger than the average arc power and a shock wave is created. This shock wave sometimes contains a considerable proportion of the arc energy[1], resulting in an unaccountable amount of the energy not being used for ignition, and indeed probably acting to prevent ignition.

In the work described here repeated pulsed arcs are employed. The advantage of such a technique is that the energy input as a function of time can be controlled and measured. For this particular case, the wave shape is very nearly square. This means that during the discharge the energy is being put into the arc at a relatively uniform controllable rate. The pulses are spaced wide enough apart so that there is sufficient time for dissipation of the thermal energy in the inter-electrode gap. Thus a reasonably accurate determination can be made.

Description of Equipment

Electrical system

A series pulse-modulator was constructed to furnish pulses of variable width, repetition rate and amplitude of peak current through an arc across a known gap. The modulator used a 3E29, driven from a Measurements Model 79B pulse generator, as a cathode-follower to drive a type 715C tube. The latter tube permitted operation up to 15 kV (tube rating 25 kV) with a plate current of 14 A at the required duty factor. The circuit diagram for this modulator is shown in *Figure 1*.

The voltage wave form across the gap was determined using a modified DuMont Model 303 oscilloscope. The case and connections to deflection plates D3 and D4 were removed. Both D3 and D4 were returned to a common power supply (G.E. Model PS-2) through 200kΩ resistors and

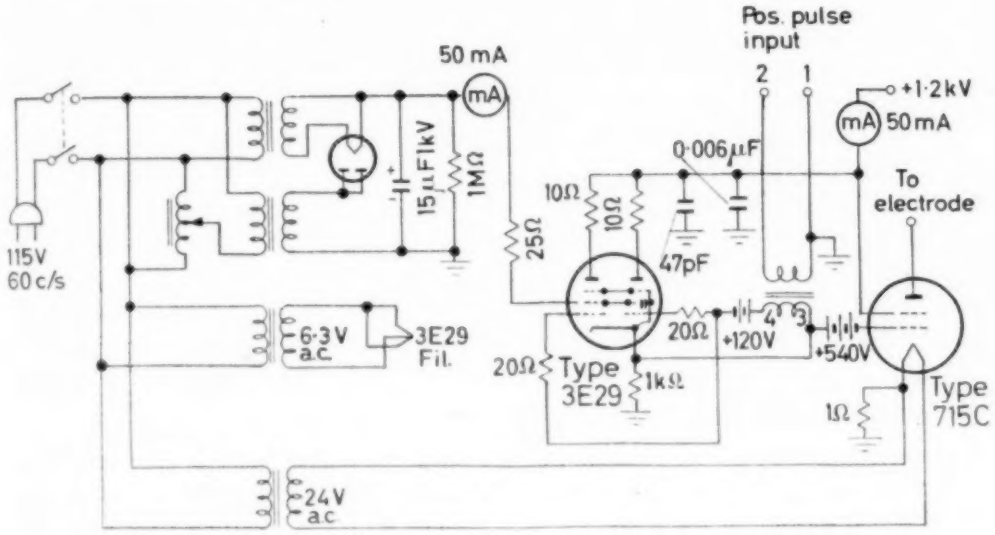

Figure 1. 15 kV *pulse modulator*

by-passed at this common point by a 0·05 μF tubular condenser and a 5000 pF disc ceramic condenser to earth. The common power supply was adjusted to between 280 and 300 V to give proper focus of the beam under pulsed conditions. Two 2500 pF, 3 kV condensers were used as coupling between each electrode at the gap and the deflection plates D3 and D4 on the oscilloscope. One-thousand ohm resistors were required in each of these leads at the point where they made connection to the electrodes to reduce the Q of the tuned circuit formed by the leads connecting the oscilloscope to the electrodes. This modification is necessary as it was found by trial that if the voltage measurements were taken on an oscilloscope (with a single-ended input) connected between the electrode attached to the plate of the modulator and earth that consecutive traces would not coincide with each other. This multiple-trace pattern is present because, at a 360 c/s repetition rate, 6 pulses will appear during one cycle of a conventional 60 c/s, half-wave power supply. Since the filter condenser does not get recharged between the pulses it is difficult to read accurately the amplitude of the voltage wave form.

Current wave forms were taken by inserting a 1-ohm resistor (ten 10-ohm resistors in parallel) between the cathode of the modulator and earth. This method gave a single-ended source for measuring the current wave form with one disadvantage, that of compensating for grid current. The cathode of the modulator tube was connected through a 1000-ohm resistor to the input of an unmodified model 514 Tektronix oscilloscope. The purpose of the resistor was to lower the Q in this portion of the circuit because a slight amount of ringing was present in the beginning of each pulse. Since

the input impedance of the oscilloscope was one megohm, the addition of the 1000-ohm resistor did not introduce sufficient error in current measurement to require compensation when using the internal calibration facilities of the oscilloscope.

Pertinent points in the design of this modulator are:

(*a*) The bias batteries are made up of Eveready No. 413 cells mounted on Plexiglas plates. These plates were mounted on one-inch ceramic stand-off insulators to lower the component capacity to earth.

(*b*) Westinghouse model 1–F–19 pulse transformer was used on the input, as the grid of the 3E29 returned to its cathode. Although pulses in the range 800 to 1000 V were obtained from the cathode of the 3E29 there was no indication of breakdown in this small pulse transformer.

(*c*) The resistor used in the cathode circuit of the 3E29 was a 1000-ohm 25-W non-inductive type manufactured by Sprague with a trade name of 'Koolohm'.

(*d*) The lead from the plate cap of the modulator to the electrode should be as short as possible. In this experiment it was about 2 in. long.

(*e*) During a portion of this experiment both the voltage oscilloscope and the current oscilloscope were triggered from the Measurements model 79B pulse generator. A delay line was inserted in the input of the pulse modulator which gave approximately one-half a microsecond of base line display before the starting of the pulse. This was quite helpful in determining exact amplitudes of pulses.

Electrode system

The micrometer cross slide from a Wilder Micro Projector was modified to hold two 1/8-in. electrodes in insulated holders. This facilitated manipulation of the electrodes in two planes, alignment in a horizontal plane and gap distance between the points of the electrodes.

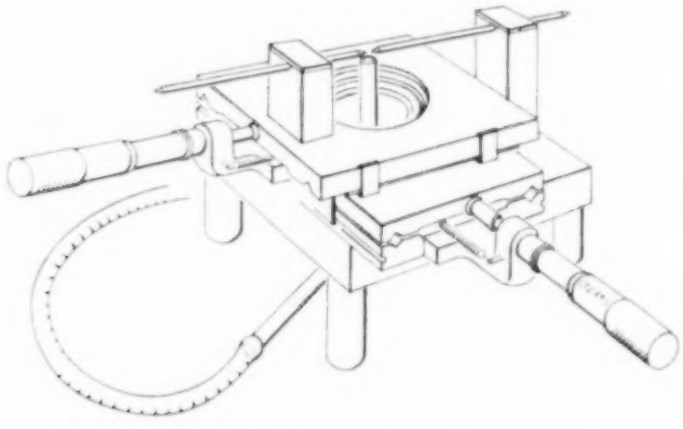

Figure 2. Electrode support and spacing equipment

A silica glass tube of 8 mm i.d. was firmly supported through a hole in the base of the cross slide and extended through the holes in the centre of the cross slide to a position 2 mm below the points of the electrodes. *Figure 2* illustrates the cross slide with the above modification.

Pure tungsten electrodes, 6 in. long by 1/8 in. in diameter, were used throughout all the experiments. The tips of the electrodes were ground to a sharp point with an included angle of 34° on a Brown and Sharpe No. 13 cylindrical grinder using a $7 \times \frac{1}{2}$ in., 120 grit diamond faced wheel. In order to obtain more consistent breakdown voltages for each pulse the electrode which was used as the cathode was given a coat of oxide[2] by being heated to 800°C for 10 minutes in air.

Photographs of the equipment, electrode set-up and typical current and voltage wave shapes are shown below (*Figures 6* to *9*). The wave shapes attest to the uniformity of energy input rate obtainable with the system used.

Flow system

A flow system indicated by the sketch in *Figure 3* was employed. The rotameters were Fischer–Porter Tri-Flat meters. The meter for airflow determination consisted of tube—02F–1/8–12–5 and stainless steel float 18, for neo-pentane 08F–1/16–16–4 and sapphire float—16.

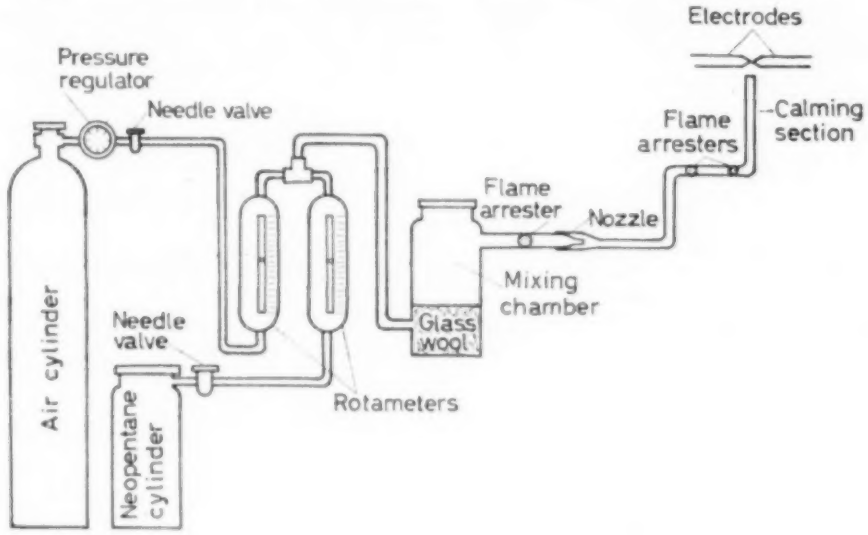

Figure 3. Fuel system

The composition of the gas mixture was chosen to give minimum ignition energy. It was determined experimentally to be 1·4 times stoichiometric (i.e. 40 per cent more neo-pentane than could be completely oxidized by the oxygen in the mixture).

The gas velocity was established by the requirement that it should be the minimum velocity that would stabilize a flame at the mouth of the 8 mm (i.d.) glass tube. The velocity thus measured was 1450 cm^3/min. This value corresponds to a Reynolds number of 256 which is well within the laminar range. C. C. SWETT[3] has shown that at this velocity the effect of gas flow on ignition energy requirements is very small.

RESULTS

Table 1 includes data taken with the multipulse system. These data are arranged to show the variation of the energy per pulse which is required

Table 1

Gap spacing mil	*Current* A	*Voltage* V	*Pulse width* μsec	*Energy* J × 10⁴
5	13·3	30	8	32·0
10	7·0	30	8	16·8
12	11·5	30	4	13·8
13	7·9	30	6	14·1
15	10·0	30	4	12·0
15	6·0	32	6	11·5
20	8·4	30	4	10·0
30	7·0	33	2	4·6
30	4·9	33	3	4·8
30	3·7	33	3	4·9
32	3·0	33	4	3·9
33	6·0	33	2	3·9
33	11·1	33	1	3·7
40	8·2	36	1	2·9
40	2·0	36	4	2·9
40	4·0	36	2	2·9
40	7·8	36	1	2·8
40	8·1	35	1	2·8
40	8·0	35	1	2·8
40	4·5	30	2	2·6
40	4·4	33	2	2·7
46	3·4	33	2	2·2
50	4·0	39	1	1·6
60	2·1	*Not readable*	1	?

to ignite the optimum mixture (1·4 times the stoichiometric on the rich side). The data were taken at a pulse repetition rate of 360 pulses per second and a pulse width of two to eight microseconds (the pulse width is shown subsequently to be independent of minimum energy requirement).

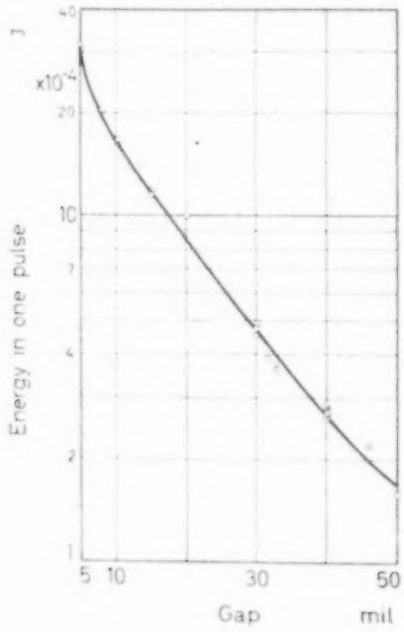

Figure 4. Pulse ignition data

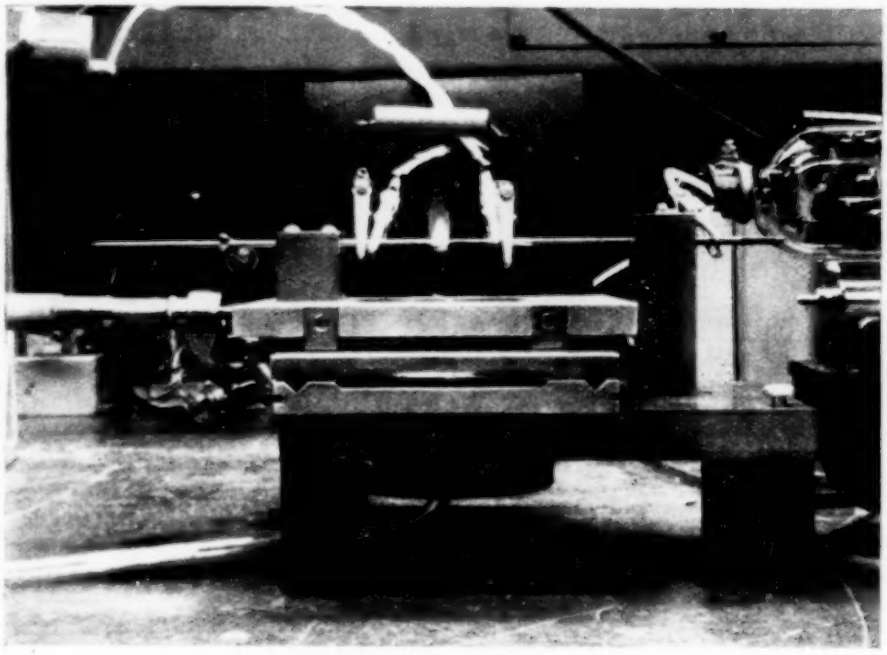

Figure 5. Arcing and ignition with laboratory set-up

The data from *Table 1* are plotted in *Figure 4* as pulse energy required for ignition versus gap spacing. *Figure 5* shows the resulting ignition, while *Figures 6* to *8* illustrate typical wave forms and *Figure 9* gives the set-up for voltage measurement.

The reproducibility was surprisingly good when two effects were eliminated. First of all, it was learned that blowing out the flame after ignition would cause enough moisture deposition around the mouth of the tube to affect results. The proper extinguishing technique was found to be a

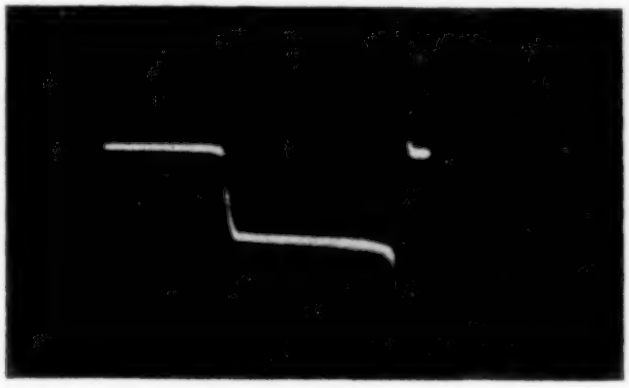

Figure 6. Voltage pulse wave form. 8 μsec. 30V

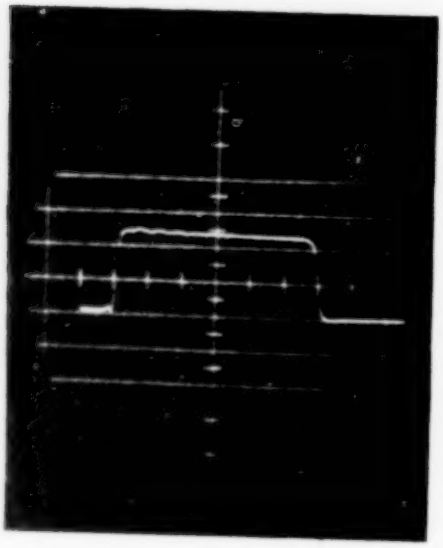

Figure 7. Current pulse wave form. 6 μsec. 4·75A

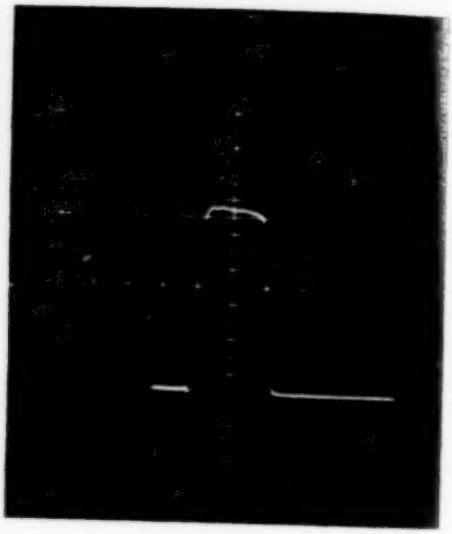

Figure 8. Current pulse wave form. 2 μsec. 10·5A

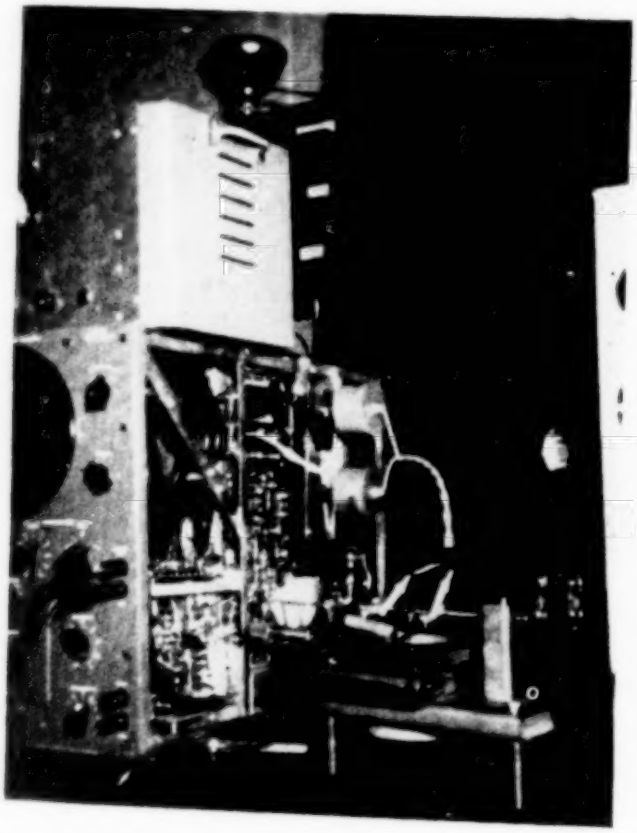

Figure 9. Electrode set-up showing connection to voltage measurement oscilloscope

'pinching-off' of the gas supply, causing a temporary flashback of the flame, then a sudden release of the supply which caused a 'blow-out'. Secondly, a time for cooling of about 15 seconds between bursts was required to ensure that the electrodes did not heat up unduly.

Effect of pulse width

An approximate analysis of the thermal dissipation—considering radiation and conduction through the electrodes—from the arc region indicated that the energy in a pulse required for ignition would be appreciably increased with decreasing energy input rate only if the time of input was of the order of milliseconds. Thus the effect in the few microsecond range would not be expected to be noticeable. This conviction was borne out by measurements at thirty and forty mil gap spacings tabulated in *Table 1* and in addition the results shown in *Table 2* at thirty four mils.

Table 2

Pulse width μsec	*Current* A	*Voltage* V	*Gap spacing* mil	*Energy* $I \times 10^3$
8	1·5	30	34	3·60
4	2·9	30	34	3·48
2	5·8	30	34	3·48

Effect of pulse repetition rate

From the results of H. WHITE[1], it was surmised that gap recovery—both ionic and thermal—is practically complete after one millisecond. This time, of course, depends on the composition of the gases involved, the gas velocity and the electrode shapes and composition. However, it was generally felt that if the pulse repetition rate did not exceed one thousand pulses per second the interpulse effects would not be noticeable. *Table 3* includes data at several pulse repetition rates.

Table 3

Pulse repetition rate p/s	*Current* A	*Voltage* V	*Gap* mil	*Energy* $J \times 10^3$
360	5·0	30	36	3·0
720	5·0	30	36	3·0
360	4·6	30	36	2·9
360	5·0	30	36	3·0
720	4·7	30	36	2·9
1440	5·6	30	36	3·4
720	5·5	30	36	3·3

These data seem to confirm the conviction stated above. At rates considerably more than 1000 p/s, the interpulse effects are presumed to be chiefly thermal until the time lag is of the order of ten microseconds. The problem of recurrent breakdown was studied by R. COOPER[2] who also gave indications of recovery time by the dielectric strength measurements.

Correlation with capacitor discharge results

There is surprisingly good agreement between the results given above and those obtained with capacitor discharge measurements. The effect of gap spacing with pointed electrodes was observed to be similar using both techniques. The pulse technique, however, did yield lower ignition energies at wide gap spacings than did the capacitor discharge method. For instance, the minimum value found by the latter technique was approximately $2{\cdot}6 \times 10^{-4}$ J at a spacing of about 80 mils, whereas only $1{\cdot}6 \times 10^{-4}$ J at 50 mils was required with the pulse technique. In addition, even lower values were indicated at wider spacings, but could not be measured accurately because of the difficulties of observing the voltage pulse under these conditions.

The authors wish to express their thanks to the Rome Air Force Development Center, Rome, New York, for sponsoring this work, and to Mr Zenn Zenon of the Heavy Military Department of General Electric for his cooperation.

G.E. Electronics Laboratory,
Syracuse, N.Y.

(*Received March 1957*)

REFERENCES

[1] LEWIS, B., VON ELBE, G. and KARLOVITZ, B. Combustion and Explosives Research Inc. Private correspondence

[2] LLEWELLYN JONES, F. *Proc. phys. Soc. Lond. B* 62 (1949) 366

[3] SWETT, C. C. *Third Symposium (International) on Combustion, Flame and Explosion Phenomena*, p. 363 Williams and Wilkins: Baltimore, 1949

[4] WHITE, H. *Z. Phys.* 88 (1934) 415

[5] COOPER, R. *J. Instn elect. Engrs* 95 (II) (1948) 378

*Temperature Stability of the Laminar Combustion Wave**

J. F. WEHNER† and J. B. ROSEN‡

The solution to a simplified form of the linearized time-dependent energy equation of a laminar flame has been considered in order to develop a criterion for the stability of such a flame. It is shown that for this energy equation the stability is determined by the behaviour of the concentration perturbation. The results also demonstrate that it is not justified without further investigation to assume that the solution to any particular steady-state flame equation is stable.

FROM accumulated knowledge about combustion a theory of laminar flame propagation has been developed[1] in which a system of steady-state conservation equations is built up and solved in varying approximations. From this theory, a relatively clear picture of the processes occurring in a laminar flame front is obtained, depending upon the approximations made.

A failure of the steady-state theory is that it gives no adequate explanation for the existence of flammability limits and possibly contradicts the experimental evidence for such limits. The theory predicts a finite value of flame velocity for all mixtures of combustible and oxidizer. However, an experimental plot of flame velocity versus composition falls very rapidly near the limit of inflammability and would appear to be extrapolated to zero at a finite concentration.

A possible explanation to the problem may be found in a study of the stability of the steady-state solutions to small perturbations. If solutions to the time-varying flame equations do not decay into the steady-state solutions, the steady-state solution is unstable and cannot be realized physically since small perturbations from the steady-state will certainly occur. An adequate explanation for flammability limits would be obtained if it could be shown that a stable steady-state solution can be changed to an unstable solution by varying the steady-state parameter corresponding to concentration.

To show whether or not the above hypothesis has any basis in fact is a difficult task because of the number of equations which must be solved simultaneously. Even in the steady state, when more than one equation is necessary, it is a major task to obtain exact solutions to the equations for even one set of steady-state parameters, and approximations have been sought to reduce the number of equations. Several investigators have studied the problem with various approximations. J. M. RICHARDSON[2] has studied the stability of a flame which can be represented by a single equation, either the continuity equation with diffusion or the energy balance

*This research was supported by the United States Air Force under Contract No. AF 33(038)-23976 monitored by the Office of Scientific Research.
†Present address: Department of Chemical Engineering, The Catholic University of America, Washington 17, D.C.
‡Present address: Shell Development Company, Emeryville, California.

equation, both of which have a similar form. He linearized the time-dependent equation about the steady state and assumed that the reaction rate is a function of temperature alone. The latter assumption is equivalent to assuming that the time-dependent concentration is instantaneously given by the steady-state value of concentration corresponding to the time-dependent temperature variation. The equation is always stable in this approximation. H. EINBINDER[3] also considered a single linearized energy equation including one more term than Richardson, but making the steady-state concentration assumption. He assigned average values of coefficients in various parts of the flame and found complete stability. D. LAYZER[4] has considered the stability of the energy equation without linearization about the steady state, but the approximation also is made of giving the concentration its steady-state variation. Layzer found no evidence for instability. J. B. ROSEN[5] has integrated the complete set of linearized time-dependent flame equations for a single reaction flame with no diffusion. He found that a temperature perturbation could grow with time—the first instance that an instability has been demonstrated for a flame where pressure effects are not taken into account. Later numerical calculations by J. B. ROSEN[6] on the ozone flame show that stability depends upon the mole fraction of ozone present initially when a three-component system is considered.

DEVELOPMENT OF SYSTEM OF EQUATIONS

Present work is an attempt to clarify the differences between previous hypotheses and to develop further a criterion for the determination of the stability of a particular set of flame equations.

Consider then a single reaction flame in which diffusion of fuel and product are allowed. The molecular weight of fuel and product are assumed equal. The thermal conductivity and specific heat of the mixture will be considered constant. The diffusivity of fuel and product is assumed to be proportional to temperature. Let the symbols have the following significance.

Nomenclature

c_p = specific heat at constant pressure
D = diffusion constant
G = fraction of mass flow due to fuel
Δh = heat of reaction
k = pre-exponential part of specific reaction rate (considered constant)
m = mass-flow perturbation
M = mass flow
$P = R/k\phi$ = dimensionless reaction rate = $P(\phi, Y)$
R = reaction rate = $R(T, Y)$
t = time
T = temperature
V = potential function (see equation 19)
x = distance
y = concentration perturbation
Y = concentration (mass fraction of fuel)
$z = (k\rho_a/M)x$ = dimensionless distance
$\beta = c_p M^2/\lambda k \rho_a$ = mass-flow eigenvalue in dimensionless form

δ = stability eigenvalue
$\eta = \Delta h / c_p T_0$ = dimensionless heat of reaction
$\theta = kt$ = dimensionless time
λ = thermal conductivity
ζ = reduced distance variable (see equation 17)
ρ = density $= \rho_0 / \phi$
τ = temperature perturbation
$\phi = T / T_0$ = dimensionless temperature
ψ = reduced temperature perturbation

Subscripts: 0 = cold gas; ∞ = hot gas

Others indicate partial derivatives except where the equation reduces to a total differential equation, where they indicate total derivatives.

Equations

The complete time-dependent flame equations with these assumptions are:
Energy balance

$$\rho c_p T_t + M c_p T_x - \lambda T_{xx} + \rho \Delta h R(T, Y) = 0 \quad \ldots . [1]$$

Continuity of individual component

$$\rho Y_t + M Y_x - D \rho Y_{xx} - \rho R = 0 \quad \ldots . [2]$$

Total continuity

$$\rho_t + M_x = 0 \quad \ldots . [3]$$

Equation of state

$$\rho = \rho_0 T_0 / T \quad \ldots . [4]$$

Steady-state equations are obtained from these equations by setting the time derivative terms equal to zero. The steady-state solutions to these equations under the boundary conditions that derivatives of temperature and concentration are zero at $\pm\infty$ are obtained as follows. If $D = 0$ or $\lambda / c_p \rho$, the problem reduces to the integration of a single equation which has M as an eigenvalue. For $D = 0$, equation 2 is substituted into equation 1 followed by a single integration. Dividing equation 2 by the result eliminates the distance variable. The resulting equation can be integrated from the hot to the cold boundary for various values of M until the boundary conditions are satisfied, if the reaction rate is assumed to vanish in the cold gas. For $D = \lambda / c_p \rho$, Y becomes a known[7] linear function of T, $Y = L(T)$. The eigenvalue problem is solved by introducing a variable G, the fraction of the mass flow due to the fuel as defined by

$$\rho Y_x = M(Y - G) / D \quad \ldots . [5]$$

By taking $\mathrm{d}/\mathrm{d}x$ of equation 5 the variable Y can be eliminated from equation 2 for steady state, giving

$$M G_x = \rho R[T, L(T)] \quad \ldots . [6]$$

Using this in equation 1 for steady state and integrating from the cold boundary gives

$$\lambda T_x = M[c_p(T - T_0) + \Delta h(G - Y_0)] \quad \ldots . [7]$$

Dividing equation 6 by equation 7 gives a single equation which together with the hot and cold boundary conditions determines the eigenvalue M

equation, both of which have a similar form. He linearized the time-dependent equation about the steady state and assumed that the reaction rate is a function of temperature alone. The latter assumption is equivalent to assuming that the time-dependent concentration is instantaneously given by the steady-state value of concentration corresponding to the time-dependent temperature variation. The equation is always stable in this approximation. H. EINBINDER[3] also considered a single linearized energy equation including one more term than Richardson, but making the steady-state concentration assumption. He assigned average values of coefficients in various parts of the flame and found complete stability. D. LAYZER[4] has considered the stability of the energy equation without linearization about the steady state, but the approximation also is made of giving the concentration its steady-state variation. Layzer found no evidence for instability. J. B. ROSEN[5] has integrated the complete set of linearized time-dependent flame equations for a single reaction flame with no diffusion. He found that a temperature perturbation could grow with time—the first instance that an instability has been demonstrated for a flame where pressure effects are not taken into account. Later numerical calculations by J. B. ROSEN[6] on the ozone flame show that stability depends upon the mole fraction of ozone present initially when a three-component system is considered.

DEVELOPMENT OF SYSTEM OF EQUATIONS

Present work is an attempt to clarify the differences between previous hypotheses and to develop further a criterion for the determination of the stability of a particular set of flame equations.

Consider then a single reaction flame in which diffusion of fuel and product are allowed. The molecular weight of fuel and product are assumed equal. The thermal conductivity and specific heat of the mixture will be considered constant. The diffusivity of fuel and product is assumed to be proportional to temperature. Let the symbols have the following significance.

Nomenclature

c_p = specific heat at constant pressure
D = diffusion constant
G = fraction of mass flow due to fuel
Δh = heat of reaction
k = pre-exponential part of specific reaction rate (considered constant)
m = mass-flow perturbation
M = mass flow
$P = R/k\phi$ = dimensionless reaction rate = $P(\phi, Y)$
R = reaction rate = $R(T, Y)$
t = time
T = temperature
V = potential function (see equation 19)
x = distance
y = concentration perturbation
Y = concentration (mass fraction of fuel)
$z = (k\rho_a/M)x$ = dimensionless distance
$\beta = c_p M^2/\lambda k \rho_a$ = mass-flow eigenvalue in dimensionless form

δ = stability eigenvalue
$\eta = \Delta h / c_p T_0$ = dimensionless heat of reaction
$\theta = kt$ = dimensionless time
λ = thermal conductivity
ζ = reduced distance variable (see equation 17)
ρ = density $= \rho_0 / \phi$
τ = temperature perturbation
$\phi = T / T_0$ = dimensionless temperature
ψ = reduced temperature perturbation

Subscripts: 0 = cold gas; ∞ = hot gas

Others indicate partial derivatives except where the equation reduces to a total differential equation, where they indicate total derivatives.

Equations

The complete time-dependent flame equations with these assumptions are:

Energy balance

$$\rho c_p T_t + M c_p T_x - \lambda T_{xx} + \rho \Delta h R(T, Y) = 0 \quad \ldots . [1]$$

Continuity of individual component

$$\rho Y_t + M Y_x - D \rho Y_{xx} - \rho R = 0 \quad \ldots . [2]$$

Total continuity

$$\rho_t + M_x = 0 \quad \ldots . [3]$$

Equation of state

$$\rho = \rho_0 T_0 / T \quad \ldots . [4]$$

Steady-state equations are obtained from these equations by setting the time derivative terms equal to zero. The steady-state solutions to these equations under the boundary conditions that derivatives of temperature and concentration are zero at $\pm\infty$ are obtained as follows. If $D = 0$ or $\lambda / c_p \rho$, the problem reduces to the integration of a single equation which has M as an eigenvalue. For $D = 0$, equation 2 is substituted into equation 1 followed by a single integration. Dividing equation 2 by the result eliminates the distance variable. The resulting equation can be integrated from the hot to the cold boundary for various values of M until the boundary conditions are satisfied, if the reaction rate is assumed to vanish in the cold gas. For $D = \lambda / c_p \rho$, Y becomes a known[7] linear function of T, $Y = L(T)$. The eigenvalue problem is solved by introducing a variable G, the fraction of the mass flow due to the fuel as defined by

$$\rho Y_x = M(Y - G) / D \quad \ldots . [5]$$

By taking d/dx of equation 5 the variable Y can be eliminated from equation 2 for steady state, giving

$$M G_x = \rho R[T, L(T)] \quad \ldots . [6]$$

Using this in equation 1 for steady state and integrating from the cold boundary gives

$$\lambda T_x = M[c_p(T - T_0) + \Delta h(G - Y_0)] \quad \ldots . [7]$$

Dividing equation 6 by equation 7 gives a single equation which together with the hot and cold boundary conditions determines the eigenvalue M

and $G(T)$. For other values of D, the integral equation methods of G. KLEIN[8] can be applied, but very much more mathematical labour is involved. In all cases, after $G(T)$ or $Y(T)$ is obtained, the variation with distance is obtained by a single integration. The consideration of the time-dependent equations to follow assumes that the steady-state equations have been solved.

If τ, y and m are first-order perturbations from the steady-state conditions for dimensionless temperature T/T_0, concentration Y, and mass flow M/M_0, and if the various terms in the time-dependent equations are written as one-term Taylor series in the perturbations, the following set of linearized equations is obtained[5]:
Energy balance

$$\rho c_p T_0 \tau_t + M_0 c_p T_0 \tau_x + \rho \Delta h [R_T T_0 \tau + R_Y y] - (\Delta h \rho^2 / \rho_0) R\tau - \lambda T_0 \tau_{xx} + M_0 c_p T_x m = 0 \quad \ldots . [8]$$

Continuity of individual component

$$\rho y_t + M y_x - \rho [R_T T_0 \tau + R_Y y] + (\rho^2 / \rho_0) R\tau - D\rho y_{xx} + M_0 Y_x m = 0 \quad \ldots . [9]$$

Total continuity

$$m_x - \rho_0 (T_0^2 / T^2) \tau_t = 0 \quad \ldots . [10]$$

The coefficients are functions of the steady-state system only and are thus assumed known.

In view of difficulties in solving these equations simultaneously, it is of value to investigate a simplified version of these equations. In order to study the temperature perturbation the energy equation is of primary interest. The difficulty lies in the terms containing y and m since each requires another equation in order to be determined. In references 3 and 4 this difficulty is eliminated by assuming that y always has the value given by the steady-state approximation

$$y = T_0 (\mathrm{d}Y / \mathrm{d}T) \tau \quad \ldots . [11]$$

and that the effect of the mass flow perturbation term involving m can be neglected.

In the following analysis the effect of m will also be neglected, but a more general assumption concerning y will be made. Setting $m = 0$, the energy equation becomes

$$(\beta / \phi) \tau_\theta - \tau_{zz} + \beta \tau_z + \beta \eta P_T \tau + \beta \eta P_Y y = 0 \quad \ldots . [12]$$

the variables being expressed in dimensionless form. We will now make the additional assumption concerning y that

$$y = r(z) \tau \quad \ldots . [13]$$

where $r(z)$ is an arbitrary continuous and bounded function of z. Special cases are $r(z) = \mathrm{d}Y / \mathrm{d}\phi$ which is the steady-state approximation equation 11, and $r(z) = 0$ which gives $y = 0$.

It is shown in what follows that the energy equation is stable provided

$$r(z) \leqslant dY/d\phi \qquad \ldots.[14]$$

and unstable if

$$r(z) > dY/d\phi \qquad \ldots.[15]$$

The case where y is given by equation 11 is therefore just stable, while $y=0$ is unstable since we will always have $(dY/d\phi) < 0$.

Using equation 13, y is eliminated from the energy equation 12 so that it involves only the temperature perturbation τ. If the perturbation is required to go to zero at the boundaries and an exponential time dependence of the form $\tau = \tau(z)\exp(-\delta\theta)$ is assumed, the following eigenvalue equation for the eigenvalue δ is obtained

$$\beta\tau_z - \tau_{zz} + [\beta\eta(P_\phi + r(z)P_Y) - (\beta/\phi)\delta]\tau = 0 \qquad \ldots.[16]$$

The sign of δ determines whether or not the equation is stable, a negative sign indicating instability. The value of δ can be more easily determined by transforming the equation to one formally equivalent to the Schroedinger equation of quantum mechanics. The transformation is

$$\tau = \phi^{1/4}\psi(\zeta)\exp(\tfrac{1}{2}\beta z); \qquad \zeta = \int_0^z \phi^{-1/2}dz \qquad \ldots.[17]$$

and the resulting equation is

$$d^2\psi/d\zeta^2 + [\delta\beta - V(\zeta)]\psi = 0 \qquad \ldots.[18]$$

where

$$V(\zeta) = \beta\eta\phi(P_\phi + rP_Y) - \tfrac{1}{4}\phi_{zz} - \tfrac{5}{16}\phi_z^2 + \tfrac{1}{4}\beta^2\phi \qquad \ldots.[19]$$

This function, $V(\zeta)$, is positive at $\zeta = \pm\infty$, and has a negative minimum $V_{min.}$ at a finite value of ζ. The set of eigenvalues which comes from a solution of such an equation consists of a continuous set of positive values which lie above $\frac{1}{4}\beta$ and a possible set of discrete values lying between $\frac{1}{4}\beta$ and $V_{min.}/\beta$ provided that the well is wide and deep enough[9]. If the discrete values exist it is possible that they may be negative.

Whether or not the lowest discrete eigenvalue (if any exists) is negative depends on the shape of the well in addition to its width and depth. In a previous note[10] concerning the case $y=0$, it was assumed that the function $V(\zeta)$ could be approximated by a square well with a depth equal to the minimum of $V(\zeta)$. On this basis it was found that, depending on the $V(\zeta)$ determined by the steady-state parameters, there were both stable and unstable solutions of equation 12. The exact analysis below shows that equation 12 is always unstable for $y=0$, so that clearly the square well approximation is not a sufficiently good one.

Consider equation 16 with $r(z) = dY/d\phi$. The terms involving P then become the total derivative $dP/d\phi$, and the resulting equation is similar to the one considered by Richardson[2]. For $\delta = 0$ it has the solution $\tau = \phi_z$. This can be shown by taking the steady-state equation obtained from equation 1 in dimensionless variables and differentiating it with respect to z. This gives

$$\beta(\phi_z)_z - (\phi_z)_{zz} + \beta\eta[P_\phi + (dY/d\phi)P_Y]\phi_z = 0 \qquad \ldots.[20]$$

so that clearly ϕ_z satsifies the same equation as τ for $\delta=0$. Furthermore, $\tau=\phi_z$ goes to zero as $\exp(\beta z)$ at $z=-\infty$ and vanishes at $z=\infty$. Therefore, $\psi(\zeta)$ obtained from this τ by equation 17 vanishes exponentially at $\pm\infty$ and is a discrete solution. Since ϕ_z is nodeless, $\tau=\phi_z$ is the lowest solution of equation 16 and $\delta=0$ is therefore the minimum eigenvalue for $r=\mathrm{d}Y/\mathrm{d}\phi$. This case is therefore just stable.

Let $\bar{V}(\zeta)$ denote the function given by equation 19 for $r=\mathrm{d}Y/\mathrm{d}\phi$. The form of reaction rate $R(T, Y)$ assumed for flame equations is always such that $P_Y<0$, except at $\pm\infty$ where it may be zero. Then $V(\zeta)<\bar{V}(\zeta)$, for any $r(z)$ satisfying equation 15. As proved in the Appendix, this requires that the minimum δ corresponding to such an $r(z)$ be negative, so that for $r(z)>\mathrm{d}Y/\mathrm{d}\phi$ the energy equation is unstable. A similar argument shows that for $V(\zeta)\geqq\bar{V}(\zeta)$ the minimum $\delta\geqq 0$. Then it follows that for $r(z)\leqq\mathrm{d}Y/\mathrm{d}\phi$ the equation is stable.

We have thus shown that if the mass flow perturbation is neglected the stability depends entirely on the behaviour of the concentration perturbation. A small change in y relative to that in τ tends to instability. A large change in y of opposite sign to that of τ will tend to stabilize. In view of this it seems necessary, even for a two-component system, to include the effect of y and possibly m as well in the energy equation in order to get an accurate determination of stability as a function of the steady-state parameters. The results obtained also demonstrate that it is not justified without further investigation to assume that the solution to any particular steady-state flame equation is stable.

The authors wish to express their gratitude to Professor R. H. Wilhelm, Princeton University, for much helpful assistance during the course of the work.

James Forrestal Research Center,
Princeton University, N.J.

(Received March 1957)

APPENDIX

Assume that

$$\psi''+(\delta-V)\psi=0$$

and

$$\bar{\psi}''+(\bar{\delta}-\bar{V})\bar{\psi}=0$$

are two Schroedinger equations with potential functions

$$V(\zeta)<\bar{V}(\zeta)$$

which satisfy the boundary conditions that ψ and $\bar{\psi}$ approach zero exponentially as $\zeta\to\pm\infty$.

Multiplying by $\bar{\psi}$ and ψ respectively gives:

$$\bar{\psi}\psi''+(\delta-V)\psi\bar{\psi}=0$$

$$\psi\bar{\psi}''+(\bar{\delta}-\bar{V})\psi\bar{\psi}=0$$

Integrating each equation from $\zeta = -\infty$ to $\zeta = \infty$ and using integration by parts to evaluate the first term gives:

$$[\bar{\psi}\psi']_{-\infty}^{\infty} - \int \psi'\bar{\psi}'d\zeta + \int (\delta - V)\psi\bar{\psi}d\zeta = 0$$

$$[\psi\bar{\psi}']_{-\infty}^{\infty} - \int \bar{\psi}'\psi'd\zeta + \int (\bar{\delta} - V)\psi\bar{\psi}d\zeta = 0$$

The first term in each equation is zero because of the boundary conditions.

Subtracting the equations and solving for $\bar{\delta} - \delta$ gives

$$\bar{\delta} - \delta = \frac{\int (\bar{V} - V)\psi\bar{\psi}d\zeta}{\int \psi\bar{\psi}d\zeta}$$

ψ and $\bar{\psi}$ are nodeless functions when δ and $\bar{\delta}$ are the lowest eigenvalues (see reference 9) and do not change sign throughout the range of integration. Therefore $\bar{\delta} - \delta > 0$ and if $\bar{\delta}$ is zero, δ is negative.

REFERENCES

[1] HIRSCHFELDER, J. O., CURTISS, C. F. and BIRD, R. B. *The Molecular Properties of Gases and Liquids* Wiley: New York, 1954

[2] RICHARDSON, J. M. *Fourth International Symposium on Combustion* Williams and Wilkins: Baltimore, 1953

[3] EINBINDER, H. *J. chem. Phys.* 21 (1953) 480

[4] LAYZER, D. *J. chem. Phys.* 22 (1954) 222

[5] ROSEN, J. B. *J. chem. Phys.* 22 (1954) 733 and 743

[6] ROSEN, J. B. *Sixth Symposium on Combustion* Reinhold: New York, 1957

[7] VON KÁRMÁN, T. and PENNER, S. S. *Selected Combustion Problems* p. 14 NATO AGARD, Butterworths: London, 1954

[8] KLEIN, G. *Univ. Wis. Nav. Res. Lab. Rep.* 9 Jun 1954, 30 Sep 1954

[9] MORSE, P. and FESHBACH, H. *Methods of Theoretical Physics* pp. 1650-1655. McGraw-Hill: New York, 1953

[10] ROSEN, J. B. *J. chem. Phys.* 22 (1954) 750

so that clearly ϕ_z satsifies the same equation as τ for $\delta=0$. Furthermore, $\tau=\phi_z$ goes to zero as $\exp(\beta z)$ at $z=-\infty$ and vanishes at $z=\infty$. Therefore, $\psi(\zeta)$ obtained from this τ by equation 17 vanishes exponentially at $\pm\infty$ and is a discrete solution. Since ϕ_z is nodeless, $\tau=\phi_z$ is the lowest solution of equation 16 and $\delta=0$ is therefore the minimum eigenvalue for $r=\mathrm{d}Y/\mathrm{d}\phi$. This case is therefore just stable.

Let $\bar{V}(\zeta)$ denote the function given by equation 19 for $r=\mathrm{d}Y/\mathrm{d}\phi$. The form of reaction rate $R(T, Y)$ assumed for flame equations is always such that $P_Y<0$, except at $\pm\infty$ where it may be zero. Then $V(\zeta)<\bar{V}(\zeta)$, for any $r(z)$ satisfying equation 15. As proved in the Appendix, this requires that the minimum δ corresponding to such an $r(z)$ be negative, so that for $r(z)>\mathrm{d}Y/\mathrm{d}\phi$ the energy equation is unstable. A similar argument shows that for $V(\zeta)\geqslant\bar{V}(\zeta)$ the minimum $\delta\geqslant 0$. Then it follows that for $r(z)\leqslant\mathrm{d}Y/\mathrm{d}\phi$ the equation is stable.

We have thus shown that if the mass flow perturbation is neglected the stability depends entirely on the behaviour of the concentration perturbation. A small change in y relative to that in τ tends to instability. A large change in y of opposite sign to that of τ will tend to stabilize. In view of this it seems necessary, even for a two-component system, to include the effect of y and possibly m as well in the energy equation in order to get an accurate determination of stability as a function of the steady-state parameters. The results obtained also demonstrate that it is not justified without further investigation to assume that the solution to any particular steady-state flame equation is stable.

The authors wish to express their gratitude to Professor R. H. Wilhelm, Princeton University, for much helpful assistance during the course of the work.

James Forrestal Research Center,
Princeton University, N.J.

(Received March 1957)

APPENDIX

Assume that

$$\psi''+(\delta-V)\psi=0$$

and

$$\bar{\psi}''+(\bar{\delta}-\bar{V})\bar{\psi}=0$$

are two Schroedinger equations with potential functions

$$V(\zeta)<\bar{V}(\zeta)$$

which satisfy the boundary conditions that ψ and $\bar{\psi}$ approach zero exponentially as $\zeta\to\pm\infty$.

Multiplying by $\bar{\psi}$ and ψ respectively gives:

$$\bar{\psi}\psi''+(\delta-V)\psi\bar{\psi}=0$$

$$\psi\bar{\psi}''+(\bar{\delta}-\bar{V})\psi\bar{\psi}=0$$

Integrating each equation from $\zeta = -\infty$ to $\zeta = \infty$ and using integration by parts to evaluate the first term gives:

$$[\bar{\psi}\psi']_{-\infty}^{\infty} - \int \psi'\bar{\psi}'d\zeta + \int (\delta - V)\psi\bar{\psi}d\zeta = 0$$

$$[\psi\bar{\psi}']_{-\infty}^{\infty} - \int \bar{\psi}'\psi'd\zeta + \int (\bar{\delta} - V)\psi\bar{\psi}d\zeta = 0$$

The first term in each equation is zero because of the boundary conditions.

Subtracting the equations and solving for $\bar{\delta} - \delta$ gives

$$\bar{\delta} - \delta = \frac{\int (\bar{V} - V)\psi\bar{\psi}d\zeta}{\int \psi\bar{\psi}d\zeta}$$

ψ and $\bar{\psi}$ are nodeless functions when δ and $\bar{\delta}$ are the lowest eigenvalues (see reference 9) and do not change sign throughout the range of integration. Therefore $\bar{\delta} - \delta > 0$ and if $\bar{\delta}$ is zero, δ is negative.

REFERENCES

[1] HIRSCHFELDER, J. O., CURTISS, C. F. and BIRD, R. B. *The Molecular Properties of Gases and Liquids* Wiley: New York, 1954

[2] RICHARDSON, J. M. *Fourth International Symposium on Combustion* Williams and Wilkins: Baltimore, 1953

[3] EINBINDER, H. *J. chem. Phys.* 21 (1953) 480

[4] LAYZER, D. *J. chem. Phys.* 22 (1954) 222

[5] ROSEN, J. B. *J. chem. Phys.* 22 (1954) 733 and 743

[6] ROSEN, J. B. *Sixth Symposium on Combustion* Reinhold: New York, 1957

[7] VON KÁRMÁN, T. and PENNER, S. S. *Selected Combustion Problems* p. 14 NATO AGARD, Butterworths: London, 1954

[8] KLEIN, G. *Univ. Wis. Nav. Res. Lab. Rep.* 9 Jun 1954, 30 Sep 1954

[9] MORSE, P. and FESHBACH, H. *Methods of Theoretical Physics* pp. 1650-1655. McGraw-Hill: New York, 1953

[10] ROSEN, J. B. *J. chem. Phys.* 22 (1954) 750

Present Status of Information on Transport Properties Applicable to Combustion Research

A. A. WESTENBERG

A survey is presented of the available experimental and theoretical information on molecular diffusion and thermal conductivity coefficients likely to be of interest in low speed combustion studies. Emphasis is placed on high temperature data and practical methods of calculation. Reliability of present information is discussed, and the great lack of experimental data is pointed out. No pretence of a complete summary is made, but most of the best existing sources are indicated. Consideration of viscosity or dense gas effects is specifically excluded.

AT the outset, let it be stated that this review has strictly limited objectives. The study of transport properties of gases is a broad and complex field in which research is being actively carried out along many lines, and has been for over a century. A general review of the subject would be out of place in this journal and beyond the author's competence. The theoretical background is covered in great detail in the exhaustive and very useful treatise by J. O. HIRSCHFELDER, C. F. CURTISS and R. B. BIRD[1], which also includes most of the important published experimental results up to the end of 1953. All workers interested in molecular properties of fluids are greatly indebted to these authors, and this reviewer readily acknowledges his own heavy reliance on their book in preparing this article. E. W. MONTROLL and M. S. GREEN[2] have reviewed the statistical mechanics of transport processes to the end of 1953. Current literature since then has been summarized in the annual reviews of chemical engineering fundamentals published in the supplement to the March issue of *Industrial and Engineering Chemistry*[3]. Presumably this very useful series will continue. E. S. CAMPBELL and J. O. HIRSCHFELDER[4] have reviewed the situation regarding transport properties specifically pertinent to the hydrogen–bromine flame, but much useful general information is included also. A thorough bibliography of transport (and thermodynamic) data compiled by the U.S. Bureau of Standards has recently been given by J. HILSENRATH[5] covering the literature from 1945 to 1954. This is a valuable reference, as it contains concise indexes to the available theoretical and experimental papers on various transport properties, and a summary of review articles and compilations.

What is presented here is a summary of the available transport property information which is of particular importance in current combustion research. Recent trends in the study of laminar flames, for example, point strongly to the need for accurate data on the diffusion and heat conduction of gases at high temperatures. Detailed temperature[6–8], aerodynamic[6], and

composition[9, 10] profiles are being obtained in laminar flames of various kinds. The analysis of these data in terms of mass[11] and heat[7] transport and chemical kinetics[12] requires reliable knowledge of molecular transport phenomena. Flame structure research of this kind has now passed the stage (characteristic of much of the earlier theoretical and experimental work) where gross approximations, average values, or complete neglect of transport processes would suffice. The new technique for studying turbulent flames involving an inert gas tracer[13] requires high temperature molecular diffusion coefficient data. The present trend to higher and higher flight speeds in aircraft and missiles has begun to stimulate research in high temperature transport properties of dissociated, excited and ionized gases.

With the aim of this review as set forth above restricted to transport properties of interest in combustion research, let us further define the field to include only thermal conductivity and ordinary (concentration) diffusion. Viscous effects are generally (and quite legitimately) neglected in low speed combustion studies of the type under discussion here, although this will no longer be possible as techniques of analysis are extended to high speed flames. The other transport processes such as thermal diffusion, pressure diffusion, etc., are too minor to be considered at present*. Another limitation of this review is that transport properties at only low and moderate pressure, are considered, so that complexities due to dense gas effects are excluded as being unimportant in combustion generally. This means that thermal conductivity and diffusion coefficients are strictly treated as independent of, and inversely proportional to, pressure respectively. One final restriction perhaps ought to be mentioned explicitly for the sake of completeness. We are assuming throughout that in most combustion problems one does not deal with gradients so great that it is impossible to define a 'simple' transport coefficient, i.e. we assume conditions are such that the Navier–Stokes equations apply (changes in macroscopic gas properties over the distance of a mean free path are small). This is certainly a good assumption.

Within these severe limitations it is hoped that this summary will be of practical use to those persons who have need for the best available information on transport properties applicable to combustion systems.

DIFFUSION COEFFICIENTS

The reaction zone in any practically attainable flame contains more than two chemical species† so that, rigorously, one must consider multi-component diffusion. The diffusion velocity of a particular species (see equation 11.2–50 on p 718 of reference 1) then depends on a set of multi-component diffusion coefficients each of which, in turn, depends in a complicated way on the ordinary binary diffusion coefficients of all the pairs in the mixture. In many common flames (notably those involving air as oxidant) one component is present in great excess so that it is possible to simplify the problem by regarding each of the other species one at a time as a trace in a binary mixture with the main component[11]. At any

*An exception to this statement is mentioned in a footnote of reference 11.
†This is true even of the ozone decomposition flame unless the oxygen atoms are ignored.

rate, the treatment of molecular diffusion depends basically on a knowledge of binary diffusion coefficients.

Experimental

Unfortunately, the data available on molecular diffusion coefficients of gases at room temperatures are quite scanty, while high temperature data are practically non-existent. The great majority of measurements have been made using the basic techniques of either J. LOSCHMIDT[14] or J. STEFAN[15], with various refinements. L. WALDMAN[16] has made interesting use of the Dufour effect (the reciprocal effect to thermal diffusion) to determine some diffusion coefficients, while the rate of approach to the steady state in thermal diffusion has been employed by P. T. NETTLEY[17] and by H. K. LONSDALE and E. A. MASON[18]. *Table 1* contains the

Table 1. Experimental binary diffusion coefficients at 298° K and 1 atm

Gas pair	*D* $cm^2\ sec^{-1}$	*Reference*	*Gas pair*	*D* $cm^2\ sec^{-1}$	*Reference*
N_2–He	0·71	19	CO_2–O_2	0·16	21
N_2–A	0·20	16	CO_2–CO	0·16	26
N_2–H_2	0·78	20	CO_2–C_2H_4	0·15	26
N_2–O_2	0·22	21	CO_2–CH_4	0·18	26
N_2–CO	0·22	22	CO_2–H_2O	0·19	24
N_2–CO_2	0·16	23	CO_2–C_3H_8	0·086	29
N_2–H_2O	0·24	24	CO_2–C_2H_4O	0·092	29
N_2–C_2H_4	0·16	23	CO_2–CS_2	0·074	15
N_2–C_2H_6	0·15	23	CO_2–C_6H_6	0·061	28
N_2–n-C_4H_{10}	0·096	23	H_2O–CH_4	0·28	24
H_2–n-C_4H_{10}	0·38	25	H_2O–C_2H_4	0·20	24
H_2–O_2	0·81	26	H_2O–O_2	0·27	24
H_2–CO	0·75	26	CO–O_2	0·21	26
H_2–CO_2	0·65	23	CO–C_2H_4	0·13	26
H_2–CH_4	0·73	23	O_2–C_6H_6	0·073	30
H_2–C_2H_4	0·60	23			
H_2–C_2H_6	0·54	23			
H_2–H_2O	0·99	24			
H_2–Br_2	0·58	27			
H_2–C_6H_6	0·34	28			

available values collected from various sources for the gas pairs likely to be of use in combustion studies. All are given for 1 atm pressure and have been slightly corrected (where necessary) to 25° C. Two significant figures are listed, although the probable accuracy may be greater or less in some cases. The data collected in *Table 1*, while containing many common flame constituents, obviously do not include many important pairs, so that there is need for a great deal more experimental work in this field.

Much more serious, however, is the nearly complete absence of experimental diffusion data at the temperatures encountered in flames, or even approaching such temperatures. To the author's knowledge, the only measurements which have been made at fairly high temperature are those

on carbon dioxide–air and water–air by T. M. KLIBANOV *et al.*[31]. They used a capillary-leak method which is closely related to the classic Loschmidt method, and obtained the results shown in *Figure 1*. The data are not

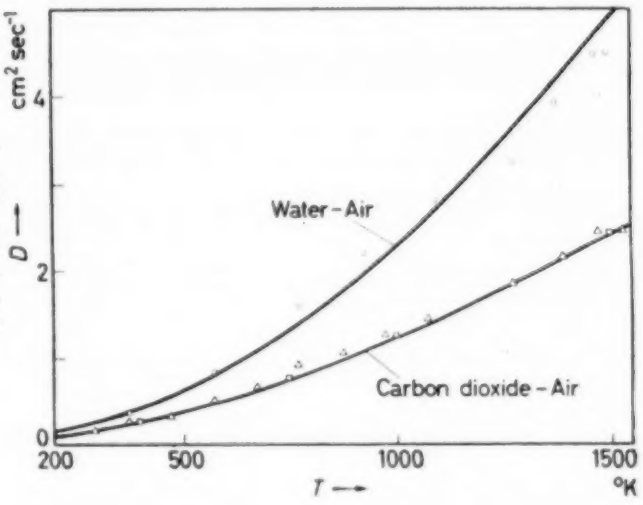

Figure 1. High temperature diffusion coefficients. Carbon dioxide–air: △, experimental data of reference 31; □, calculated from equation 1; ——, calculated from equation 4. Water–air: ○, experimental data of reference 31; ——, fitted by $T^{1.89}$

very precise, as each point represents an average over several runs in which the experimental scatter is as much as 20 per cent. These measurements are of great interest, however, since the temperature range up to 1500°K is much the highest covered so far, and the gas pairs used are certainly pertinent to combustion. The nearest approach to this work from the point of view of temperature attained appears to be the data on noble gases obtained recently by K. SCHÄFER and K. SCHUHMANN[32] over a temperature range of 90° to 473°K. R. A. STREHLOW'S[23] high precision measurements extended to 430°K. No other published results known to the author have exceeded about 400°K. The reasons for this are fairly obvious. Diffusion measurements are difficult even at ordinary temperatures, and extension of the conventional techniques to higher temperature multiplies the problems enormously. All of the common static methods require very careful temperature control to avoid thermal convection currents which would completely upset the molecular transfer process. Recently, some preliminary room temperature results with an entirely different technique have been reported by A. A. WESTENBERG and R. E. WALKER[33]. This involves injecting one gas as a tracer from a tiny tube (point source) into a slow laminar stream of the second gas. From measurements of the concentration downstream the diffusion coefficient can be derived. By heating the main carrier gas, the possibility of extending these (quite precise) measurements to high temperatures seems promising, and research in this direction is continuing.

Experimental data on diffusion in systems of more than two components which would be of application to flames are almost completely lacking. A few such measurements have been reported[34], but the field is a fertile one for further research.

Theoretical

Aside from its own great intrinsic interest, the scarcity of experimental data pointed out above has made the theoretical treatment of molecular diffusion indispensable in practical applications—especially at high temperature. There have been a good many empirical or quasi-theoretical relations proposed for predicting binary diffusion coefficients and their temperature dependence. The better known of these have been reviewed recently and compared by C. R. WILKE and C. Y. LEE[35], and will not be discussed here since they are of historical importance only. The best estimates of diffusion coefficients presently possible are those based firmly on the rigorous Chapman–Enskog kinetic theory of dilute gases. This is thoroughly discussed by Hirschfelder, Curtiss and Bird[1]. In their notation, the first approximation‡ to the binary diffusion coefficient for spherical, non-polar molecules is given ($cm^2\ sec^{-1}$) by

$$D = \frac{0{\cdot}00263\,[T^3(M_1+M_2)/2M_1M_2]^{\frac{1}{2}}}{P\sigma_{12}^{\,2}\Omega^{(1,1)*}} \qquad \ldots.[1]$$

where T is the temperature in °K, M_1 and M_2 are the molecular weights of species 1 and 2, and P is the pressure in atmospheres. The parameter σ_{12} (Ångstrom units) is characteristic of the interaction potential energy between the two species (the average collision diameter of simple kinetic theory), and $\Omega^{(1,1)*}$ is the so-called collision integral also determined by the interaction potential. These integrals have been numerically calculated for the physically realistic Lennard-Jones (6-12) potential by Hirschfelder, Curtiss and Bird[1], and for the modified Buckingham (exp – 6) potential by E. A. MASON[36]. Both are tabulated as a function of $T^* = Tk/\varepsilon_{12}$, where ε_{12} is another potential parameter (depth of the minimum in potential energy of interaction) and k is Boltzmann's constant. Since there has been a great deal more use made of the Lennard-Jones potential than of the modified Buckingham one, we shall not consider the latter any further. Even though it should allow better fit to experimental data than the Lennard-Jones potential (it has three adjustable parameters instead of two), the advantages of the modified Buckingham potential are usually very slight or negligible[37-39].

In order to make use of equation 1 and the tabulated integral $\Omega^{(1,1)*}$ for the Lennard-Jones (6-12) potential, it is necessary to have values of σ_{12} and ε_{12}/k. In principle, the best way of obtaining these is by an empirical fit to measurements of the diffusion coefficient over a range of temperature. This has been done in only a few cases[19, 20, 25]. The alternative procedure is to deduce these quantities from the corresponding ones for the pure components by means of empirical 'combining laws'. Usually, these are simply

$$\sigma_{12} = (\sigma_1 + \sigma_2)/2;\ \ \varepsilon_{12} = (\varepsilon_1\varepsilon_2)^{\frac{1}{2}} \qquad \ldots.[2]$$

where σ_1, ε_1 and σ_2, ε_2 are obtained by fitting the (much more abundant) experimental viscosity or second virial coefficient data to the appropriate

‡To this approximation, the very slight concentration dependence of D does not appear.

kinetic theory relations. This is not entirely satisfactory, since the parameters which work well for one property of a pure gas are usually not the same as those applicable to another property of a mixture, nor is there any firm basis yet for such combining laws as equations 2. Nevertheless, this is the best available scheme, and tables of σ and ε for many common molecules are given in reference 1. It is recommended that, wherever possible, the viscosity parameters be used for transport property calculations rather than those derived from second virial coefficients. Parameters for gases of interest in combustion have been selected from this compilation and are given in *Table 2*.

Table 2. Parameters from viscosity for use in transport property calculations (from reference 1)

Gas	σ Å	ε/k °K	*Gas*	σ Å	ε/k °K
H_2	2·92	38	SO_2	4·29	252
D_2	2·95	39	C_2H_2	4·22	185
He	2·58	10·2	C_2H_4	4·23	205
A	3·46	116	C_2H_6	4·42	230
N_2	3·75	80	C_3H_8	5·06	254
O_2	3·54	88	n-C_4H_{10}	5·00	410
CO	3·71	88	i-C_4H_{10}	5·34	313
CO_2	3·90	213	n-C_5H_{12}	5·77	345
NO	3·60	91	C_6H_6	5·27	440
N_2O	3·82	237	CS_2	4·44	488
CH_4	3·80	144	*Air*	3·69	84

Hirschfelder, Curtiss and Bird[1] have used the calculation scheme described above on most of the gas pairs given in *Table 1*—the main exceptions being those involving water. The results generally agree with the experimental room temperature values to within five per cent, which is often within the experimental precision. Due to the lack of high temperature diffusion data, the theoretical predictions have not been tested much above room temperature. The only available case is that of carbon dioxide–air (considered as a binary mixture) shown in *Figure 1*, where theoretical calculations give the points plotted as squares. The generally satisfactory result is a hopeful sign that the theory may be considered fairly reliable for diffusion calculations at flame temperatures. On the other hand, the data of Schäfer and Schuhmann[32] on neon–argon and argon–krypton do not fit the Lennard-Jones calculations very well ($\sim$ 10 per cent) even to 473 °K. It seems likely, however, that this is mainly the fault of the viscosity parameters used, since the experimental temperature dependences of $T^{1\cdot73}$ and $T^{1\cdot75}$ for the two pairs are fairly close to the predicted values (see below). Schäfer and Schuhmann themselves used a square-well potential in their theoretical discussion, which is less realistic but has the empirical advantage of using three parameters.

This reviewer has had occasion to make an empirical approximation to the theory which has been very useful in flame calculations. The collision

integral for the Lennard-Jones (6-12) potential may be fitted by

$$\Omega^{(1,1)*} \simeq 1{\cdot}12(T^*)^{-0{\cdot}17} \quad \ldots . [3]$$

within two per cent in the range $3 \leqslant T^* \leqslant 200$. Using this relation in equation 1 yields

$$D = \frac{0{\cdot}00235[(M_1+M_2)/2M_1M_2]^{\frac{1}{2}}T^{1{\cdot}67}}{P\sigma_{12}^2(\varepsilon_{12}/k)^{0{\cdot}17}} \quad \ldots . [4]$$

This equation was used in the carbon dioxide–air example giving the curve† shown as the lower solid line in *Figure 1*. The only justification for such a purely empirical relation as equation 4 is convenience. In mathematical manipulations it is often handy to have an analytical function to represent the temperature dependence of diffusion coefficients. In flame work, conditions are such that T^* is nearly always greater than 3, so that equation 4 is valid. It should be emphasized, however, that this empirical relation rapidly breaks down for $T^* < 3$, and for such cases only the accurate, tabulated functions should be used.

Thus far all the theoretical discussion has been strictly applicable only to spherical non-polar molecules. Fortunately, most of the common, stable flame constituents fall into this category—or nearly enough so that the theory can be applied. The main exception, of course, is water which is strongly polar. It is possible, in principle, to apply interactions of the Lennard-Jones form to mixtures containing one polar and one non-polar component, provided different combining laws are used. These are discussed by Hirschfelder, Curtiss and Bird[1] (p 600) and some sample calculations given for the diffusion of water into several non-polar gases. The results agree with the limited experimental data fairly well (~ 10 per cent) near room temperature. It seems likely that the deviations would be much more serious at high temperatures, since the water–air data of *Figure 1* follow approximately a $T^{1{\cdot}89}$ dependence (shown by the solid line) while the tabulated Lennard-Jones functions would predict $T^{1{\cdot}67}$. For the interaction of two polar molecules, the potential is strongly angular-dependent and the Stockmayer potential is physically fairly realistic. No calculations on transport properties have been made with this as yet, however, so that there are no good theoretical predictions possible at present for transport involving polar molecules.

The formal development of a kinetic theory for rigid, non-spherical molecules has been initiated[10-12], but practical transport calculations are a long way off. The estimation of diffusion coefficients for atoms, radicals, and electronically excited species which are so important in combustion is largely a matter of guesswork at present, since no experimental data are available and no satisfactory theory. J. O. Hirschfelder and M. A. Eliason[13] have recently made an interesting start on this problem. They indicate how one can make crude estimates of transport properties for these species, and show that, because of their great size, electronically

†The authors of reference 31 fit their data to an equation of the form

$$\frac{D}{D_c} = \frac{T_c+C}{T+C}\left(\frac{T}{T_c}\right)^{3/2}$$

where C is a constant. This relation works very little better than equation 4.

excited atoms and molecules would be expected to have abnormally low diffusion coefficients.

THERMAL CONDUCTIVITY

The transport of heat by molecular processes in any real polyatomic gas is considerably more complex than that of mass. The reason for this is that energy is carried in, and interchanged among, the internal degrees of freedom of the molecules as well as by translation, and these complications become more pronounced at high temperatures. Despite these difficulties (or perhaps because of them) there has been a good deal more effort spent on thermal conductivity (λ) than on ordinary diffusion, especially along experimental lines. There may be a practical reason for this in view of the importance of thermal conduction in engineering heat transfer applications. Consideration of any real flame involves heat transport in a mixture of polyatomic gases, but the properties of the mixture depend ultimately on the thermal conductivities of the individual components.

Experimental

Most of the measurements of gaseous thermal conductivity have been made in steady state systems subject to simple solutions of the appropriate equation of heat conduction, such as concentric cylinders, parallel plates, etc. The techniques are difficult, require many corrections and careful refinements, and, as usual, the problems increase as the temperature is raised. Nevertheless, the amount of data available is considerably greater than for diffusion—both with regard to variety of gases and range of temperature covered. The best available source for the thermal conductivities (as well as the thermodynamic functions) of several of the common flame gases is certainly the extensive and critical compilation of the National Bureau of Standards[44] (NBS). These tables were prepared from equations empirically fitted to the experimental data, and extrapolated somewhat in most cases. Entries are given at temperature intervals close enough so that linear interpolation is valid. The gases tabulated, along with their temperature ranges in °K, are as follows: air (80 to 1000), argon (90 to 1500), carbon dioxide (180 to 600), carbon monoxide (70 to 600), hydrogen (10 to 700), nitrogen (100 to 1200), oxygen (80 to 600), and water (300 to 800). The estimated reliability of the tables (i.e. the fit to the data) varies between two and five per cent in the temperature range of the experimental data. In the extrapolated ranges, the reliability is less. The literature is covered up to 1952.

The absolute reliability (accuracy) of the above tabulations may sometimes be more questionable. For nitrogen, the high temperature thermal conductivities (above 300 °K) were obtained from the data of D. W. STOPS[45], while those for carbon dioxide were from various sources at much lower temperatures*. More recently, A. J. ROTHMAN and L. A. BROMLEY[46] have reported careful measurements on these gases up to about 1100 °K.

* For reasons unknown to this reviewer, the data of Stops[45] on carbon dioxide were not used in the NBS tabulations.

Their values are compared with the NBS values in *Figures 2* and *3*. Stops's data on carbon dioxide are also included. The nitrogen curves agree remarkably well—the maximum difference is about five per cent—although the NBS values are uniformly higher. For carbon dioxide, the limited NBS values deviate rather sharply even at moderate temperature, while

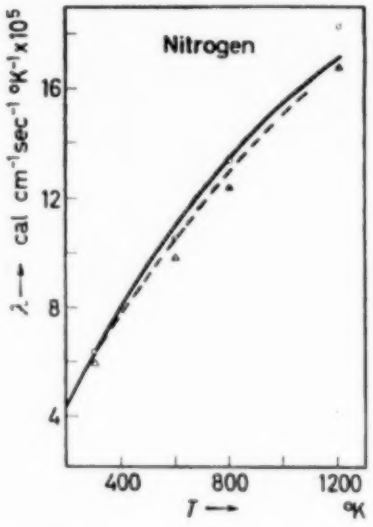

Figure 2. High temperature thermal conductivity of nitrogen. ——, NBS values; - - -, experimental data of reference 46; △, calculated from equation 5 and original Eucken correction; ○, calculated from equation 5 and modified Eucken correction

those of the other experimenters are in heartening agreement up to the highest temperatures reported. Rothman and Bromley also measured argon and their values agree closely with those of the NBS, as might be expected for a monatomic gas.

There are no other even moderately high temperature data to report for comparison with the NBS tables, so that for the present they must be taken at face value. In view of the above discussion, however, the tables should not be used uncritically, especially for the triatomic gases at high temperatures.

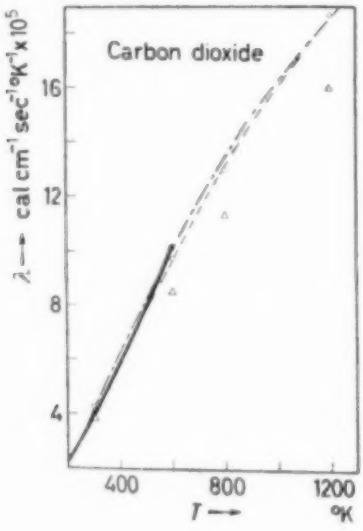

Figure 3. High temperature thermal conductivity of carbon dioxide. ——, NBS values; - - -, experimental data of reference 46, — · —, experimental data of reference 45; △, calculated from equation 5 and original Eucken correction; ○, calculated from equation 5 and modified Eucken correction

The NBS compilation includes some of the most important of the common flame gas components. The main exceptions are the hydrocarbons and other organic compounds. R. G. VINES and L. A. BENNETT[47] have reported measurements on some thirty one organic materials at various temperatures from room temperature to 160°C. The species of likely combustion interest include methanol, ethylene oxide, acetaldehyde, acetone, benzene, hexane, propane, and ethane. Other reported measurements are: bromine[48], hydrogen bromide[48], deuterium[49], ethylene[50], and methane[51]. None of these extends more than about 300° above room temperature.

As with diffusion, measurements of thermal conductivity at realistic flame temperatures are practically non-existent. In view of this, recent work by E. F. SMILEY[52] is of particular importance. A shock-tube technique was employed to estimate the thermal conductivity of argon up to 3300°K. Extension of the work to other gases is anticipated.

Experimental data on mixtures are very scarce. Rothman and Bromley[46] measured various carbon dioxide–nitrogen mixtures up to 950°K finding that above about 360°C λ goes through a maximum as a function of concentration. Hydrogen in binary mixtures with carbon dioxide, carbon monoxide, and nitrogen has been measured near room temperature by T. L. IBBS and A. A. HIRST[53], and with oxygen by A. WASSILJEWA[54]. L. A. BENNETT and R. G. VINES[55] reported an interesting set of data on several organic vapour mixtures, and showed that maxima in λ exist for polar–non-polar mixtures but not for non-polar mixtures. An explanation is offered, but in view of the above results on carbon dioxide–nitrogen (non-polar) there is undoubtedly more to the story. Similar maxima have also been reported for water–nitrogen by F. G. KEYES[56].

Theoretical

The calculation of thermal conductivity is, generally, in the least satisfactory state of development of any of the transport properties. For simple monatomic gases with spherically symmetrical potentials, the rigorous kinetic theory[1] gives to the first approximation

$$\lambda \times 10^5 = 19{\cdot}89\,(T/M)^{\frac{1}{2}}/\sigma^2\Omega^{(2,2)*}\ \text{cal sec}^{-1}\text{cm}^{-1}\ {}^\circ\text{K}^{-1} \qquad \ldots [5]$$

where M is the molecular weight, σ the 'collision diameter', and $\Omega^{(2,2)*}$ an integral determined by the interaction potential. The latter has been tabulated as a function of T^* for the Lennard-Jones (6-12) potential in reference 1 and for the modified Buckingham potential in reference 36. With viscosity parameters (σ and ε/k), this equation gives excellent agreement with experiment over the modest temperature range available (90° to 580°K) for noble gases. Even up to the 3300°K attained in Smiley's recent work[52] on argon, the Lennard-Jones calculations appear to be in reasonable agreement—probably within experimental error[57].

It is with the polyatomic gases, generally of more practical interest (certainly in combustion), that difficulties arise due to the presence of internal degrees of freedom. The rigorous treatment of this problem

involves the relaxation times for energy transfer between translational and internal (particularly vibrational) degrees of freedom and is not possible at present. Thus it has become customary to employ the Eucken correction for the thermal conductivity of polyatomic gases. In its original, simplest form[58], the monatomic result of equation 5 is multiplied by a correction term

$$[(4/15)(C_v/R)+(3/5)]$$

C_v being the molar heat capacity at constant volume and R the gas constant. J. O. HIRSCHFELDER[59] has recently given a very illuminating discussion of this correction. A polyatomic gas is considered as a reacting mixture of species in the various internal energy states. In order to define a thermal conductivity at all, i.e. to equate the flux of heat to the product of λ and the temperature gradient, two crucial assumptions are necessary: first, that the distribution of species among the internal states is that which is characteristic of local thermodynamic equilibrium (Maxwellian) and a function only of temperature, and second, that all the species have the same diffusion coefficient. Under these conditions a generalized Eucken correction can be derived. Making use of the tabulated collision integrals for realistic potentials (Lennard-Jones or modified Buckingham) an improved Eucken correction $(0{\cdot}354\,C_v/R + 0{\cdot}469)$ is obtained.

Using equation 5 and the viscosity parameters of *Table 2*, it is interesting to compare the values of λ calculated with both the original Eucken correction and the modified form of Hirschfelder with the experimental data of *Figures 2* and *3*. Specific heats were obtained from a standard source[11]. For nitrogen, the modified form is slightly superior until the higher temperatures where it gives values considerably too high. For carbon dioxide, the agreement using the modified correction is excellent, while the older form falls far short at the higher temperatures. It would appear from these results that calculations based on Lennard-Jones interaction and the modified Eucken correction may be expected to give reasonably reliable results at moderately high flame temperatures.

In the same paper[59], Hirschfelder points out that the assumption of thermodynamic equilibrium is not valid for species in metastable electronic states, so that an Eucken-type approximation would not hold. In fact, a thermal conductivity cannot be defined strictly. The other assumption, namely, that species in various quantum states have the same diffusion coefficients, is violated for excited electronic species, which are abnormally large. Either or both of these violations might be expected in very hot flames, and heat transfer calculations become correspondingly more difficult.

As for diffusion, it is often convenient to have an analytical expression for the thermal conductivity of a gas without internal freedom as a function of temperature. The collision integral of equation 5 for the Lennard-Jones (6-12) potential may be fitted empirically by

$$\Omega^{(2,2)*} \simeq 1{\cdot}22(T^*)^{-0{\cdot}16} \quad \ldots . [6]$$

to within two per cent in the range $3 \leqslant T^* \leqslant 200$. Substitution in equation 5 gives

$$\lambda \times 10^5 = 16{\cdot}3\, T^{0{\cdot}66}/\sigma^2(\varepsilon/k)^{0{\cdot}16}M^{\frac{1}{2}} \quad \ldots . [7]$$

The theoretical treatment of mixtures of monatomic gases is extremely cumbersome and complicated, but may be performed rigorously for various assumed potentials. The appropriate equations and tables are given in reference 1. For polyatomic mixtures no rigorous treatment is possible at present. J. O. HIRSCHFELDER[60] has indicated how Eucken-type corrections can be applied to this case after first calculating λ as though only monatomic species were present. Good agreement with room temperature measurements on hydrogen–carbon dioxide was obtained, but high temperature calculations are extremely uncertain.

For practical calculations in combustion research these methods for polyatomic, multicomponent mixtures are prohibitively complex, and too uncertain to justify themselves. For many common flames involving air, the best present alternative is to regard the system as pure nitrogen and use the experimental data (where available) and theory as outlined above to estimate the thermal conductivity. In systems involving hydrogen in appreciable quantities it may be desirable to include it as a binary mixture with nitrogen. Similarly, other binary combinations may be calculated if necessary, but where the mixture is made up largely of three or more components all present in roughly the same concentration the calculation becomes exceedingly awkward. In such cases it is probably necessary to resort to devices such as a linear interpolation between estimated values at a high and a low temperature[4].

Various empirical relations for the thermal conductivity of binary mixtures as a function of composition have been proposed. The best known is probably that of A. L. LINDSAY and L. A. BROMLEY[61] which is reasonably successful for non-polar gases, but does not predict the cases showing maxima such as carbon dioxide–nitrogen and water–nitrogen. As a general rule, for non-polar mixtures the variation of λ with composition is nearly linear, but there are many exceptions.

The author is grateful to Drs E. A. Mason and W. H. Avery for critical readings of this manuscript, and to Dr R. M. Fristrom for helpful discussions. Permission to reproduce part of the data of Table 1 and all of the data of Table 2 from the source cited is acknowledged with gratitude.

Applied Physics Laboratory,
The Johns Hopkins University,
Silver Spring, Maryland

(Received May 1957)

REFERENCES

1 HIRSCHFELDER, J. O., CURTISS, C. F. and BIRD, R. B. *Molecular Theory of Gases and Liquids* Wiley: New York, 1954
2 MONTROLL, E. W. and GREEN, M. S. *Annu. Rev. phys. Chem.* 5 (1954) 449–476
3 JOHNSON, E. F. *Industr. Engng Chem. (Industr.)* 47 (1955) 599
WILKE, C. R. *Industr. Engng Chem. (Industr.)* 47 (1955) 658
JOHNSON, E. F. *Industr. Engng Chem. (Industr.)* 48 (1956) 582
WILKE, C. R. and PRAUSNITZ, J. M. *Industr. Engng Chem. (Industr.)* 48 (1956) 669
WILKE, C. R. and PRAUSNITZ, J. M. *Industr. Engng Chem. (Industr.)* 49 (1957) 577

JOHNSON, E. F. *Industr. Engng Chem.* (*Industr.*) 49 (1957) 614
[4] CAMPBELL, E. S. and HIRSCHFELDER, J. O. *Univ. Wis. Naval Res. Lab. Rep. No. CF-2180* (1953)
[5] HILSENRATH, J. *Selected Combustion Problems* Vol. II, pp. 199-244, AGARD, Butterworths: London, 1956
[6] FRISTROM, R. M. *J. chem. Phys.* 24 (1956) 888
[7] FRIEDMAN, R. and BURKE, E. *J. chem. Phys.* 22 (1954) 824
[8] BURGOYNE, J. H. and WEINBERG, F. J. *Proc. Roy. Soc. A* 224 (1954) 286
[9] FRISTROM, R. M., PRESCOTT, R. and GRUNFELDER, C. *Combustion & Flame* 1 (1957) 102
[10] FRIEDMAN, R. and CYPHERS, J. A. *J. chem. Phys.* 23 (1955) 1875
[11] FRISTROM, R. M. and WESTENBERG, A. A. *Combustion & Flame* 1 (1957) 217
[12] See remarks by WESTENBERG, A. A. in the Panel Discussion on High Speed Reactions, *Sixth Symposium* (*International*) *on Combustion* Reinhold: New York, 1957
[13] WESTENBERG, A. A. *J. chem. Phys.* 22 (1954) 814
[14] LOSCHMIDT, J. *S.B. Akad. Wiss. Wien* 61 (1870) 367
[15] STEFAN, J. *S.B. Akad. Wiss. Wien* 63 (1871) 63
[16] WALDMAN, L. *Naturwissenschaften* 32 (1944) 223
[17] NETTLEY, P. T. *Proc. phys. Soc. Lond. B* 67 (1954) 753
[18] LONSDALE, H. K. and MASON, E. A. *Univ. Maryld Inst. molec. Phys. Report* 1957
[19] RUMPEL, W. F. *Univ. Wis. Naval Res. Lab. Rep. No. CM-851* (1955)
[20] BUNDE, R. E. *Univ. Wis. Naval Res. Lab. Rep. No. CM-850* (1955)
[21] BOARDMAN, L. E. and WILD, N. E. *Proc. Roy. Soc. A* 162 (1937) 511
[22] CHAPMAN, S. and COWLING, T. G. *The Mathematical Theory of Non-Uniform Gases* Cambridge University Press: London, 1939
[23] BOYD, C. A., STEIN, N., STEINGRIMSSON, V. and RUMPEL, W. F. *J. chem. Phys.* 19 (1951) 548
[24] SCHWERTZ, F. A. and BROW, J. E. *J. chem. Phys.* 19 (1951) 640
[25] STREHLOW, R. A. *J. chem. Phys.* 21 (1953) 2101.
[26] VON OBERMAYER, A. *S.B. Akad. Wiss. Wien* 96 (1887) 546
[27] MACKENZIE, J. E. and MELVILLE, H. W. *Proc. Roy. Soc. Edinb.* 53 (1933) 255
[28] LEBLANC, M. and WUPPERMAN, G. *Z. phys. Chem.* 91 (1916) 143
[29] WALL, F. T. and KIDDER, G. A. *J. phys. Chem.* 50 (1946) 235
[30] SCHMIDT, R. *Ann. Phys., Lpz.* 14 (1904) 801
[31] KLIBANOV, T. M., POMERANTSEV, V. V. and FRANK-KAMENETSKY, D. A. *J. tech. Phys. U.S.S.R.* 12 (1942) 14
[32] SCHÄFER, K. and SCHUHMANN, K. *Z. Elektrochem.* 61 (1957) 246
[33] WESTENBERG, A. A. and WALKER, R. E. *J. chem. Phys.* 25 (1957) 1753
[34] FAIRBANKS, D. and WILKE, C. R. *Industr. Engng Chem.* (*Industr.*) 42 (1950) 471
[35] WILKE, C. R. and LEE, C. Y. *Industr. Engng Chem.* (*Industr.*) 47 (1955) 1253
[36] MASON, E. A. *J. chem. Phys.* 22 (1954) 169
[37] MASON, E. A. and RICE, W. E. *J. chem. Phys.* 22 (1954) 522
[38] MASON, E. A. and RICE, W. E. *J. chem. Phys.* 22 (1954) 843
[39] MASON, E. A. *J. chem. Phys.* 23 (1955) 49
[40] CURTISS, C. F. *Univ. Wis. Naval Res. Lab. Rep. No. Wis-NSF-1* (1955)
[41] CURTISS, C. F. and MUCKENFUSS, C. *Univ. Wis. Naval Res. Lab. Rep. No. Wis-NSF-6* (1955)
[42] DAHLER, J. S. *Univ. Wis. Naval Res. Lab. Rep. No. Wis-ONR-23* (1956)
[43] HIRSCHFELDER, J. O. and ELIASON, M. A. *Univ. Wis. Naval Res. Lab. Rep. No. Wis-AF-1* (1956)
[44] HILSENRATH, J. *et al.* 'Tables of Thermal Properties of Gases.' *Circ. U.S. Bur. Stand. No. 564* Washington, 1955
[45] STOPS, D. W. *Nature, Lond.* 164 (1949) 966
[46] ROTHMAN, A. J. and BROMLEY, L. A. *Industr. Engng Chem.* (*Industr.*) 47 (1955) 899
[47] VINES, R. G. and BENNETT, L. A. *J. chem. Phys.* 22 (1954) 360
[48] FRANCK, E. U. *Z. Elektrochem.* 55 (1951) 636
[49] UBBINK, J. B. *Physica, 's Grav.* 14 (1948) 165
[50] KEYES, F. G. *Trans. Amer. Soc. mech. Engrs* 76 (1954) 809
[51] SCHOTTKY, W. F. *Z. Elektrochem.* 56 (1952) 889
[52] SMILEY, E. F. Doctoral *Dissertation*, Catholic University of America, 1957
[53] IBBS, T. L. and HIRST, A. A. *Proc. Roy. Soc. A* 123 (1929) 134
[54] WASSILJEWA, A. *Phys. Z.* 5 (1904) 737
[55] BENNETT, L. A. and VINES, R. G. *J. chem. Phys.* 23 (1955) 1587
[56] KEYES, F. G. *Project Squid. Tech. Rep. No. 37* Massachusetts Institute of Technology, 1952

[57] Private communication with SMILEY, E. F.
[58] EUCKEN, A. *Phys. Z.* 14 (1913) 324
[59] HIRSCHFELDER, J. O. *J. chem. Phys.* 26 (1957) 282
[60] HIRSCHFELDER, J. O. *Univ. Wis. Naval. Res. Lab. Rep. No. CM–880* (1956)
[61] LINDSAY, A. L. and BROMLEY, L. A. *Industr. Engng Chem.* (*Industr.*) 42 (1950) 1508

Scale Effect in a Gas Turbine Combustion Chamber fitted with a Swirl Atomizer—Part I

M. V. HERBERT and J. A. BAMFORD

The scale test conditions required to obtain agreement in performance between geometrically similar spray combustion chambers are examined, with special reference to fuel atomization criteria. Theoretical considerations do not yield a unique specification, but an optimum compromise can be derived, which in a practical case will enable suitable atomizers to be matched to chambers of different scales. Test conditions may then be chosen by which one scale combination of chamber and atomizer can be used to predict the performance of another. Two combustion chambers with a scale ratio of two have been tested under highly sensitive conditions, and an experimental correlation obtained in terms of spray momentum and droplet size, which agrees well with the theoretical analysis.

A GENERAL theoretical study of the contributory processes of combustion has been made by D. G. STEWART[1, 2]. Various requirements were produced, in many cases mutually conflicting, which should be satisfied when testing geometrically similar combustion chambers. The fuel spray functions in particular were confusing, and easily upset by variation in the practical qualities of atomizers. While, therefore, accepting the basic aerodynamic factors which emerged, it was the purpose of this work to consider their application to a specific type of chamber, and establish the additional requirements governing the air–fuel mixture pattern.

To this end, a more restricted analysis has been employed, concentrating on those factors to which the performance of a spray chamber is thought to be most critical. A concurrent experimental programme has provided data on atomizer scale behaviour, enabling the optimum matching to be predicted. Comprehensive combustion tests on two scales of aircraft-pattern tubular chamber have been carried out, to confirm the results of this theoretical treatment. Scale agreement has been tested throughout at simulated altitude idling conditions, where combustion can be expected to be most sensitive to minor differences in air flow pattern and fuel spray characteristics.

The benefit in terms of plant capacity to be derived from part-size scale testing of chambers under development was stated by Stewart[1]. While this is indeed true, interest in scale techniques is also directed towards use of linear scale as a further test variant, which becomes available in experimental research into combustion processes.

SCALE TEST REQUIREMENTS

The ultimate interest of this section is to select operating conditions for a half scale model chamber to reproduce full scale performance. It is assumed

that the conditions of testing will allow the following factors to be constant between full size unit and model: (*i*) length/diameter ratio, (*ii*) fuel properties, and (*iii*) operating temperatures.

The most important considerations then are:

(*a*) Aerodynamic flow pattern, governed by Reynolds number and Mach number

(*b*) Air–fuel mixture distribution, which will be dependent on penetration scale, evaporation rate, air/fuel momentum ratio, and geometric similarity of fuel spray

(*c*) Chemical combustion processes, including the effects of ignition delay, limiting reaction rate, and flame propagation.

Items (*a*) and (*c*) may conveniently be considered together, in the absence of fuel injection effects, which will be treated separately.

Homogeneous combustion

The notation is set out in Appendix I. For independent variation in v, p and l:

$$R_e \propto vlp = \text{constant}^* \quad \ldots [1]$$

$$M_a \propto v = \text{constant} \quad \ldots [2]$$

$$S \propto v/(pl)^x = \text{constant} \left[\begin{matrix}\text{See Appendix II,} \\ \text{`Stability'}\end{matrix}\right] \ldots [3]$$

Of these relations, the Reynolds number and the stability criterion are likely to have the most effect, and combination of equations 1 and 3 leads to:

$$lp = \text{constant} \quad \ldots [4]$$

and

$$v = \text{constant} \quad \ldots [5]$$

The Mach number requirement is thus also satisfied although in point of fact the influence of compressibility will be negligible in the range of velocities covered by these tests.

Hence, for this work, the scale ratios will be:

$$\sigma_l = 1/n \; : \; \sigma_p = n \; : \; \sigma_v = 1$$

leading to

$$\sigma_Q = 1/n, \quad \text{since } Q \propto pl^2v$$

Air–fuel mixture

The object is to ensure that the air and fuel are in the same proportion and state at relative positions throughout each scale of chamber. Provided that the atomization is suitably scaled, as will be considered later in the

*The stability parameter S already contains a dependence on R_e. The further introduction of R_e at this point is, however, necessary to allow for the much increased importance of aerodynamic influences in a combustion chamber of such complex form. It is also of importance in some of the heat transfer processes controlling loss of heat from the chamber (see ref. 1). The extent to which the assumption of constant temperatures throughout is violated by these losses, changing the reaction zone wall temperature in different scales, is examined theoretically in ref. 12. From this it appears that with a 2:1 scale change in accordance with equations 4 and 5 above, the effect on wall temperature should be almost negligible, the larger size of chamber having slightly higher temperatures.

light of these mixing requirements, this calls for scaling of the simultaneous processes of penetration and evaporation.

A necessary corollary to any analysis of penetration is the preservation of air/fuel momentum ratio similarity, so that the relative motion between air and fuel droplets is scaled. To a first approximation, indeed, this relation is of sole importance. Limited correlations[3, 4] exist with combustion efficiency; and with atomizers 'A,' 'C' and 'D' used in this work (see Appendix III) the agreement obtained with momentum alone scaled is quite reasonable.

The requirement is

$$\frac{M_f}{M} \propto \frac{Q_f V}{Q v} = \text{constant} \qquad \ldots . [6]$$

and since, for matching of air/fuel ratios between full-size and model chambers, $Q_f/Q = \text{constant}$,

$$\frac{M_f}{M} \propto \frac{V}{v} = \text{constant} \qquad \ldots . [6a]$$

Our experiments have shown, however, that a further factor must be called upon to explain the ultimate matching of the fuel spray, and that this is some function of droplet size. The inter-relation of spray velocity and drop size is considered in the next section.

Analysis of a typical primary zone geometry has produced the further relation for simultaneous penetration and evaporation [See Appendix II, 'Simultaneous penetration and evaporation']

$$d^2 v/l = \text{constant} \qquad \ldots . [7]$$

Using the values of the previous section, this yields

$$\sigma_d = 1/n^{0.5}$$

It is of interest to compare this result with a relation derived by F. J. BAYLEY[5], also with simultaneous evaporation, but considering only stagnant air and unidirectional motion. The assumption of equation 6a is thus again implicit, and leads to

$$d^{1.84} V^{0.84}/lp^{0.16} = \text{constant} \qquad \ldots . [8]$$

Although there is no very close similarity between his system and the practical case, it is worthy of note that equation 8 yields for these conditions

$$\sigma_d = 1/n^{0.46}$$

Of some further interest are several attempts which have been made to correlate droplet penetration into a moving air stream with injector orifice size, omitting evaporation effects. R. A. RICE[6] and L. J. CHELKO[15] have given two relations for cross-stream injection [*Figure 11(a)*]:

$$\frac{x}{D} \propto \frac{V}{v^{1.206}} \frac{\rho_f}{\rho_a^{0.566}} \left(\frac{y}{D}\right)^{0.333} D^{0.118} \qquad \ldots . [9]$$

$$\frac{x}{D} \propto \left(\frac{V}{v}\right)^{0\cdot95} \left(\frac{\rho_f}{\rho_a}\right)^{0\cdot74} \left(\frac{y}{D}\right)^{0\cdot23} \quad \ldots.[10]$$

while C. N. KING[7] gives for upstream injection [*Figure 11(b)*]

$$\frac{x}{D} \propto \left(\frac{V}{v}\right) \left(\frac{\rho_f}{\rho_a}\right)^{0\cdot5} \quad \ldots.[11]$$

The dimension of y may be omitted from equations 9 and 10 for a scale ratio calculation. For $\sigma_x = 1/n$, equations 9, 10 and 11 then yield respective values of $\sigma_D = 1/n^{0\cdot553}$, $1/n^{0\cdot338}$ and $1/n^{0\cdot5}$.

The upstream value thus accords fairly with a mean of the cross-stream results. This requirement may then be written using equation 6a and with $x \propto l$

$$D^2 \propto l^2 p \quad \ldots.[11a]$$

Hence, from equation 7

$$d^2/D^2 \propto 1/vlp$$

which, by equations 4 and 5, gives

$$d/D = \text{constant} \quad \ldots.[12]$$

Atomization

The conclusions of the previous section throw the onus of preserving similarity of mixture distribution on the atomizer (equations 6a and 12).

The behaviour of scaled atomizers will in practice depend upon a number of factors, which may be listed thus:

(*a*) Mechanical features
- (*i*) geometric similarity of design
- (*ii*) accuracy of manufacturing finish.

These will affect:

(*b*) Physical properties
- (*i*) change of cone angle
- (*ii*) change of discharge coefficient
- (*iii*) change of atomizer efficiency (i.e. effect of viscous losses)

} with pressure.

If the discharge coefficient and efficiency could be made equal for each atomizer, and constant throughout the working range, then the flow numbers would also be constant, and could be directly scaled. However, when the very low pressure end of the atomizer range is used, changes in all the above properties become significant. Hence, in practice, atomizer matching is very critical; and it may even be expected that several small scale atomizers will be necessary to match over different parts of a full size atomizer range.

A rather superficial argument[2] was as follows.

From equation 6a $\sigma_V = \sigma_v = 1$

Now $V \propto (\Delta P)^{\frac{1}{2}}$ (this assumes constant atomizer efficiency)

$$\therefore \sigma_{\Delta P} = 1$$

Hence $$\sigma_N = \sigma_{Q_f} / (\sigma_{\Delta P})^{\frac{1}{2}} = 1/n$$

Early tests with various scaled atomizers of two types showed a mutual similarity in pattern of the results for one type, which differed from that for the other. This indicated that close geometric similarity must be maintained; and, in addition, there was evidence that some reduction in nominal flow number scale ratio was necessary. A range of seven special atomizers was therefore obtained and calibrated for fuel spray momentum. Details are given in Appendix III, and all test results quoted were obtained using these atomizers.

The foregoing requirements specify both spray velocity and drop size leaving an atomizer. Since these must in practice be physically related for a given atomizer, it is clearly necessary to know its performance in detail before accurate scaling of a fuel spray can be achieved. The real problem now becomes one of physical properties of an atomizer, and it remains to be seen whether both drop size and fuel velocity requirements can be satisfied. In any case, actual calibration of a number of atomizers for spray momentum and SMD will be necessary before one can be chosen to give good scale matching.

The general equations may be written:

$$Q_f = \rho_f \, . \, C_D \, . \, A \, . \, V \qquad \ldots . [13]$$

$$M_f = Q_f V / g \qquad \ldots . [14]$$

$$\Delta P = (1/2g) \, \rho_f \, (V/\eta_m)^2 \qquad \ldots . [15]$$

$$N = 6{\cdot}25 \, Q_f / \rho_f \, (\Delta P)^{\frac{1}{2}} \qquad \ldots . [16]$$

Rearranging, the following forms are of interest:

$$Q_f^2 \propto \Delta P \, (A C_D \, \eta_m)^2 \qquad \ldots . [17]$$

$$N \propto A C_D \, \eta_m \qquad \ldots . [18]$$

$$M_f \propto Q_f^2 / A C_D \qquad \ldots . [19a]$$

$$\propto (\eta_m / N) \, Q_f^2 \qquad \ldots . [19b]$$

C_D and η_m are both nearly constant over the higher flow range, with fairly sharp increase and decrease respectively at the low pressure end. Equation 18 shows the effect on N: a slight net increase with decreasing pressure.

It is interesting to note that if, to a first approximation, $A \, . \, C_D \propto D^2$, then equation 13 automatically satisfies the requirement of equation 11a for $\sigma_D = 1/n^{0{\cdot}5}$.

Considering now the drop size requirement of equation 7, various empirical formulae for spray SMD from a swirl atomizer are in existence. The two most worthy of note are:

(*i*) The Lucas[8] relation

$$d = 335\, N^{0\cdot209}\, \nu^{0\cdot215} / \Delta P^{0\cdot348}$$

for kerosine, this leads to

$$d = 261\, Q_f^{0\cdot209} / \Delta P^{0\cdot453} \quad \ldots\ldots [20]$$

(*ii*) H. C. NEEDHAM'S relation[9]

$$d = 182\, Q_f^{0\cdot25} / \Delta P^{0\cdot40} \quad \ldots\ldots [21]$$

In either case we see that, for momentum to be matched, V is determined for a given Q_f (i.e. $A \,.\, C_D$ is fixed); but a variation in drop size—being a function of ΔP—may still be possible, depending on η_m.

The calibrations of atomizers used in these tests are examined in Appendix III and the following scale ratios for optimum matching are deduced:

$$\sigma_N = 1/n^{1\cdot32} \quad : \quad \sigma_{\Delta P} = n^{0\cdot64}$$

$$\sigma_{AC_D} = 1/n \quad : \quad \sigma_{\eta_m} = 1/n^{0\cdot32}$$

Putting $\sigma_{Q_f} = 1/n$ and $\sigma_{\Delta P} = n^{0\cdot64}$ in equations 20 and 21 gives respective values of $\sigma_d = 1/n^{0\cdot499}$ $(=0\cdot707)$ and $1/n^{0\cdot506}$ $(=0\cdot704)$. This agreement is remarkably close, and exactly satisfies the requirement of equation 7. It may therefore be expected that the half scale atomizer with this particular set of properties will show the closest agreement in performance tests with the full size chamber.

TEST EQUIPMENT

A scaled version was made of a typical aircraft turbo-jet engine tubular chamber, whose altitude performance had already been thoroughly assessed. From the point of view of test convenience, a half scale model was chosen; and simulated altitude idling conditions have been used throughout, where combustion can be expected to be most sensitive to minor differences in air flow pattern and fuel spray characteristics.

A true half scale sheet metal flame-tube was obtained after some difficulty in ensuring sufficient accuracy of detail, while the air casing was only scaled internally. Both scales of chamber were tested with an upstream rig adaptor shaped in the segment of an annulus, carrying a row of straight vanes to simulate the final row of compressor stator blades. Eleven-diameter pressure traversing sections were used to check the air velocity profiles at inlet to the diffusers. Outlet temperature was measured by means of a sonic suction pyrometer in a 60-point traverse.

General scale agreement

Figures 1 and *2* show total head traverses at inlet to full size and half size chambers, both chambers being tested at atmospheric outlet pressure, and air mass flow scaled to give equal velocity. Very reasonable matching is evident.

Table 1 gives the air flow distribution in the separate circuits of both scales of chamber, set up to have inlet total head pressures proportional to those in *Figures 1* and *2*. Air mass flow was measured with other circuits

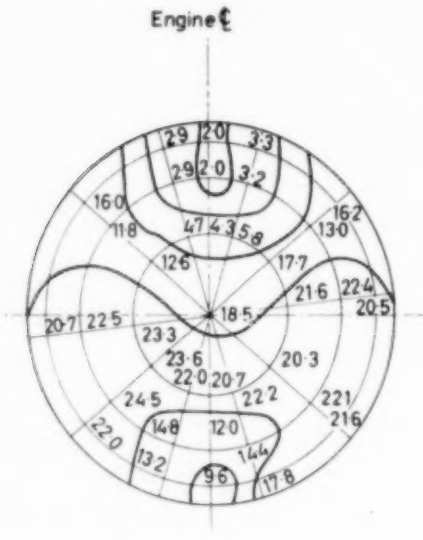

Mean value of total head 15·34 in water

Figure 1. Inlet total head pressure traverse—full scale chamber.

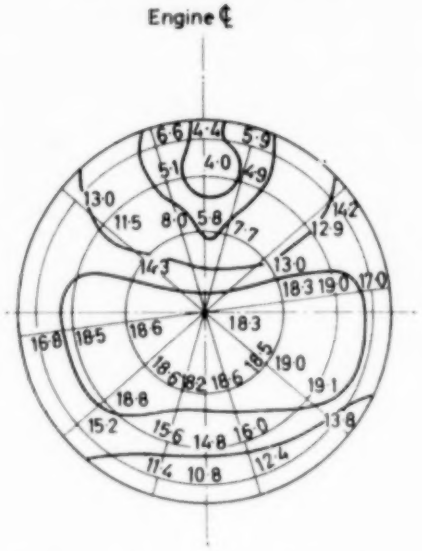

Mean value of total head 14·29 in water

Figure 2. Inlet total head pressure traverse—half scale chamber.

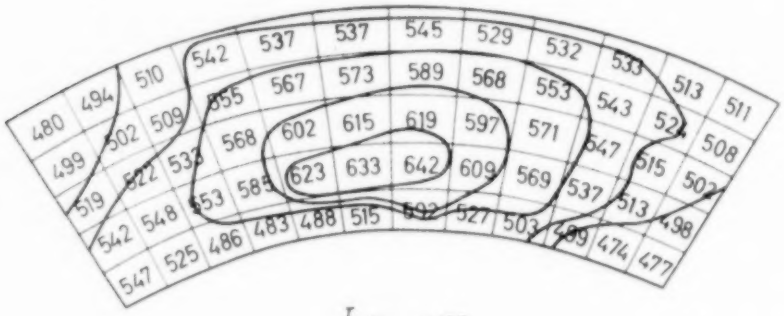

$$\frac{T_{max}}{T_{mean}} = 1{\cdot}187$$

Figure 3. Exhaust temperature traverse—full scale chamber

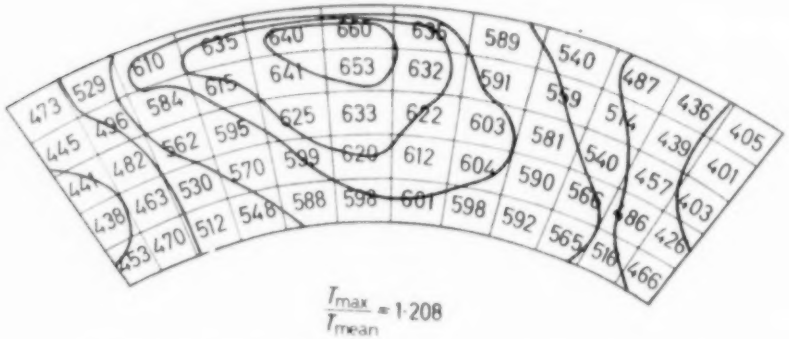

$$\frac{T_{max}}{T_{mean}} = 1{\cdot}208$$

Figure 4. Exhaust temperature traverse—half scale chamber

successively blanked off. The overall agreement of primary and secondary circuits is good, but despite the care in manufacture the half scale swirler accepts an excess of primary air. Test results suggest that there is no very serious effect on combustion performance due to this error.

Table 1. Air flow distribution in scaled chambers

Separate circuits	*Cold air flow per cent whole chamber*					
	Full scale chamber			*Half scale chamber*		
	Test 1	*Test 2*	*Mean*	*Test 1*	*Test 2*	*Mean*
Secondary	78·7	76·3	77·5	74·0	79·4	76·7
Primary (incl. swirler)	42·8	44·75	43·8	40·3	42·4	41·4
Primary (less swirler)	37·3	39·3	38·3	33·15	35·6	34·4
Swirler	7·82	9·12	8·47	11·75	12·67	12·21

Note: Tests 1 and 2 had inlet total head pressures in the ratio of 1·5:1.

Typical outlet temperature traverses are shown in *Figures 3* and *4* for the two scales of chamber. The agreement in $T_{max.}/T_{mean}$ is very good, but a characteristic shift of contour is noticeable. A similar difference in pattern has been observed[8] elsewhere.

Combustion tests

Table 2 gives the chamber inlet conditions used in these tests. The fuel used in both scales was kerosine RDE/F/KER S.R.312. Test results for 40000, 50000, and 60000 feet are shown in *Figures 12* to *17*, for the full size chamber and atomizers 'A' to 'E' in the half scale (see Appendix III).

Table 2. Combustion test conditions for scaled chambers

Equivalent altitude ($ft \times 10^{-3}$)	*Inlet temperature* (°C)	*Inlet static pressure (in. of mercury abs.)*		*Air mass flow (lb/sec)*	
		Full scale	*Half scale*	*Full scale*	*Half scale*
30	+5	15·94	31·88	0·798	0·399
40	−7	10·35	20·70	0·546	0·273
50	−7	6·40	12·80	0·338	0·169
60	−7	3·95	7·90	0·208	0·104

Although the range of these tests is somewhat restricted, a region of efficiencies substantially below 100 per cent is necessary for the effects of minor differences in air flow pattern and fuel spray characteristics to be distinguished. Ref. 8 affords confirmation of the matching between scales at conditions of higher chamber loading (efficiency approximately constant at 100 per cent). In this region, however, the atomization criteria seem to have been wholly outweighed.

In order to justify the very critical effects which seemed to be attributable to the atomizers, it was necessary to determine what degree of scatter might be due simply to idiosyncrasies in individual hardware. A range of full

scale chambers was accordingly tested at each altitude, with the same atomizer; and *Figures 15* to *17* show that there is in fact negligible difference in result.

Early work on the half scale chamber indicated that atomizers of half the full scale flow number produced a spray too coarse to match (i.e. $\sigma_d > 0{\cdot}707$), while smaller flow number atomizers could be used to refine the spray sufficiently to increase efficiency above the full scale curve

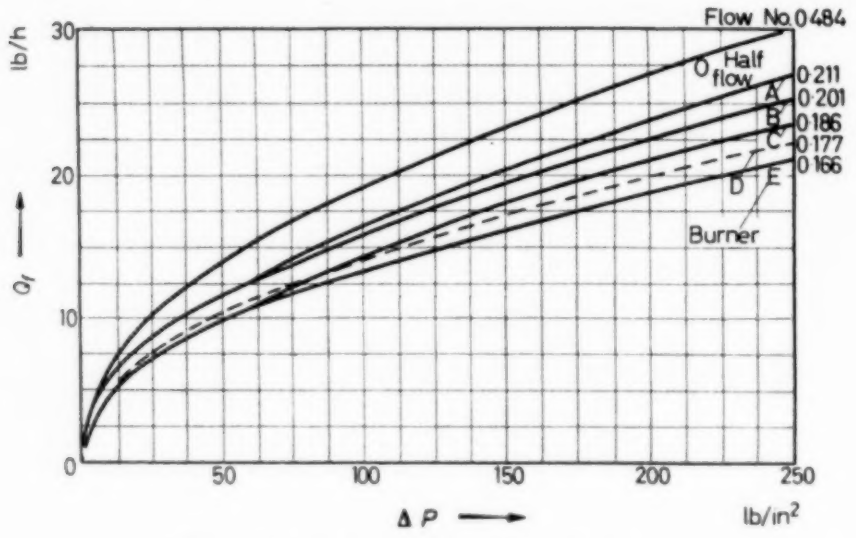

Figure 5. Atomizer flow number calibration

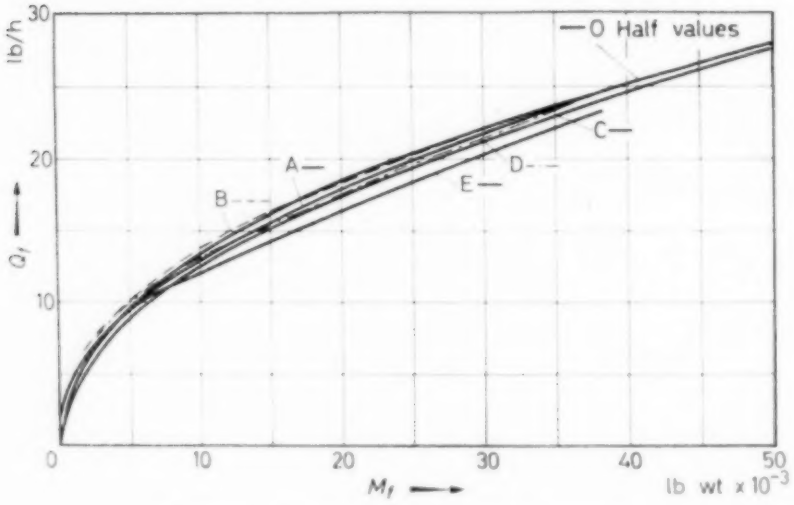

Figure 6. Atomizer momentum calibration

(σ_d then $< 0{\cdot}707$). The latter effect might be expected solely from spray momentum considerations, and it agrees with H. M. NICHOLSON's conclusion[3], that, other things being equal, efficiency depends only on spray characteristics.

The results for half scale atomizers show that in practice $\sigma_{\eta_m} < 1$: see 'Atomization' above. A. RADCLIFFE and J. M. HAWKINS[4] obtained results

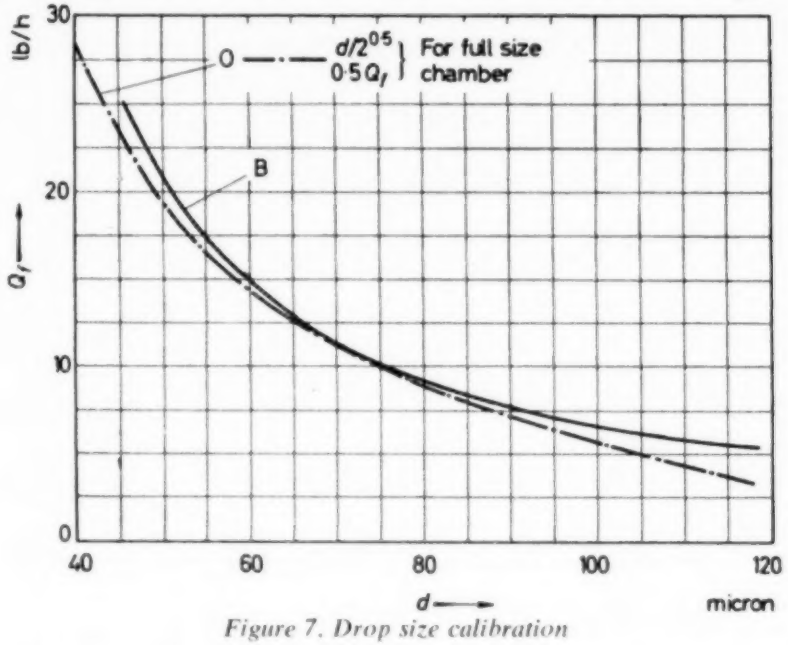

Figure 7. Drop size calibration

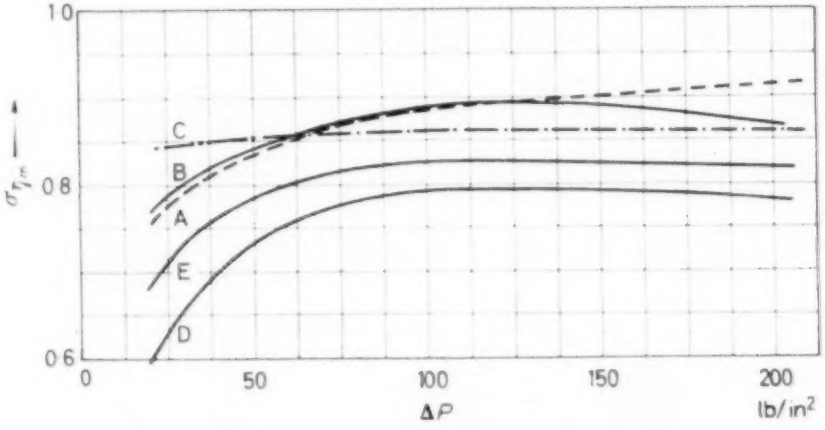

Figure 8. Atomizer efficiency scale ratios

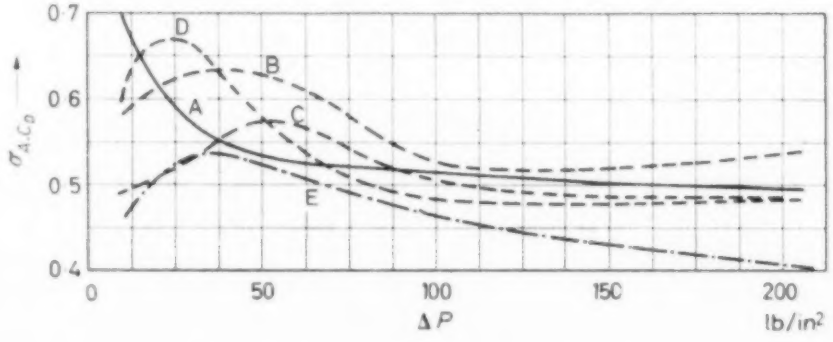

Figure 9. Atomizer orifice size scale ratios

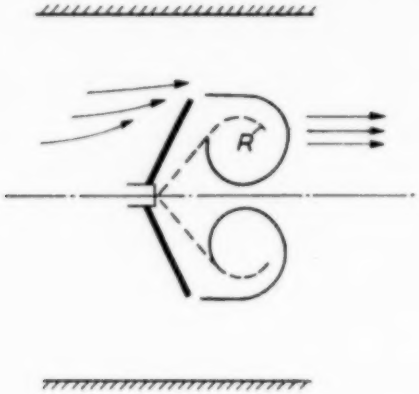

Figure 10. Primary zone of a spray combustion chamber (schematic)

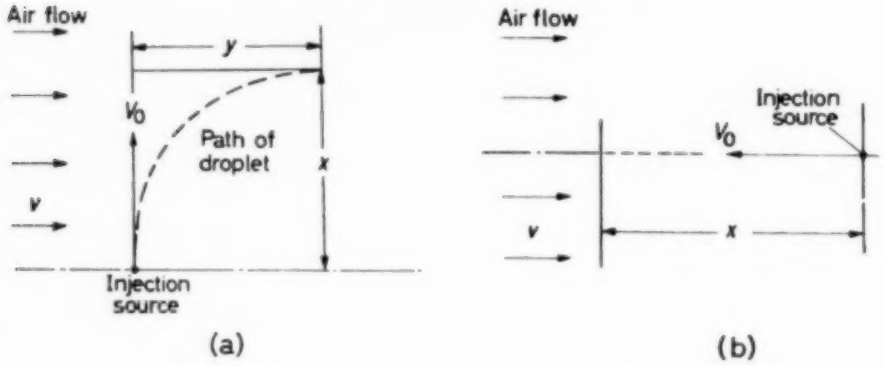

Figure 11. Droplet penetration experiments

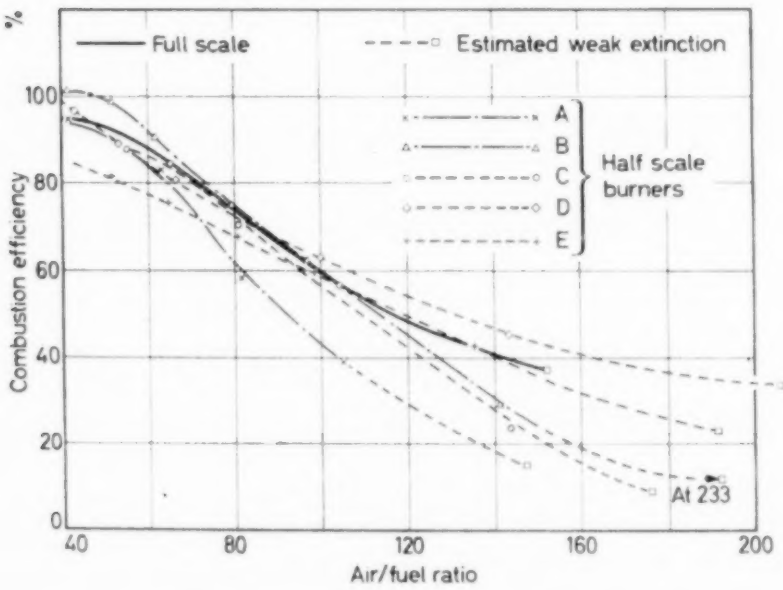

Figure 12. Scale performance comparison under altitude idling conditions—40000 f

showing a fall in η_m with flow number, and, for a particular small atomizer, with ΔP. It was by now clear that scale matching was dependent on atomizer performance.

For all the range of atomizers tested, *Figures 12* to *14* show very reasonable agreement on weak extinction.

Spray momentum correlation—As mentioned in Appendix III, atomizer 'B' shows closest agreement with the full size throughout the range, while 'A' and 'D' improve towards the rich end. Results for 40000 and

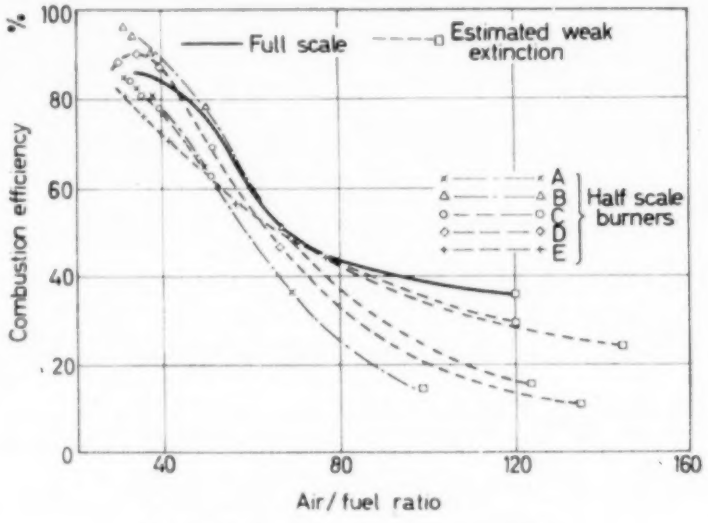

Figure 13. As Figure 12, but 50000 ft

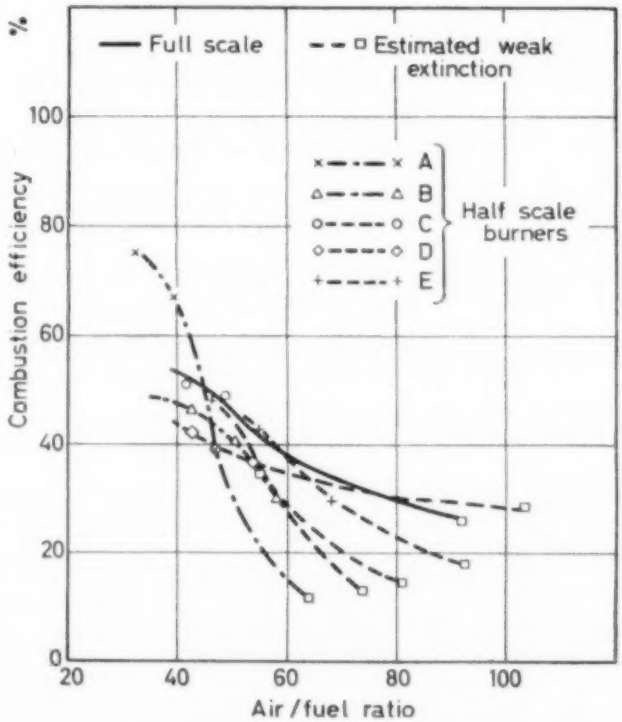

Figure 14. As Figure 12, but 60000 ft

50000 feet (*Figures 12* and *13*) agree well with these trends, while 60000 (*Figure 14*) is evidently too critical to offer much useful information. At

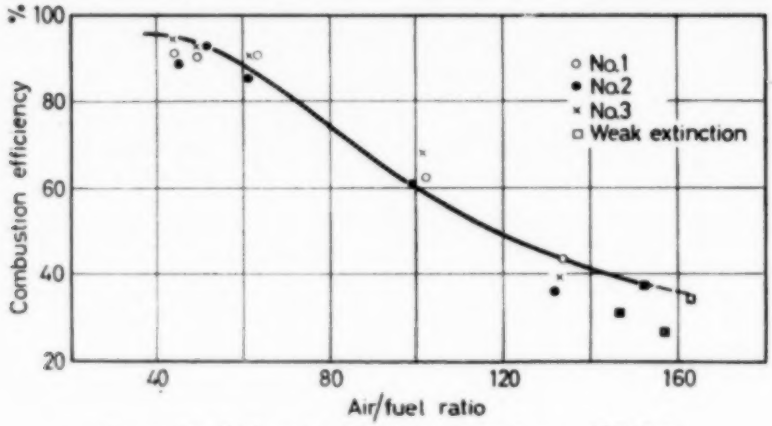

Figure 15. Full scale chamber comparison—40000 ft

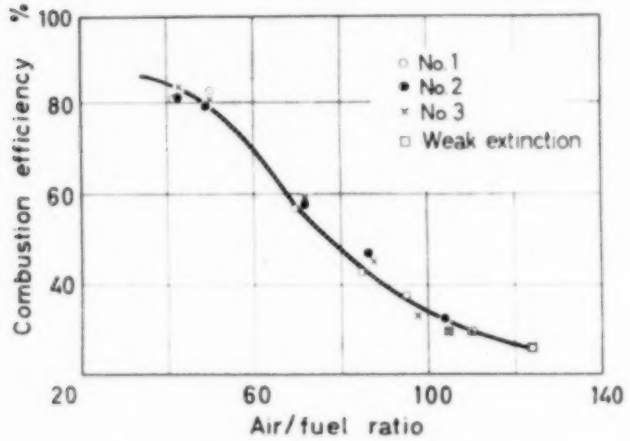

Figure 16. As Figure 15, but 50000 ft

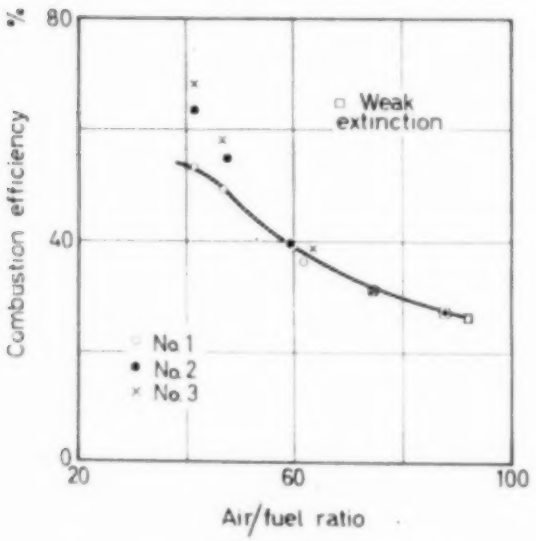

Figure 17. As Figure 15, but 60000 ft

the weak end, the accuracy of the momentum calibrations is too low for detailed correlation.

However, the effect of increasing momentum at the rich end (e.g. 'E' with highest momentum and lowest efficiency) can only be explained in terms of the parallel factor of spray penetration.

Spray penetration correlation—Above a certain air/fuel ratio, increased penetration must lower efficiency by unduly spreading the combustion zone, eventually weakening the primary until the flame is chilled out. Conversely, below the air/fuel ratio for peak efficiency, reduced penetration will also adversely affect combustion by causing local over-richness and incomplete burning of fuel pockets.

In 'air–fuel mixture' above, it is shown that, where momentum is matched, it is sufficient to consider penetration as a function of drop size only. *Figure 7* is drawn for this condition, and a scale ratio of $\sigma_d = 1/2^{0.5}$. This shows only atomizer 'B,' since the necessary condition of $\sigma_V = 1$ is not always satisfied in the cases of 'A,' 'C,' 'D' and 'E.' *Figure 7* shows perfect agreement in the middle of the range, while increased drop size and penetration at either end forecast a higher efficiency at the rich end, and a low efficiency at the weak. Reference to *Figures 12* and *13* shows this to be so. The position of this cross-over of efficiency curves is determined by the value of Q_f, the air/fuel ratio differing according to air mass flow. Identical matching can only be achieved, therefore, by some change in atomizers through the fuel flow range. However, the agreement already obtained with 'B' should be adequate for all practical purposes.

CONCLUSION

Theoretical analysis of the main factors to be preserved in geometric scaling of spray combustion chambers has produced a set of conditions which may be summarized as follows:

(*i*) Temperature = constant

(*ii*) Velocity = constant

(*iii*) Pressure × length = constant

(*iv*) Air/fuel momentum ratio = constant.

(*v*) Drop size $\propto$ (length)$^{\frac{1}{2}}$.

The combination of (*iv*) and (*v*) constitutes a problem in atomizer design, which may only be solved in practice by detailed calibration of a range of model atomizers.

Experiment has shown that, under the above conditions, very good scale agreement in performance can be achieved.

The work reported above was carried out at the National Gas Turbine Establishment during 1954 and is published by permission of the Director.
Crown Copyright reserved.

National Gas Turbine Establishment,
Pyestock, Hants.

(*Received March 1957*)

APPENDIX I. NOTATION

R_e = Reynolds number
$R_{e,d}$ = Droplet Reynolds number
M_a = Mach number
A = Area of atomizer orifice
C_D = Discharge coefficient
d = Droplet diameter (d_0—initial diameter)
D = Fuel orifice diameter
l = Chamber scale length
M = Air momentum
M_f = Fuel spray momentum
N = Atomizer flow number
n = Size factor = full size dimension / model dimension
p = Chamber pressure
ΔP = Atomizer fuel pressure drop
Q = Air mass flow
Q_f = Fuel flow
R = Radius from vortex centre
S = Stability factor
t = Time
v = Air velocity
V = Fuel droplet velocity (V_0—injection velocity)
x, y = Penetration coordinates
α = Flow angle
η_m = Atomizer efficiency = measured momentum / theoretical momentum
η_c = Combustion efficiency
λ = Evaporation constant
μ_a = Air viscosity (absolute)
ν = Fuel viscosity (kinematic)
ρ_a = Air density
ρ_f = Fuel density
σ = Scale ratio = value of quantity in model / value of quantity in full size unit (suffices refer to quantity being scaled)
τ = Ignition delay time
ϕ = A function
ψ = Air loading group Q/l^3p^2

APPENDIX II. NOTES ON SCALE FACTORS

STABILITY

In ref. 2, the criterion for stability was taken as

$$\frac{\text{Ignition delay time}}{\text{Reaction zone residence time}} = \text{constant}$$

For kerosine[10], ignition delay time $\propto 1/p$, while the residence time may be written as $\propto l/v$. Thus v/lp = constant, and the air loading group $Q/l^3p^2 = \psi$ = constant.

It is, however, doubtful whether this is altogether valid as a practical criterion. The question of stability is a complex one, but it might reasonably be considered as a conjunction of mixing and heat release effects. Now the mixing is a function of aerodynamic flow pattern, governed, say, by Reynolds number; while the above parameter ψ is purely a measure of the chemical limitations governing reaction with perfect mixing—i.e. homogeneous combustion. Even for fully premixed and vaporized fuel injection then, it might be expected that the stability will be controlled by a balance between aerodynamics and chemistry, i.e. between R_e ($\propto Q/l$) and ψ ($= Q/l^3p^2$).

A survey[11] of available data on both 'can' and baffle stabilizing systems supports this argument, and shows that the stability correlating group always conforms closely to a common relation of the form

$$S \propto v/(lp)^x$$

where $0 < x < 1$. It may be noted that as $\sigma_l = l/\sigma_p$, the value of x is unimportant here.

SIMULTANEOUS PENETRATION AND EVAPORATION

The primary zone of a spray combustion chamber may be represented by the system shown in *Figure 10*. Fuel drops after disruption of the conical film leaving the atomizer are entrained by air in the recirculation zone, and ideally proceed in a diminishing spiral path until evaporation is complete.

There is thus no real comparison between conditions existing in such a chamber and those assumed by Bayley[5], where a fuel spray was diffusing, albeit with simultaneous evaporation, into a region of stagnant air. His criterion of penetration distance is of less interest *per se* than for the agreement it gives with other requirements for drop size scale ratio.

Some further consideration will therefore be made of the system of *Figure 10*, to find the optimum scale of drop size for similarity of air–fuel mixture distribution. Omitting for simplicity of analysis any circumferential swirl of the vortex, such as would be promoted by a swirler in the baffle plate, and considering only a 'bluff body' recirculation system, each droplet may be regarded as following a two-dimensional path.

It must be assumed for this analysis that air–fuel velocity similarity is maintained, according to equation 6a. Hence the relative velocity of fuel drops to air may be regarded as proportional to either absolute velocity. From the equations for radial and tangential equilibrium relative to the air flow, it may be shown that

$$\frac{dV}{dt} + \frac{2}{R} V^2 \tan \alpha - \frac{18 \rho_a^{1-r} \mu_a^{r} V^{2-r}}{d^{1+r} \rho_f} = 0 \qquad \ldots . [22]$$

The value of r will depend upon $R_{e,d}$, and for typical altitude test conditions

$$0{\cdot}75 < R_{e,d} < 3{\cdot}5$$

for initial injection. Both d and V will decrease to zero as evaporation and diffusion of the spray proceed, and a reasonable compromise is to confine attention to the region in which Stokes's law applies ($R_{e,d} < 0{\cdot}5$). Hence equation 22 becomes more readily soluble

$$\frac{dV}{dt} + \frac{2}{R} V^2 \tan \alpha - \frac{18 \mu_a V}{d^2 \rho_f} = 0 \qquad \ldots . [22a]$$

Ref. 13, for example, states that the evaporation rate of a drop is proportional to its diameter, or

$$d^2 = d_0^2 - \lambda t \qquad \ldots . [23]$$

For the purpose of the next steps in the analysis, it will be assumed that λ is constant; the variation with $R_{r,d}$ is considered later.

Equation 23 leads to its own scale requirements, viz.

$$d^2/t = \text{constant} \quad \ldots . [24]$$

Combining the differential of equation 23 with 22a, one obtains as a solution

$$\frac{1}{V} = \frac{2\rho_f \tan \alpha d^2}{R\,(18\mu_a - \lambda\rho_f)} \quad \ldots . [25]$$

leading to

$$Vd^2/R = \text{constant} \quad \ldots . [26]$$

Equations 24 and 26 then both give $\sigma_d = 1/n^{0.5}$.

Variation of evaporation constant with drop size—Heat transfer to an evaporating droplet is mainly by convection (> 80 per cent) and hence we may write as an approximation[13]

$$\lambda \propto 1 + k\,(R_{r,d})^{0.5}$$

Putting $k = 0{\cdot}246$, and $R_{r,d} = vd\rho_a/\mu_a \propto d$, we have by equation 26

$$R_{r,d} \propto p\,(l/v)^{0.5} \text{ and } \sigma R_{r,d} = n^{0.5}$$

whence

$$\sigma_\lambda = [1 + k\,(n)^{0.25}]/(1 + k)$$

The extreme values of $R_{r,d}$ for the full size chamber in our tests (0·75 and 3·5) yield

$$1{\cdot}033 < \sigma_\lambda < 1{\cdot}06$$

according to which the effect of variation in λ is clearly negligible.

Effect of pressure—The results obtained in the foregoing analysis are independent of chamber pressure. Reverting, however, to equation 22, a term p^{1-r} will be included if we depart from the range of validity of Stokes's law. To investigate the order of this effect, consider a simplified system where conditions are constant. The counterpart of equation 25 would be

$$\frac{1}{V^r} = \frac{\rho_f d^{1+r}}{18 R \mu_a{}^r \rho_a{}^{1-r} \tan^2 \alpha}$$

Hence $\sigma_d = (2)^{-r/(1+r)}$ for a half scale model chamber. For the extreme range

$$1 > r > 0{\cdot}65$$

the corresponding change in σ_d is

$$0{\cdot}707 > \sigma_d > 0{\cdot}760$$

For this work therefore, the effect of change in $R_{e,d}$ is small, and it is reasonable to accept the form of equation 22a as giving sufficiently close results.

Hence the geometry of a primary zone may be regarded as independent of pressure. However, the air–fuel mixture distribution, being dependent on evaporation rate, may still be affected if λ is itself a function of pressure. Ref. 14 gives

$$\mathrm{d}m/\mathrm{d}t \propto d_p^{0\cdot25} \quad \text{(where } m = \text{droplet mass)}$$

in the range 1 to 20 atm. Below 1 atm, however, the trend is towards a power less than 0·25. It may then introduce little error to assume that in our work the evaporation rate is also independent of pressure.

APPENDIX III. CALIBRATION OF SCALED ATOMIZERS

Details of the atomizers used in these tests are set out in *Table 3*.

Table 3

Type	*Designation*	*Nominal flow number*	*Operating calibration flow number/cone angle at 200 lb/in²*
Full size	*O*	0·48	0·484/68
	A	0·24	0·211/66
	B	0·22	0·201/70
	C	0·20	0·186/68
Half scale	*D*	0·18	0·177/74
	E	0·16	0·166/70
	F	0·14	*Not used*
	G	0·12	*Not used*

The close agreement in cone angle satisfactorily avoids the need to consider effects of this factor. *Figures 5* and *6* give the calibration for flow number and spray momentum.

Considering now the scale matching, from *Figure 6* the atomizer most nearly satisfying the requirement $\sigma_Y = 1$ is 'B.'

Hence $\sigma_X \rightleftharpoons 0\cdot201/0\cdot484 = 0\cdot4 = 1/n^{1\cdot32}$

$\therefore\ \sigma_{\Delta p} = (\sigma_{Q_f}/\sigma_X)^2 = (0\cdot5/0\cdot4)^2 = 1\cdot56 = n^{0\cdot64}$

Reference to *Figure 5* checks this value.

Now since $\sigma_Y = 1$

$$\sigma_{(A,C_D)} = \sigma_{Q_f} = 0\cdot5 = 1/n \text{ (cf. } \textit{Figure 9}\text{)}$$

And from equation 18

$$\eta_m \propto N/AC_D$$

$\therefore\ \sigma_{\eta_m} = 0\cdot4/0\cdot5 = 0\cdot8 = 1/n^{0\cdot32}$ (cf. *Figure 8*).

REFERENCES

[1] STEWART, D. G. 'Scaling of gas turbine combustion systems.' *Selected Combustion Problems II*. AGARD; Butterworths: London, 1956

[2] STEWART, D. G. 'The scale model testing of swirl atomizer gas turbine chambers.' Unpublished M.O.S. *Report*, September 1942

[3] NICHOLSON, H. M. 'The correlation of combustion efficiency and burner characteristics under simulated altitude idling conditions.' Unpublished M.O.S. *Report*, April 1951

[4] RADCLIFFE, A. and HAWKINS, J. M. 'The correlation of atomizer parameters and combustion chamber efficiency at altitude.' Unpublished M.O.S. *Report*, June 1953

[5] BAYLEY, F. J. 'A preliminary investigation of the physical aspects of gas turbine combustion.' Unpublished M.O.S. *Report*, August 1951

[6] RICE, R. A. 'Penetration of a liquid fuel in a gas stream.' *Internal Rep. Rolls-Royce*, October 1952

[7] KING, C. N. 'Fuel distribution experiments in a turbulent airstream.' Unpublished M.O.S. *Report*, May 1954

[8] Joseph Lucas Ltd. 'Some results obtained from initial tests with a scale model of a conventional Lucas combustion chamber.' Unpublished *Report*, April 1953. Joseph Lucas Ltd. 'The results of further experiments with scale models of a conventional Lucas combustion chamber.' Unpublished *Report*, March 1955

[9] NEEDHAM, H. C. 'Correlation of particle size data on pressure jet atomizers.' Unpublished Power Jets *Report*, May 1946

[10] MULLINS, B. P. 'Studies on the spontaneous ignition of fuels injected into a hot air stream.' *Fuel, Lond.* 32 (1953) 211

[11] HERBERT, M. V. 'A theoretical analysis of reaction rate controlled systems.' Part I: *Combustion Researches and Reviews*, AGARDograph No. 15, Butterworths: London, 1957. Part II. To be published

[12] HERBERT, M. V. 'Scale effect in a gas turbine combustion chamber fitted with a swirl atomizer'—Part II. To be published

[13] GODSAVE, G. A. E. 'Studies of the combustion of drops in a fuel spray—the burning of single drops of fuel.' *Fourth Symposium (International) on Combustion, 1952*, Williams and Wilkins: Baltimore, 1953

[14] DIEDRICHSEN, J. and HALL, A. R. 'The burning of single drops of fuel in air at pressures up to twenty atmospheres.' *Fourth Symposium (International) on Combustion, 1952*, p. 837. Williams and Wilkins: Baltimore, 1953

[15] CHELKO, L. J. 'Penetration of liquid fuel jets into high velocity air stream.' *NACA RM E50F21* (1950)

Recent Developments and Notes

BURNING OF METHANE FLAMES AT HIGH PRESSURE

J. DIEDERICHSEN and H. G. WOLFHARD have studied the burning velocities of methane–oxygen and methane–air flames at pressures of 0·05 to 2 and 0·1 to 40 atm respectively [*Trans. Faraday Soc.* 52 (1956) 1102]. These appear to be the first of such measurements over so wide a range of pressures. The bunsen burner method was used on cylindrical and rectangular burners and the experimental data were evaluated by the total area method. Comparable flames were produced by keeping the Reynolds number constant at 1200 so as to make the error in all measurements the same.

It was found that the burning velocity of stoichiometric methane–air mixtures decreases appreciably but not uniformly over the whole pressure range, whereas the burning velocities of methane–oxygen flames appear to be independent of pressure. This latter result is not in accord with measurements made by B. LEWIS, from which he found that the velocity of methane–oxygen flames decreased with decreasing pressure (*Selected Combustion Problems*, p 176. Butterworths: London, 1954).

Whilst the burning velocity in methane–air flames was found to be strongly dependent on pressure, flame temperatures are not dependent on pressure. There is, moreover, a rapid decrease in the concentration of radicals, at least [H] and [O], with pressure and there is a close relation between this and the dependence of burning velocity on pressure. Therefore flame temperature appears to have little influence on flame propagation. The results suggest that the burning velocity dependence on pressure is a function of radical concentration rather than burning velocity itself as suggested by B. Lewis. If burning velocity depended only on the concentration of radicals and atoms in the burnt gas of methane–air flames, then flame propagation would cease at pressures of about 1000 atm. As this is not conceivable, at very high pressures where radicals become unimportant a purely thermal mechanism of flame propagation may predominate.

FLAMMABILITY LIMITS

The theory of steady-state flame propagation does not indicate the occurrence of limits of flammability of gases. Some special behaviour appears to be characteristic of flame reaction which does not influence the steady conditions of flame propagation but only becomes important for compositions of mixtures near the limits. Energy losses from the flame may be a partial explanation of limits. Investigation of a possible effect of this nature, using lower-limit flames of methane in air, has been made recently by G. DIXON-LEWIS and G. L. ISLES, Gas Research Laboratory, University of Leeds [*Trans. Faraday Soc.* 53 (1957) 193].

The burning velocities of these flames were measured on a modified form of the flat-flame burner first used by J. POWLING [*Fuel, Lond.* 28 (1949) 25]. The top gauze which was originally used in this burner was replaced by an

electrically heated, perforated top plate. The effect of this may be to reduce the possibility of quenching by a comparatively cool surface such as the wire gauze, not externally heated, which is normally above the flame.

For a given temperature of the burner matrix, an approximate straight-line relationship between burning velocity and composition was found. When the temperature level in the system rises, due to electrical heating at the top, the lower-limit burning velocity decreases. But even at the highest temperatures used, 900°C at the top plate, there is still a lower limit to the burning velocity, even though 900°C is sufficient to ignite an unignited mixture just inside the limit. Gas flow patterns suggest that convection may be important in placing a lower limit on the burning velocity, and hence producing a composition limit in the flat-flame burner type of system.

ACOUSTIC PROPERTIES OF COMBUSTION SYSTEMS

The most usual type of oscillations in combustion systems is that of the organ-pipe. In oscillations of this kind the wavelength is related to the length of the combustion chamber, usually the path of gas travel through the chamber and exhaust pipes. The practical consequences of combustion oscillations may be of considerable importance in industrial burners and furnaces and also in rockets. A comprehensive survey of investigations on the subject has been made by A. A. PUTNAM and W. R. DENNIS, of Battelle Memorial Institute, Ohio, along with an account of their own work which was conducted under the sponsorship of the Aeronautical Research Laboratory, Wright Air Development Center, United States Air Force [*J. acoust. Soc. Amer.* 28 (1956) 246 and 260].

The singing flame, flash tubes, gauze tones, rocket-shaped burners, combustion chambers using secondary air and ram-jet type burners are described in respect of their acoustical behaviour. The hypothesis advanced by Lord Rayleigh is used as a basis for discussion of the various oscillatory systems. The hypothesis is that for a heat-driven oscillation to occur there must be a varying rate of heat release having a component in phase with the varying component of the pressure. The authors regard this theory as being satisfactory in a general way for the interpretation of combustion-oscillation phenomena in practice. There are considerable difficulties involved in formulating the theory mathematically. It is useful, however, to picture the combustion chamber as a driver which causes certain changes in the rest of the system, ultimately affecting the rate of heat production. According to Rayleigh's criterion, if the heat is added within the correct time intervals, driving continues. Damping effects can be allowed for in a qualitative manner.

In their recent investigations the authors have used a combustion tube supplied by a burner consisting of a bank of about 170 long ports, the internal diameter of each port being 0·023 in., and a moderately large plenum chamber. Both the diameter and length of the combustion chamber were varied. It was found that the combustion chamber could be regarded as a driver which forced slugs of gas in the ports to oscillate. These slugs

constituted incremental pulses of combustible mixture which supplied energy to the oscillations when they burned in phase with the oscillating component of the pressure in the chamber. The phasing depended on a time-lag factor which was a function of the velocity of the gases through a space, similar to a dark space, between the burner ports and the mean burning points, and the width of the space itself. The oscillations not only ceased when there was a failure to satisfy the timing criterion, but also upon approach to either rich or lean blow-off limits.

DESIGN OF HIGH-INTENSITY COMBUSTION CHAMBERS

D. B. SPALDING, Reader in Applied Heat, Imperial College of Science and Technology, London, presented a paper in January to the Internal Combustion Engine Group of the Institution of Mechanical Engineers, on the use of an electric analogue for the design and development of high-intensity combustion chambers [*Chart. mech. Engr* 3 (1956) 516]. In the case of gas turbines, for example, that are to operate at high altitudes, it is not possible to predict the performance of an untested design theoretically, due to lack of knowledge of the aerodynamics of the turbulent flows with recirculation that are necessary to maintain the existence of flame. The trial-and-error testing of a full-scale combustion chamber, which has been necessary for development to proceed, requires large volumes of air, often at pressures much below atmospheric, and is costly. A further hindrance to progress is that instrumentation in flames is difficult.

The electric analogue described is being developed to make speedier testing possible in the early stages of a project when the main features of the design are being established. Through the model of the combustion chamber in question air alone flows, and heater coils, sufficiently fine not to disturb the flow seriously, are distributed through the chamber. Thermocouples measure the air temperature near each coil and the heat input at each heater is adjusted by external controls to bear the same relation to the local temperature as the volumetric reaction rate of the combustion mixture does to the local temperature of the flame. This latter relation is supposed to be known from reaction rate theory, with fuel/air ratio as parameter.

The analogue yields a prediction of all the flame properties, shape, extinction condition, efficiency, and also enables the causes of the behaviour of a particular design of combustion chamber to be discerned, since all changes take place in slow motion. Amongst several different kinds of tests carried out were some on simple baffles of the type used for stabilizing flames in streams of premixed fuel and air, as in jet-engine reheat. The predicted blow-out velocities were found to agree very well with values reported in the literature and this would appear to indicate that even the prototype electric analogue which was built to test the principle of operation, can be useful in design. Considering also the qualitative reasonableness of the results obtained from other designs of differing flow pattern, for which flame data are not available, it is concluded that the underlying theory of the interaction of aerodynamic and chemical factors in flames is substantially correct.

COMBUSTION OF SOLID FUELS IN THIN BEDS

During the past fifty years the U.S. Bureau of Mines has made many studies of the fundamentals affecting the burning of solid fuels on grates. These have been reported in about 100 publications beginning with the early investigations by Randall, Flagg, Kreisinger and their co-workers on the principles of overfeed combustion and continuing with the work of Barkley, Sherman, Rice, Nicholls, and others on underfeed and other burning and gasification processes. In the past few years a continuation of this work has been specially directed to investigating the ignition and burning of solid fuels in thin beds, as on travelling, or chaingrate, stokers, and pure crossfeed combustion. An account of this later work has now been published by E. P. CARMAN, E. G. GRAF and R. C. COREY, in the belief that significant new material and conclusions have resulted on the behaviour of fuels burning under these conditions [U.S. Dept of Interior, Bureau of Mines, *Bull. No. 563* (1957)].

IGNITION TEMPERATURE OF SOOT

A new instrument that has been developed to measure the ignition temperature of soot has been described by D. R. ANDERSON and W. R. WATSON, of the National Aluminate Corporation [*Combustion* (*int. Combust. Engng Corp.*) 28 (Oct 1956) 43]. This instrument has been devised for measuring the effect of various catalysts on the burning of soot from oil flames and provides a simple, rapid and reliable method. The apparatus consists essentially of a piece of aluminium foil wrapped round a cylindrical holder and sooted in a suitable flame. A fuel oil solution or finely divided oil suspension of the material to be tested is sprayed on to the soot. The holder is then placed in an electric heater supported in a Pyrex glass tube, where it is heated at a uniform rate until the soot disappears, the temperature being very closely controlled. The temperature at which the foil becomes again visible in the area surrounding a thermocouple junction is recorded as the soot ignition temperature.

A variation in ignition temperature from 565° to 600°C was recorded for soots from different fuel oils and a temperature of over 700°C for graphite soot. The effect of oil-soluble metal-organic compounds was studied and lead, sodium, potassium and copper were found to have strong catalytic action in reducing the ignition temperature by between 180° and 120°C. In general these results agree with those of P. NICHOLLS and C. W. STAPLES in their work on combustion catalysts for solid fuel [U.S. Dept of Interior, Bureau of Mines, *Bull. No. 360* (1932)]. Non-metallic substances are generally ineffective, but the catalytic activity of many oil-soluble, metal-organic compounds is increased by the addition of certain non-metals. The effect of copper plus chlorine is an example of this combined action, but phosphorus produces the opposite effect from that of chlorine.

REACTION ZONE IN DETONATIONS

G. B. KISTIAKOWSKY and P. H. KYDD, of the Gibbs Chemical Laboratory, Harvard University, Massachusetts, have continued their series of papers

on gaseous detonations by the recent publication of one on a study of the reaction zone by gas density measurements [*J. chem. Phys.* 25 (1956) 824].

An x-ray absorption photometer capable of measuring gas densities with extreme rapidity and reasonable accuracy was developed to study the reaction zone in detonation waves. At low initial pressures this zone is observable as a density peak at the wave front lasting a few microseconds.

These investigators have found that in general the results agree with the hydrodynamic theory of the detonation wave. The observed densities at the end of the reaction zone (the Chapman–Jouguet state) compare well with the results of approximate equilibrium calculations, and the observed shape of the density profile qualitatively confirms kinetic predictions. The observed peak densities, however, are substantially lower than expected and the initial chemical reaction rates are faster. It is suggested that this may be due to the comparatively slow equilibration of translational energy with the internal degrees of freedom which allows substantial progress of the chemical reactions to take place.

The duration of the reaction zone in stoichiometric mixtures of hydrogen and oxygen is inversely proportional to the initial pressure of the detonating gas. On varying the composition of these gas mixtures the duration was found to be inversely proportional to the partial pressure of hydrogen and independent of that of the oxygen. An increase of the total pressure by the addition of rare gas accelerates the reaction. Nitrogen and water vapour act as inert additives.

Methane reacts with oxygen at a rate which is comparable with that observed for hydrogen, while acetylene oxidation is very much faster.

SHOCK TUBES

A short review of the principles of operation of shock tubes and of their applications has been published by A. KNOWLER [*Research, Lond.* 10 (1957) 132]. P. VIEILLE in 1899, in connection with his researches on the detonation wave, was the first to demonstrate a shock tube, and in more recent years such tubes were used by W. PAYMAN and W. C. F. SHEPPARD [*Proc. Roy. Soc. A* 186 (1946) 293] for similar investigations. At present various shock tubes are being used or built for research in universities or government establishments both in this country and in the U.S.A.

In principle the shock tube is a parallel-sided tube in which gas at high pressure at one end is separated initially by a diaphragm from gas at low pressure at the other end. When the diaphragm is burst the high pressure gas flows into the low pressure region. In the complex flow pattern produced there is a column of gas in which the flow is uniform and in which the temperature is high. It is this column of gas which has many important research applications. A comprehensive account of the flow in shock tubes has been given by J. LUKASIEWICZ [Shock tube theory and applications, *Report No.* MT–10, National Research Council, Canada, 1950].

Temperatures of 18 000° C have been produced using argon in a shock tube and at this temperature it was found that 40 per cent of the argon was ionized. The time available for measurements with the stronger shock

waves is only of the order of microseconds. In addition to studies involving very high temperatures, in aerodynamic investigations the shock tube can provide speeds up to fifteen times that of sound.

WESTERN STATES SECTION (U.S.A.) OF THE COMBUSTION INSTITUTE

At a meeting on 29 May 1957 at the Marquardt Aircraft Co., Van Nuys, California, a Western States Section of The Combustion Institute was provisionally organized, encompassing California, Oregon, Washington, Idaho, Nevada, Utah and Arizona. This meeting resulted from suggestions made at the Sixth Symposium on Combustion and the new section will promote greater interchange of information among combustion workers in the western U.S.A., especially those who have not as yet attended Combustion Symposia. It plans to embrace the entire field of combustion without particular direction towards either pure science or pure engineering applications.

The organizational meeting consisted of a technical session and a business session. At the technical session (*Chairman*, E. E. ZUKOSKI, California Institute of Technology) six papers were presented: 'Recent advances in the theory of metal ignition' by R. D. SCHULTZ (Aerojet-General Corpn); 'A direct method for predicting laminar burning velocities of both hydrocarbon and non-hydrocarbon fuels' by J. R. PERRIN (Marquardt Aircraft Co.); 'Flame reaction rates' by A. L. BERLAD (Convair Scientific Research Laboratory); 'An investigation of the combustion of composite propellants containing ammonium nitrate' by W. H. ANDERSEN, K. W. BILLS, E. MISHUCK, G. MOE and R. D. SCHULTZ; 'Chemical aspects of Mollier diagrams for combustion products' by C. H. BUILDER and G. S. BAHN (Marquardt Aircraft Co.); and 'Scaling parameters for small gas turbine combustors' by E. S. STARKMAN and A. J. LADERMAN (University of California) with L. H. MACLEOD (Aerojet-General Nucleonics) and V. E. TJULANDER (Marquardt Aircraft Co.).

At the business session (*Chairman*, A. L. BERLAD) a prospectus was adopted outlining the procedure by which the Section may be organized and may seek formal recognition by the Board of Directors of The Combustion Institute. An executive committee was elected to pursue the objectives of the prospectus. Serving on the executive committee are: W. J. BENNET, Marquardt Aircraft Co., Chairman; A. F. CHARWAT, University of California at Los Angeles, Vice-chairman; G. S. BAHN, Marquardt Aircraft Co., Secretary; M. W. RIGG, Office of Naval Research, Treasurer; J. A. DONNELLY, Radioplane Co.; R. D. STEWART, American Potash and Chemical Corpn; M. GOLDSMITH, the RAND Corpn; H. WISE, Stanford Research Institute; and S. S. PENNER, California Institute of Technology.

W. A. KIRKBY

FUEL

Attention is drawn to the following *Notes* which were published in the July 1957 issue of *Fuel* and which may be of interest to readers of *Combustion and Flame*:

Catalytic combustion of industrial fumes and exhaust gases
Engineers and clean air